eISSN 2500-0632

МИСИС
УНИВЕРСИТЕТ

Mining Science and Technology

Горные науки и технологии

Vol. Том 8 №3
2023

https://mst.misis.ru/

MINING SCIENCE AND TECHNOLOGY (Russia)

Горные науки и технологии

SCIENTIFIC AND PRACTICAL E-JOURNAL

eISSN 2500-0632

2023

Vol. 8, no. 3

https://mst.misis.ru/

Activities of the ***Mining Science and Technology (Russia) (Gornye nauki i tekhnologii)*** international journal are aimed at developing international scientific and professional cooperation in the field of mining.

The journal target audience comprises researchers, specialists in the field of mining, representatives of academic and professional communities.

The journal publishes original papers describing research findings, experience in the implementation of projects in mining industry, review publications.

The journal seeks to develop interdisciplinary areas that contribute to progress in mining, for example, technological and environmental safety, project organization and management in mining industry, development of territories, legal aspects of natural resource use, and other areas studied by researchers and practitioners. The journal always welcomes new developments. Papers are accepted in English or Russian.

QUARTERLY

FOUNDED in 2016

REGISTRATION

The journal science and applied research journal is registered by the Federal Service for Communication, IT and Mass Communication Control on August 10, 2015.
Registration Certificate E-No. ФС77-62652

INDEXATION

Scopus, CAS, EBSCO, DOAJ, РИНЦ, ВИНИТИ РАН, Dimensions, BASE, J-Gate, Jisc Library Hub Discover.

FOUNDER AND PUBLISHER

The National University of Science and Technology MISiS (NUST MISiS)

CONTACT

4 Leninsky Prospect, Moscow 119049, Russian Federation
Phone: +7 (495) 955-00-77
e-mail: send@misis.ru

ГОРНЫЕ НАУКИ И ТЕХНОЛОГИИ
Mining Science and Technology (Russia)
ЭЛЕКТРОННЫЙ НАУЧНО-ПРАКТИЧЕСКИЙ ЖУРНАЛ

eISSN 2500-0632
2023
Т. 8, № 3
https://mst.misis.ru/

Деятельность научно-практического журнала «Горные науки и технологии» (Mining Science and Technology (Russia)) направлена на развитие международного научного и профессионального сотрудничества в области горного дела.
Целевая аудитория журнала – исследователи, специалисты в области горного дела, представители академического и профессионального сообществ.
В журнале публикуются оригинальные статьи, описывающие результаты исследований, опыт реализации проектов в горнопромышленном комплексе, обзорные публикации.
Журнал стремится развивать такие междисциплинарные направления, как технологическая и экологическая безопасность, организация и управление проектами в горной промышленности, развитие территорий, правовые аспекты использования природных ресурсов и другие, которые способствуют прогрессу в горном деле и реализуются исследователями и практиками.

ПЕРИОДИЧНОСТЬ 4 раза в год

ОСНОВАН в 2016 году

РЕГИСТРАЦИЯ
Зарегистрирован Федеральной службой по надзору в сфере связи, информационных технологий и массовых коммуникаций 10 августа 2015 года.
Свидетельство о регистрации Эл № ФС77-62652.

ИНДЕКСИРОВАНИЕ
Scopus, CAS, EBSCO, DOAJ, РИНЦ, ВИНИТИ РАН, Dimensions, BASE, J-Gate, Jisc Library Hub Discover.

OPEN ACCESS Журнал открытого доступа.

УЧРЕДИТЕЛЬ И ИЗДАТЕЛЬ
МИСИС УНИВЕРСИТЕТ НАУКИ И ТЕХНОЛОГИЙ
Национальный исследовательский технологический университет «МИСиС» (НИТУ «МИСиС»)

АДРЕС УЧРЕДИТЕЛЯ И ИЗДАТЕЛЯ
119049, г. Москва, Ленинский проспект, д. 4

КОНТАКТЫ РЕДАКЦИИ
Адрес: 119049, г. Москва, Ленинский проспект, д. 4
Телефон: +7 (495) 955-00-77
e-mail: send@misis.ru

MINING SCIENCE AND TECHNOLOGY (Russia)
Горные науки и технологии
SCIENTIFIC AND PRACTICAL E-JOURNAL
eISSN 2500-0632
2023
Vol. 8, no. 3
https://mst.misis.ru/

CONTENTS

ГОРНЫЕ НАУКИ И ТЕХНОЛОГИИ
Mining Science and Technology (Russia)
ЭЛЕКТРОННЫЙ НАУЧНО-ПРАКТИЧЕСКИЙ ЖУРНАЛ
eISSN 2500-0632
2023
Т. 8, № 2
https://mst.misis.ru/

СОДЕРЖАНИЕ

eISSN 2500-0632
https://mst.misis.ru/

MINING ROCK PROPERTIES. ROCK MECHANICS AND GEOPHYSICS

Research paper

https://doi.org/10.17073/2500-0632-2023-01-75
UDC 691.21:553.89

Dolomite type nephrite processing wastes and their application

E. V. Kislov[1] ✉, **L. I. Khudyakova**[2], **A. G. Nikolaev**[3]

[1] *Dobretsov Geological Institute of Siberian Branch of the Russian Academy of Sciences (GIN SB RAS), Ulan-Ude, Russian Federation*

[2] *Baikal Institute of Nature Management of Siberian Branch of the Russian Academy of Sciences (BIP SB RAS), Ulan-Ude, Russian Federation*

[3] *Kazan (Privolzhsky) Federal University (KFU), Kazan, Russian Federation*

✉ *evg-kislov@ya.ru*

Abstract

The demand for ornamental stone material has led to an increase in the amount of rock mass being processed. However, the production of lapidary works and jewelry result in a significant amount of waste. This study aims to investigate the material composition and physical and mechanical properties of the solid wastes generated during the processing of dolomite type nephrite in the Vitim region. The accumulation of such waste leads to increased costs of transportation, storage, security, and negative environmental impact. The majority of dolomite type nephrite deposits are located in the Northwest, Northeast, and South of China, in South Korea, Australia, Italy, and Poland, with a large deposit in the Vitim region of Russia. In this study, the waste from the Kavoktinsky deposit, the most productive in Russian, was used. A visual and petrographic examination of nephrite, skarn and amphibolite which are components of the solid waste, was conducted. The macro- and microchemical composition of nephrite of different colors was studied, and X-ray phase analysis was performed. The decorative properties of the waste were determined. A radiation and hygienic certificate was obtained. The waste has a crushability grade of 1200, abrasion grade of I1, and frost resistance of F400. The study has shown that the waste does not contain grains of incompetent rocks, clay, dust, and clay particles. The solid waste form the Vitim nephrite processing is of high quality and meets the requirements of GOST 8267-93, except for an increased content of flagstone (flattened) and large size fragments. It can be used for the production of ordinary, decorative, and mosaic concrete, decorative plates, interior decoration of premises, bathrooms, and saunas, and the manufacture of souvenir products. However, further research is needed to investigate the application of the waste as a raw material for stone casting and a slow-release fertilizer. The utilization of this waste not only solves the problem of waste disposal but also improves economic performance of mineral extraction.

Keywords

nephrite, processing, processing waste, the Vitim region, mineral composition, chemical composition, decorative properties, physical and mechanical properties, utilization

Acknowledgments

The manuscript has been greatly improved thanks to remarks made by the reviewer of the editorial board. The authors would like to express their gratitude to Oriental Way Ltd. for providing stone material, to the Geospectr Center (TsKP) of the Institute of Geology of SB RAS, Ulan-Ude, and to the Geoanalitik of the Institute of Geology and Geochemistry, UB RAS, Yekaterinburg, for the analyses performed. The research was supported by grant No. 22-27-20003 form the Russian Science Foundation, https://rscf.ru/project/22-27-20003.

For citation

Kislov E.V., Khudyakova L.I., Nikolaev A.G. Dolomite type nephrite processing wastes and their application. *Mining Science and Technology (Russia)*. 2023;8(3):195–206. https://doi.org/10.17073/2500-0632-2023-01-75

СВОЙСТВА ГОРНЫХ ПОРОД. ГЕОМЕХАНИКА И ГЕОФИЗИКА

Научная статья

Отходы переработки аподоломитового нефрита и направление их использования

Е.В. Кислов[1] ✉, **Л.И. Худякова**[2], **А.Г. Николаев**[3]

[1] *Геологический институт им. Н.Л. Добрецова Сибирского отделения Российской академии наук (ГИН СО РАН), г. Улан-Удэ, Российская Федерация*

[2] *Байкальский институт природопользования Сибирского отделения Российской академии наук (БИП СО РАН), г. Улан-Удэ, Российская Федерация*

[3] *Казанский (Приволжский) федеральный университет (КФУ), г. Казань, Российская Федерация*

✉ *evg-kislov@ya.ru*

Аннотация

Камнесамоцветное сырье пользуется повышенным спросом, что приводит к возрастающему объему перерабатываемой горной массы. Обогащение исходного сырья, изготовление камнерезных и ювелирных изделий сопровождаются образованием большого количества отходов. Представленное исследование направлено на изучение вещественного состава и физико-механических свойств твердых отходов переработки аподоломитового нефрита Витимского региона. Образование отходов в значительном количестве приводит к затратам на перевозку, хранение и охрану, ухудшает экологическую обстановку. Месторождения аподоломитового нефрита находятся в Витимском регионе России. Наибольшее их количество сосредоточено на Северо-Западе, Северо-Востоке и Юге Китая, в меньшей мере – в Южной Корее, Австралии, Италии и Польше. В работе использованы отходы переработки наиболее продуктивного российского месторождения аподоломитового нефрита – Кавоктинского. Проведено визуальное и петрографическое изучение нефрита, скарна и амфиболита твердых отходов. Изучен макро- и микрохимический состав нефрита различного цвета, выполнен рентгенофазовый анализ. Определены декоративные свойства. Получен радиационно-гигиенический сертификат. Отходы имеют марки по дробимости 1200, по истираемости – И1, по морозостойкости – F400. Проведенные исследования показали, что в их составе не содержатся зерна слабых пород, а также глина, пылевидные и глинистые частицы. Твердые отходы переработки нефрита Витимского региона имеют высокое качество, соответствуют требованиям ГОСТ 8267–93, за исключением повышенного содержания фрагментов лещадных (уплощенных) и повышенного размера. Они могут использоваться в производстве обычного, декоративного и мозаичного бетонов, декоративных плит, внутренней отделки помещений, бань и саун, для изготовления сувенирной продукции. Использование в качестве сырья для каменного литья и пролонгированного удобрения требует дополнительного рассмотрения. Все это позволит не только решить проблему утилизации отходов, но и улучшить экономические показатели добычи минерального сырья.

Ключевые слова

нефрит, обогащение, отходы переработки, Витимский регион, минеральный состав, химический состав, декоративные свойства, физико-механические свойства, утилизация

Благодарности

Замечания рецензента редколлегии позволили значительно улучшить рукопись статьи. Авторы признательны ООО «Ориентал Вэй» за предоставление каменного материала, ЦКП «Геоспектр» ГИН СО РАН, Улан-Удэ, и «Геоаналитик» ИГГ УрО РАН, Екатеринбург, за проведенные анализы. Исследование выполнено за счет гранта Российского научного фонда № 22-27-20003, https://rscf.ru/project/22-27-20003.

Для цитирования

Kislov E.V., Khudyakova L.I., Nikolaev A.G. Dolomite type nephrite processing wastes and their application. *Mining Science and Technology* (*Russia*). 2023;8(3):195–206. https://doi.org/10.17073/2500-0632-2023-01-75

Introduction

The demand for ornamental stone material has led to an increase in the amount of rock mass being processed. This processing, which includes the production of lapidary works and jewelry, results in the generation of two types of waste: hard fragments and scraps of host rock and substandard nephrite, which are produced during the extraction of grade stone and manufacturing of products, as well as the slime formed during cutting and processing. This slime is a mixture of water, abrasive material, and small stone particles. The volume of these wastes can range from 10 to 35 % of the primary stone material. The increasing amount of waste generated has resulted in higher costs associated with transportation, storage, and security. Moreover, it has a negative impact on the environment and human health [1–4]. Therefore, recycling of such waste to obtain marketable products is essential.

The slime generated from ornamental stone processing is mainly used for the production of cement, concrete, and ceramics, which enhances their performance. Slimes from granite [5], marble [6–8] are utilized in the production of cements. They replace natural sand in cement mortars [9]. The addition of slime to the clay mixture is beneficial for the production of ceramic materials [10–13]. Solid waste from marble processing is mostly used to produce lime [14]. Granite waste is employed for stabilizing loose grounds [15], whereas marble dust is suitable for clay grounds [16]. Additionally, chips and fragments are used in the production of artificial decorative stones for pedestrian sidewalks [17] and floors of residential and industrial buildings [18].

All of the aforementioned examples are related to the processing waste of granite and marble. While some studies have been devoted to the possibility of utilizing substandard serpentinite type nephrite [19, 20], the processing waste of dolomite type nephrite has not yet been considered, despite its intensive use.

As of January , 2022, 26 nephrite deposits were in the register of the State Balance of Reserves of Russia. In 2021, seven deposits in Buryatia were developed, including Kavoktinsky, Nizhne-Ollominsky, Sergeevsky, and Khaitinsky dolomite type nephrite deposits. As for other dolomite type nephrite deposits, the Voymakansky in Buryatia was being prepared for extraction, while the Udokan in the Trans-Baikal Territory, and Buromsky in Buryatia were being explored. There are no deposits of dolomite type nephrite in the non-licensed stock of prospects/areas. All the deposits are located in the Vitim nephrite-bearing region, with the largest deposit being the Kavoktinsky which had 346.81 tons of C2 category reserves as of January 1, 2022. In 2021, 70.36 tons of nephrite were extracted, amounting to 28.58 % of the Russian production.

Most of the dolomite type nephrite deposits abroad are located in China. The largest known deposits are located in the northwestern provinces of Chin, in the Hetian nephrite-bearing belt located in Xinjiang Uygur autonomous region. This region has been being developed for 6,000 years, both for primary nephrite deposits [21–23], among which the best known and studied is Alamas [24–25], and for famous placer nephrite deposits, Yurungkash ("the river of white nephrite") and Karakash ("the river of black nephrite") [26–28]. The Hetian belt is adjoined from the east by the Altyn Tagh [29, 30] and Southern Altyn Tagh [31, 32] nephrite-bearing districts. Further eastward, the Golmud and other deposits in Qinghai Province are located [33, 34]. A number of deposits are located in the northeastern provinces of China such as Tieli in Heilongjiang Province [35–37], Panshi in Girin Province [38], and Xiuyan and Sangpiyu in Liaoning Province [39, 40]. In East China, the Xiaomeiling deposit in Jiangsu Province is known [41, 42]. In South Central China, the Luanchuan deposits in Henan Province [43, 44] and Dahua deposits in the Guangxi Zhuang Autonomous Region are presented [45–47]. In Soutwest China, the Longxi deposit in Sichuan Province [48] and Luodian deposit in Guizhou Province [49] are known.

In addition, the Chuncheon deposit in South Korea [50, 51], the Cowell area on the Eyre Peninsula in South Australia [52, 53], the Alpe Mastabia deposit (Val Malenco) in Lombardy, Italy [54], and the Zloty Stok deposit in Lower Silesia, Poland [55–57] are noteworthy.

The aim of this study is to investigate the physical and mechanical characteristics of solid wastes generated during dolomite type nephrite processing and determine potential areas of their utilization.

Research Materials and Methods

This research focuses on the solid waste generated during processing of dolomite type nephrite in the Vitim region, specifically the Kavoktinsky. Oriental Way LLC provided the waste for this study.

Sampling for laboratory analysis was conducted using the point method. A square grid was overlaid onto the batch of waste laid out horizontally, and samples were taken from the center of each grid cells. To ensure the maximum representation of all types of nephrite processing waste, a total of 20 sample weights, weighing 200 kg, were collected from the batch. These representative samples were then used for a detailed examination of the materia (Fig. 1).

Fig. 1. Nephrite processing waste

The study examined the waste generated from the processing of nephrite to assess its conformity with the technical requirements specified in GOST 8267–93 "Crushed stone and gravel of solid rocks for construction works. Technical conditions" and GOST 8269.0–97 "Crushed stone and gravel of solid rocks and industrial waste for construction works. Methods of physical and mechanical tests".

The research methodology comprised of a mineralogical-petrographic analysis, chemical testing, evaluation of decorative properties, physical and mechanical tests of the waste, and a comparison of the obtained results with the stipulated GOST parameters.

A visual petrographic and mineralogical analysis was conducted on the solid waste samples by obtaining representative samples, measuring their size, and describing their shape using a measuring tape. The samples were then weighed using portable electronic scales, and their fracture and Mohs scale were determined. The presence of fractures and carbonate minerals were identified through of fracturing and diagnosis of carbonate minerals 5 % hydrochloric acid solution, respectively. Petrographic analysis of thin sections was carried out using a polarizing microscope POLAM L-213 in the Geological Institute in Ulan-Ude, Russia.

Silicate analysis was conducted at Geospectr TsKP of GIN SB RAS, Ulan-Ude, using a UNICO 1201 spectrophotometer (United Products and Instruments, USA) that operated in the spectral range of 315–1000 nm. Additionally, we employed a SOLAAR-6M atomic-absorption spectrophotometer (Unicam, England) with appropriate software. We utilized various methods including atomic absorption, flame photometric, gravimetric, and titrimetric methods. For weighing, we used VSL-200/0,1A electronic scales (CJSC VES-SERVICE, St. Petersburg, Russia) with a weighing range of 0.01 to 205 g.

The trace elements grades were determined using a high-resolution HR ICP-MS ELEMENT2 (ThermoFinnigan) mass spectrometric system for multi-element analysis of geological material at the TsKP Geoanalitik of the Institute of Geology, Ural Branch of the Russian Academy of Sciences, Yekaterinburg. Quality control of the results was ensured through parallel analyses of internal control samples and standard rock samples, including SG-1A, SGD-1A, BCR-2. Standard samples BCR2 (U.S. Geological Survey) were included in the normal sample flow for analysis at frequency of 1:5–1:10.

Optical properties such as transparency, color, optical effects, and inclusions were investigated using a MBS-10 binocular and a 20x magnification gemological magnifying glass at KFU in Kazan. The GIA color scale and the requirements of TU 117-3-0761-7-00 were utilized for determining color, color hue, tone, and saturation. The studies were carried out by optical absorption spectroscopy method, and a standardized MSFU-K spectrophotometer was used to record optical absorption spectra in the wavelength range of 400–800 nm in increments of 1 nm. The method of calculating chromaticity coordinates according to the XYZ international colorimetric system was used to measure and describe the coloration of samples. The colorimetric results were placed on the standard color triangle of the Commission International d'Eclairage (ICE-1931), and color coordinates were converted into the GIA systems used for color evaluation. The "Spectrum" specialized program was employed to calculate colorimetric parameters of the minerals according to the CIE Lab international system. All experimental studies were carried out at room temperature, and five spectra were taken from each sample.

The physical and mechanical properties were determined in BIP SB RAS, Ulan-Ude, following the requirements of GOST 8267–93 "Crushed stone and gravel of solid rocks for construction works. Technical Specifications" and GOST 8269.0–97 "Crushed stone and gravel of solid rocks and industrial waste for construction works. Methods of physical and mechanical tests". A fraction of 40–70 mm was selected from the waste to determine the grain composition, while the fraction over 70 mm was crushed using a jaw crusher. The samples were brought to a constant weight, and the moisture content was determined using a ShSU-M1 drying cabinet (JSC Electropribor, St. Petersburg, Russia), with a heating temperature ranging from 50 to 300 °C and the time of heating to the maximum temperature not exceeding 120 minutes. Particle size distribution testing was conducted using a standard set of sieves, and weighing was carried out on MK-15.2-A22/10540 electronic scales (CJSC "Massa-K", St. Petersburg, Russia). X-ray phase analysis was performed using a D8 Advance powder automatic diffractometer of BrukerAXS (Germany) with appropriate software at a rate of 2° per minute in the range from 5 to 70°. For mechanical tests, a PGM-500 hydraulic test press (LLC "SKB Stroypribor", Chelyabinsk, Russia) with a load range up to 50 tons and a speed of plate movement of 10 ± 1 mm min^{-1} was used. To determine abrasion, an abrasion testing machine KP 123 ("Novoe Delo" LLC, St. Petersburg, Russia) with a diameter of 700 mm, length of 500 mm, and a shelf 100 mm wide on the inner surface was employed.

A radiation and sanitary audit was conducted in compliance with the requirements of GOST 30108–2016 "Materials and products for construction. Determination of specific effective activity of natural radionuclides". The specific effective activity of natural radionuclides found in nephrite processing waste was measured in the Test Laboratory Center of the Federal Public Health Institution "Center for Hygiene and Epidemiology in the Republic of Buryatia" using an integrated universal spectrometer, USK "Gamma-plus".

Findings

The batch of solid waste consists of angular, isometric to flattened fragments, and irregularly shaped pieces of light-colored raw nephrite. The largest dimension of 75 % of the fragments ranges from 4 to 12 cm, while 25 % of the fragments range from 12 to 15 cm. The coloring of the stone varies from uniform to heterogeneous, sometimes spotted or banded, and includes light-green, grayish-white, often with a bluish tint, light gray, dark gray, brown (honey). The fragments may occasionally contain light green patches and brown margins staining on fractures and surfaces. Visually distinguishable isometric grains of tremolite, calcite, epidote, chlorite, black and emerald-green phenocrysts, dendrites of black manganese hydroxides, and flaky aggregates of brown iron hydroxides may be present in some fragments. The fragments are covered with white matte crusts with dendrites of black manganese hydroxides, and dendrites of black manganese hydroxide, white films of calcite, and brown films of iron hydroxides may also be observed along fractures. Some fragments consist of areas of white matte tremolite-calcite skarns and variously colored metasomatized amphibolite., while others are entirely composed of skarn and amphibolite.

Under binocular microscope magnification, the nephrite includes inclusions of individual crystals and aggregates of calcite and broad-prismatic tremolite, dendrites of manganese hydroxides, flaky aggregates of iron hydroxides, and veins of calcite-tremolite skarn. Fresh chips show uneven, splintered, conchoidal fractures.

Under a petrographic microscope, nephrite is observed to be a practically monomineral aggregate of crystals and the finest fibers of mainly tremolite amphibole with a tangled-fibrous (fibroblast) structure characteristic of nephrite, with individual fibers ranging from a few microns to 0.1 × 0.5 mm. The shape of the aggregates is mostly parallel-fibrous, fan-shaped, and felt-like. Inclusions of individual crystals and aggregates of calcite, broad-prismatic tremolite of isometric or elongated shape with grain size up to 1–10 mm may be observed in places in nephrite. The nephrite is heterogeneously polished, with significant shagreening in places. The areas of nephrite with the inclusions of other minerals and their aggregate clusters do not take a polish; they are matte and rough. Transparency along the edge of a hand specimen is to a depth of 5 cm.

In the skarn, tremolite is represented by several varieties, including solid porcelain-like tremolite, consisting of tiny, shapeless radiated aggregates with slices, fuzzy aggregates of finely dispersed calcite, and traces of prismatic tremolite crystals. Large shapeless aggregates with relics of split prismatic tremolite replaced by thin-fibrous tremolite, and fine-grained multioriented tremolite with grain sizes ranging from 0.01 × 0.03 to 0.6 × 1.3 mm are also present. Lenticular aggregates of fine-grained calcite in various proportions with tremolite are found, and in another case, numerous single grains, panicle-like, radial-beam aggregates of tremolite with apatite alternate with nephrite-like areas composed of micro- and fine-grained tremolite. Diopside and plagioclase are also present.

The predominant mineral found in amphibolite is tremolite, with the occasion presence of actinolite. Tremolite is commonly observed in large calcite grains, where it appears as thin, elongate needle-like prisms that penetrate the host mineral parallel to one another. Actinolite is typically inequigranular, forming aggregates with rare calcite and intergrowths of prismatic epidote. These aggregates may form radial fibrous intergrowths, with potassium feldspar occasionally present in small angular interstices. The calcite grains contain inclusions of dolomite, epidote, chlorite, and quartz which can occupy up to 30 % of the host mineral area. Zoisite grains and fine-scaly chlorite, and they can form unusual spot-like aggregates among calcite grains. Xenomorphic quartz grains are often found saturated with rhombic, needle-like crystals of tremolite and/or epidote, which can occupy up to 25 % of the host mineral area. In some cases, plagioclase is more abundant and can be partially replaced by granular aggregates of epidote and clinozoisite, sometimes forming independent interstitial aggregates that may also contain potassium feldspar. Finally, apatite, sphene, and zircon are present as well.

Tables 1 and 2 provide a detailed breakdown of macro- and micro-components found in nephrite of various colors that were extracted from the solid waste.

The solid waste mineral composition is confirmed by the results of X-ray phase analysis (Fig. 2).

The X-ray diffraction pattern revealed that the primary reflexes of the studied samples corresponded to the minerals tremolite, diopside, chlorite, talcum and calcite.

The visual description of the samples included color characteristics such as primary color, hue, tone, saturation. Based on these characteristics, two main varieties were identified. The first variety is referred to as white nephrite, which ranges from pure white to slightly saturated grayish or yellowish-brown, and may appear brown (honey-colored) due to iron oxidation, as illustrated in Fig. 3. The second variety is known as light-green (greenish) nephrite, which ranges from bluish to yellow-greenish and may appear brown (honey-colored) due to oxidation, as depicted in Fig. 4.

The primary color types of the nephrite include white as well as gray with a pale green hue, bright light bluish-green, and bluish-green tones occur. The pattern of the nephrite is uniform, with brown staining edges, and may contain inclusions of prismatic tremolite, calcite and white-colored diopside, which are noticeable due to cleavage.

Table 1

Chemical composition of nephrite

Sample	Grade															
	%													g/t		
	SiO_2	TiO_2	Al_2O_3	Fe_2O_3	FeO	MnO	MgO	CaO	Na_2O	K_2O	P_2O_5	LOI	Total	F	Cr	Co	Ni
KS-6	58.2	<0.02	0.3	<0.1	0.2	0.04	25.77	12.5	0.08	0.06	<0.1	2.72	99.87	0	<5	6	9.5
KS-7	57.5	<0.02	0.6	<0.1	0.16	0.02	24.98	12.92	0.08	0.04	<0.1	2.9	99.2	0	<5	9.5	8
KS-8	56.8	<0.02	0.7	<0.1	0.22	0.03	25.36	13.15	0.1	0.07	<0.1	2.28	98.71	0.32	9	9.8	8

Note: hereinafter, the analyses of nephrites refer to: KS-6 – brown, KS-7 – light-green, and KS-8 – white nephrite.

Table 2

Concentration of trace elements in nephrite, g/t

Element	KS-6	KS-7	KS-8	Element	KS-6	KS-7	KS-8
Li	4	7	6	Te	< 0.01	< 0.01	0.026
Be	11	17	9	Cs	1.8	2.1	0.7
Sc	1	1	0.6	Ba	6	5	8
Ti	50	80	18	La	0.2	0.4	0.35
V	8	17	8	Ce	0.47	0.8	0.59
Cr	2.4	4.7	15	Pr	0.06	0.1	0.07
Mn	180	80	140	Nd	0.25	0.41	0.3
Co	4	6	5	Sm	0.06	0.09	0.07
Ni	11	6	9	Eu	0.01	0.02	0.018
Cu	4.1	6	50	Gd	0.065	0.094	0.069
Zn	14	20	14	Tb	0.01	0.014	0.01
Ga	0.8	2.4	0.9	Dy	0.07	0.09	0.06
Ge	0.5	0.5	0.6	Ho	0.015	0.02	0.012
As	90	86	80	Er	0.043	0.058	0.033
Se	0.2	0.17	0.15	Tm	0.006	0.009	0.0036
Rb	2.4	2.9	2.3	Yb	0.04	0.05	0.02
Sr	70	60	60	Lu	0.006	0.008	0.0028
Y	0.4	0.6	0.5	Hf	0.041	0.06	0.06
Zr	2.1	2.7	2.8	Ta	0.019	0.06	< 0.001
Nb	0.06	0.37	0.12	W	16	30	40
Mo	0.22	0.16	0.6	Tl	0.013	0.012	0.005
Ag	< 0.0004	0.027	0.079	Pb	4	8	12
Cd	0.05	0.05	0.09	Bi	< 0.0005	0.057	0.065
Sn	0.11	0.2	0.28	Th	0.008	0.14	0.03
Sb	0.08	0.18	0.24	U	0.026	0.6	0.047

One common feature observed in the optical absorption spectra of the nephrite is the presence of a broad absorption band in the near-infrared region, located near 990 nm, as shown in Fig. 5. Further investigation into configuration of this line, combined with chemical analyses of the nephrite, suggests that this band is associated with the spin-allowed transitions $^5T_2$ (^5D) → ^5E (^5D) in Fe^{2+} ions that occupy positions M1, M2, M3, replacing Mg^{2+}. In addition, the absorption bands observed around 440 nm and 650 nm in the spectrum of the nephrite are attributed to the spin-allowed transitions from the basic state $^4A_{2g}$ (^4F) to higher energy levels, $^4T_{1g}$ (^4F) and $^4T_{2g}$ (^4F), respectively [58, 57].

The specific effective activity of natural radionuclides present in the nephrite processing waste was found to be less than 50 Bq/kg.

As the waste is composed of remnants from sawing larger than 40 mm, only the fraction within the range of 40–70 mm can be used as ballast stone, while the remaining material must undergo crushing. The distribution of grain size in the resulting crushed waste is presented in Fig. 6.

The data obtained indicate that the majority of crushed waste (62 %) ranges from 5 to 15 mm in size, whereas 21.5 % of the waste falls under to the fraction – 5 mm.

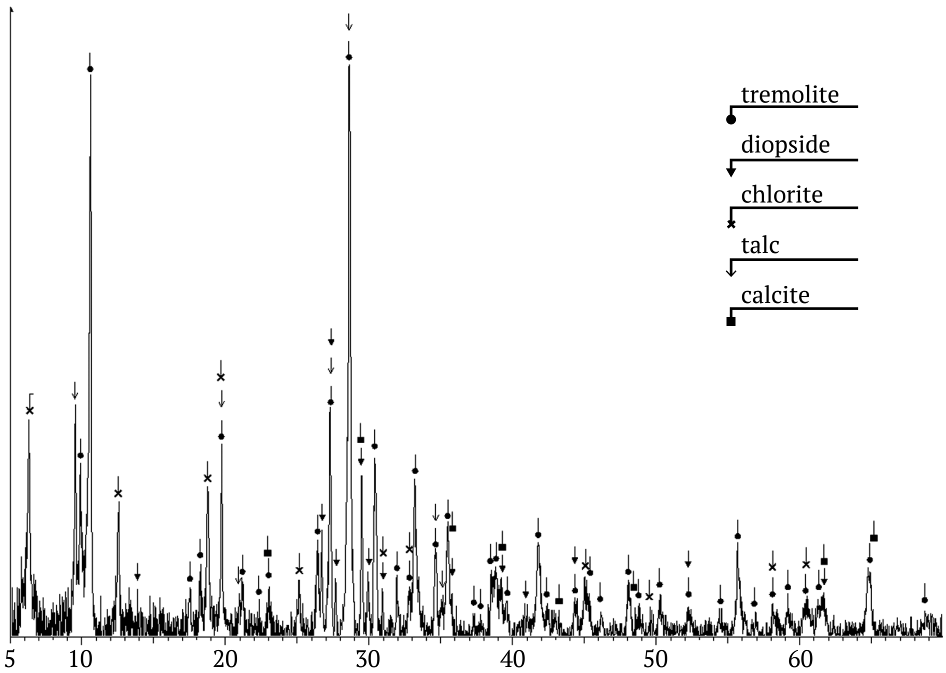

Fig. 2. X-ray diffraction pattern of nephrite processing waste

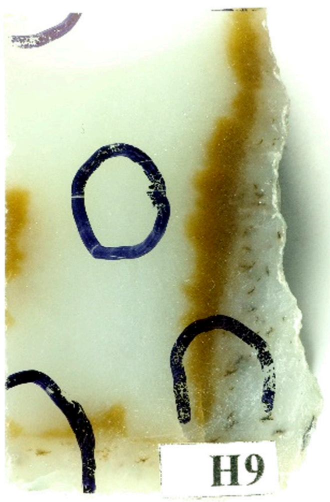

Fig. 3. Nephrite H9 white w with brown edges br and weathering crust with black manganese hydroxides

Fig. 4. Nephrite H11 bluish-green bG (light l, moderately strong light saturation mst), brown staining crust Brn (light l to extremely dark exdk with strong light saturation st)

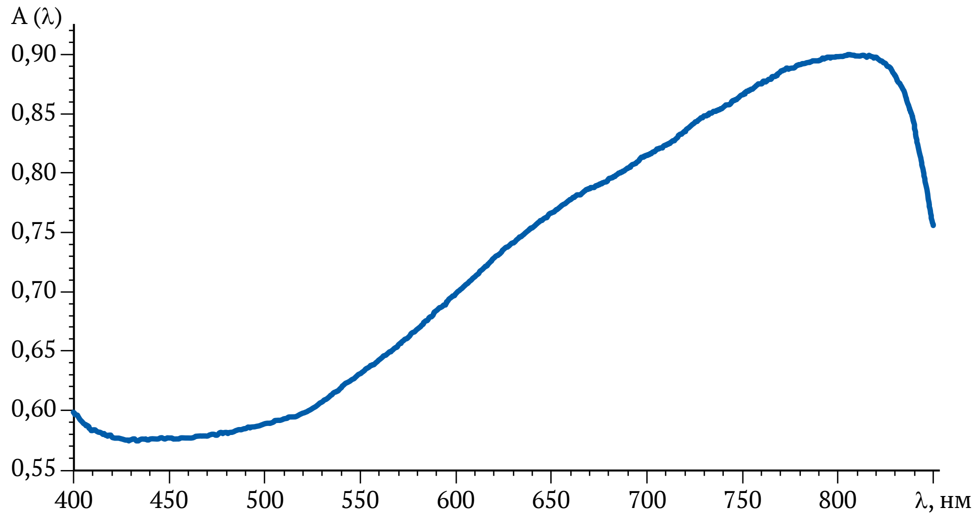

Fig. 5. Optical spectrum of white nephrite H9. Lab 55.0938: −5.4096: −5.7374 (CIE Lab)

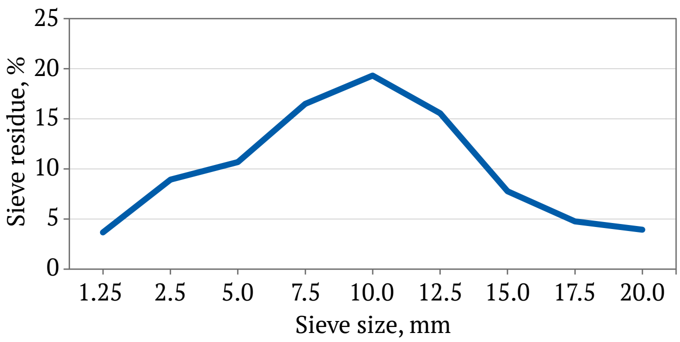

Fig. 6. Crushed stone grain size distribution

Nephrite, due to its tangled-fibrous microstructure and high viscosity, is challenging to crush. Consequently, a significant percentage of needle-shaped and flaky grains are observed, accounting for 23.4 % of the crushed stone from nephrite processing waste. This categorizes the waste into the third group of crushed stone according to GOST 8267–93.

The waste has a crushability grade of 1200, abrasion grade of I1, and frost resistance of F400. The studies reveal that the waste does not contain grains of incompetent rocks, clay, dust, or clay particles. Table 3 summarizes the study results and demonstrate that the solid nephrite processing waste from the Vitim region adheres to the requirements of GOST 8267–93.

Discussion

The investigation of the composition of the nephrite processing waste from the Vitim region revealed the absence of harmful components and impurities, including minerals, macro- and micro- chemical components). The decorative properties, including coloring, pattern, translucency, polishability, and defects, meet the existing standards.

The specific effective activity of natural radionuclides of the waste is below 50 Bq/kg, which complies with the NRB–99/2009, GOST 8267–93, and the 1st safety class norm, allowing its use as ornamental and facing stone for all types of construction work.

The waste material has a crushability grade of 1200, abrasion grade of I1, and frost resistance of F400. The studies revealed that the waste does not contain grains of incompetent rocks or clay particles. The solid waste of Vitim nephrite processing meets the requirements of GOST 8267–93, except for the increased content of flagstone and large fragments, which can be sold as crushed stone is possible by mutual agreement.

After crushing, the nephrite processing waste can be used as crushed (ballast) stone for construction works, including the production of ordinary concrete, decorative and mosaic concrete for finishing and lining walls and floors, as well as decorative floor slabs using cement and polymer binder compositions. The waste material is compliant with the requirements of GOST 9479–2011 “Blocks of rocks for the production of facing, architectural and construction, memorial and other products” and GOST 24099–2013 “Decorative plates based on natural stone. Technical Specifications”.

Furthermore, the nephrite processing waste can be utilized as a facing material for interior decoration, such as hallways and bathrooms, owing to its high density (2,900 kg/m^3), durability (M1200), low water absorption (0.2 %), resistance to corrosive environments, temperature differences, high melting point (approximately 1,250 °C) and low thermal conductivity.

Table 3

Physical and mechanical parameters of nephrite processing waste

Item No.	Indicator	Nephrite processing waste	Requirements (GOST 8267–93)
1	Total residue on check sieves, % by weight	98.73	d 90 to 100
		48.34	0.5(d+D) 30 to 60
		6.10	D to 10
		0.32	1.25D to 0.5
2	Contents of lamellar (flaky) and needle-shaped grains, % by weight	36.6	–
3	Crushability grade	1,200	–
4	Abrasion grade	I1	–
5	Content of grains of incompetent rocks, % by weight	0	Less than 5
6	Frost resistance	F400	–
7	Content of dust and clay particles, % by weight	0	Less than 1
8	Clay content in clumps, % by weight	0	< 0.25
9.	Presence of harmful components and impurities	None	–
10	Resistance against all types of decay (mass loss on decay, %)	0	Less than 3
11	True density, g/cm^3	2.8426	–
12	Average density, g/cm^3	2.8995	–
13	Bulk density, kg/m^3	1314.29	–
14	Moisture content, %	0.083	–
15	Water absorption, %	0.1937	–

Nephrite processing waste is a valuable for souvenir production, as a raw material for stone casting and slow-release fertilizer, particularly in areas with low calcium and magnesium due to the predominant development of granite, such as Buryatia.

Conclusion

The processing waste form nephrite has high quality and, with few exceptions, meets Russian standards. This waste can be utilized in the production of crushed stone for various purposes such as ordinary, decorative, and mosaic concrete. It is also suitable for the production of decorative slabs when corporated into cement and polymer binder compositions. Moreover, as an independent material it has potential for interior decoration and serves a valuable raw material for souvenir production. Furthermore, this waste can be used as a raw material for stone casting and slow-release fertilizer, especially in areas with unsufficient calcium and magnesium due to the predominance of granite, as in Buryatia. These multiple application not only solve the waste disposal problem but also enhance the economic viability of mineral extraction.

References

1. Emmanuel A.Y., Jerry C.S., Dzigbodi D.A. Review of environmental and health impacts of mining in Ghana. *Journal of Health and Pollution*. 2018;8(17):43–52. https://doi.org/10.5696/2156-9614-8.17.43

2. Jain M.K., Das A. Impact of mine waste leachates on aquatic environment: A review. *Current Pollution Reports*. 2017;3(1):31–37. https://doi.org/10.1007/s40726-017-0050-z

3. Wellen C., Shatilla N.J., Carey S.K. The influence of mining on hydrology and solute transport in the Elk Valley, British Columbia, Canada. *Environmental Research Letters*. 2018;13(7):074012. https://doi.org/10.1088/1748-9326/aaca9d

4. Strzałkowski P. Characteristics of waste generated in dimension stone processing. *Energies*. 2021;14(21):7232. https://doi.org/10.3390/en14217232

5. Medina G., Sáez del Bosque I.F., Frías M., et al. Mineralogical study of granite waste in a pozzolan/Ca(OH)$_2$ system: Influence of the activation process. *Applied Clay Science*. 2017;135:362–371. https://doi.org/10.1016/j.clay.2016.10.018

6. Prošek Z., Nezerka V., Tesárek P. Enhancing cementitious pastes with waste marble sludge. *Construction and Building Materials*. 2020;255:119372. https://doi.org/10.1016/j.conbuildmat.2020.119372

7. Wang T., Yang W., Zhang J. Experimental studies on mechanical properties and microscopic mechanism of marble waste powder cement cementitious materials. *Crystals*. 2022;12(6):868. https://doi.org/10.3390/cryst12060868

8. Ahmed A., Abbas S., Abbass W., et al. Potential of waste marble sludge for repressing alkali-silica reaction in concrete with reactive aggregates. *Materials*. 2022;15(11):3962. https://doi.org/10.3390/ma15113962

9. Moreira P.I., de Oliveira Dias J., de Castro Xavier G., et al. Ornamental stone processing waste incorporated in the production of mortars: Technological influence and environmental performance analysis. *Sustainability*. 2022;14(10):5904. https://doi.org/10.3390/su14105904

10. Gadioli M.C.B., Ponciano V.M., Bessa B.H.R., et al. Characterization of ornamental stones wastes for use in ceramic materials. *Materials Science Forum*. 2019;958:129–134. https://doi.org/10.4028/www.scientific.net/MSF.958.129

11. Xavier G.C., Azevedo A.R.G., Alexandre J., et al. Determination of useful life of red ceramic parts incorporated with ornamental stone waste. *Journal of Materials in Civil Engineering*. 2019;31(2). https://doi.org/10.1061/(ASCE)MT.1943-5533.0002590

12. Munir M.J., Kazmi S.M.S., Wu Y.-F., et al. Thermally efficient fired clay bricks incorporating waste marble sludge: An industrial-scale study. *Journal of Cleaner Production*. 2018;174:1122–1135. https://doi.org/10.1016/j.jclepro.2017.11.060

13. Ahmad S., Shah M.U.H., Ullah A., at el. Sustainable use of marble waste in industrial production of fired clay bricks and its employment for treatment of flue gases. *ACS Omega*. 2021;6:22559–22569. https://doi.org/10.1021/acsomega.1c02279

14. Soltan A.M., Taman Z., El-Kaliouby B. Recycling of ornamental stones hazardous wastes. *Natural Resources*. 2011;2(4):244–249. https://doi.org/10.4236/nr.2011.24031

15. Abdelkader H.A.M., Ahmed A.S.A., Hussein M.M.A., et al. An experimental study on geotechnical properties and micro-structure of expansive soil stabilized with waste granite dust. *Sustainability*. 2022;14(10):6218. https://doi.org/10.3390/su14106218

16. Ibrahim H.H., Alshkane Y.M., Mawlood Y.I., at el. Improving the geotechnical properties of high expansive clay using limestone powder. *Innovative Infrastructure Solutions*. 2020;5(3):112. https://doi.org/10.1007/s41062-020-00366-z

17. Carvalho E.A.S., Vilela N.F., Monteiro S.N., et al. Novel artificial ornamental stone developed with quarry waste in epoxy composite. *Materials Research*. 2018;21(1):e20171104. https://doi.org/10.1590/1980-5373-MR-2017-1104

18. Silva F.S., Ribeiro C.E.G., Rodriguez R.J.S. Physical and mechanical characterization of artificial stone with marble calcite waste and epoxy resin. *Materials Research*. 2018;21(1). https://doi.org/10.1590/1980-5373-MR-2016-0377

19. Khudyakova L.I., Kislov E.V., Paleev P.L., Malyshev A.V. Comprehensive use of substandard nephrite. *Bulletin of the Tomsk Polytechnic University. Geo Assets Engineering*. 2020;331(8):68–76. (In Russ.) https://doi.org/10.18799/24131830/2020/8/2769

20. Khudyakova L.I., Kislov E.V., Paleev P.L., Kotova I.Yu. Nephrite-bearing mining waste as a promising mineral additive in the production of new cement types. *Minerals*. 2020;10(5):394. https://doi.org/10.3390/min10050394

21. Liu Y., Zhang R., Zhang Zh., et al. Mineral inclusions and SHRIMP U-Pb dating of zircons from the Alamas nephrite and granodiorite: Implications for the genesis of a magnesian skarn deposit. *Lithos*. 2015;212–215:128–144. https://doi.org/10.1016/j.lithos.2014.11.002

22. Zhang X., Shi G., Zhang X., Gao G. Formation of the nephrite deposit with five mineral assemblage zones in the Central Western Kunlun Mountains, China. *Journal of Petrology*. 2022;63(11):egac117. https://doi.org/10.1093/petrology/egac117

23. Nangeelil K., Dimpfl P., Mamtimin M., et al. Preliminary study on forgery identification of Hetian Jade with Instrumental Neutron Activation Analysis. *Applied Radiation and Isotopes*. 2023;191:110535. https://doi.org/10.1016/j.apradiso.2022.110535

24. Liu Y., Deng J., Shi G.H., et al. Chemical Zone of Nephrite in Alamas, Xinjiang, China. *Resource Geology*. 2010;60(3):249–259. https://doi.org/10.1111/j.1751-3928.2010.00135.x

25. Liu Y., Deng J., Shi G., et al. Geochemistry and petrology of nephrite from Alamas, Xinjiang, NW China. *Journal of Asian Earth Sciences*. 2011;42(3):440–451. https://doi.org/10.1016/j.jseaes.2011.05.012

26. Jing Y., Liu Y. Genesis and mineralogical studies of zircons in the Alamas, Yurungkash and Karakash Rivers nephrite deposits, Western Kunlun, Xinjiang, China. *Ore Geology Reviews*. 2022;149:105087. https://doi.org/10.1016/j.oregeorev.2022.105087

27. Liu Y., Deng J., Shi G., Sun X., Yang L. Geochemistry and petrogenesis of placer nephrite from Hetian, Xinjiang, Northwest China. *Ore Geology Reviews*. 2011;41(1):122–132. https://doi.org/10.1016/j.oregeorev.2011.07.004

28. Liu Y., Zhang R.-Q., Maituohuti A., et al. SHRIMP U-Pb zircon ages, mineral compositions and geochemistry of placer nephrite in the Yurungkash and Karakash River deposits, West Kunlun, Xinjiang, northwest China: Implication for a Magnesium Skarn. *Ore Geology Reviews*. 2016;72(1):699–727. https://doi.org/10.1016/j.oregeorev.2015.08.023

29. Jiang Y., Shi G., Xu L., Li X. Mineralogy and geochemistry of nephrite jade from Yinggelike deposit, Altyn Tagh (Xinjiang, NW China). *Minerals*. 2020;10(5):418. https://doi.org/10.3390/min10050418

30. Liang H., Shi G., Yuan Y., et al. Polysynthetic twinning of diopsides in the Niewang and Tatliksu nephrite deposits, Xinjiang, China. *Minerals*. 2022;12(12):1575. https://doi.org/10.3390/min12121575

31. Gao K., Shi G., Wang M. et al. The Tashisayi nephrite deposit from South Altyn Tagh, Xinjiang, northwest China. *Geoscience Frontiers*. 2019;10(4):1597–1612. https://doi.org/10.1016/j.gsf.2018.10.008

32. Liu X., Gil G., Liu Y. Timing of formation and cause of coloration of brown nephrite from the Tiantai Deposit, South Altyn Tagh, northwestern China. *Ore Geology Reviews*. 2021;131:103972. https://doi.org/10.1016/j.oregeorev.2020.103972

33. Yu H.Y., Wang R.C., Guo J.C., et al. Color-inducing elements and mechanisms in nephrites from Golmud, Qinghai, NW China: Insights from spectroscopic and compositional analyses. *Journal of Mineralogical and Petrological Sciences*. 2016;111(5):313–325. https://doi.org/10.2465/jmps.151103

34. Yu H.Y., Wang R.C., Guo J.C., et al. Study of the minerogenetic mechanism and origin of Qinghai nephrite from Golmud, Qinghai, Northwest China. *Science China Earth Sciences*. 2016;59:1597–1609. https://doi.org/10.1007/s11430-015-0231-8

35. Gao S., Bai F., Heide G. Mineralogy, geochemistry and petrogenesis of nephrite from Tieli, China. *Ore Geology Reviews*. 2019;107:155–171. https://doi.org/10.1016/j.oregeorev.2019.02.016

36. Xu H., Bai F. Origin of the subduction-related Tieli nephrite deposit in Northeast China: Constraints from halogens, trace elements, and Sr isotopes in apatite group minerals. *Ore Geology Reviews*. 2022;142:104702. https://doi.org/10.1016/j.oregeorev.2022.10470

37. Xu H., Bai F., Jiang D. Geochemical characteristics and composition changes of tremolite at various stages in the mineralization process of nephrite from Tieli, Heilongjiang, Northeastern China. *Arabian Journal of Geosciences*. 2021;14:204. https://doi.org/10.1007/s12517-021-06578-6

38. Bai F., Li G., Lei J., Sun J. Mineralogy, geochemistry, and petrogenesis of nephrite from Panshi, Jilin, Northeast China. *Ore Geology Reviews*. 2019;115:103171. https://doi.org/10.1016/j.oregeorev.2019.103171

39. Zhang C., Yu X., Jiang T. Mineral association and graphite inclusions in nephrite jade from Liaoning, northeast China: Implications for metamorphic conditions and ore genesis. *Geoscience Frontiers*. 2019;10(2):425–437. https://doi.org/10.1016/j.gsf.2018.02.009

40. Zheng F., Liu Y., Zhang H.-Q. The petrogeochemistry and zircon U-Pb age of nephrite placer deposit in Xiuyan, Liaoning. *Rock and Mineral Analysis*. 2019;38(4):438–448. (In Chinese). https://doi.org/10.15898/j.cnki.11-2131/td.201807310089

41. Li P., Liao Z., Zhou Zh., Wu Q. Evidences from infrared and Raman spectra: Xiaomeiling is one reasonable provenance of nephrite materials used in Liangzhu Culture. *Spectrochimica Acta Part A: Molecular and Biomolecular Spectroscopy*. 2021;261:120012. https://doi.org/10.1016/j.saa.2021.120012

42. Li P., Liao Z., Zhou Zh. The residual geological information in Liangzhu jades: Implications for their provenance. *Proceedings of the Geologists' Association*. 2022;133(3):256–268. https://doi.org/10.1016/j.pgeola.2022.04.003

43. Chen D., Yang Y., Qiao B., et al. Integrated interpretation of pXRF data on ancient nephrite artifacts excavated from Tomb No. 1 in Yuehe Town, Henan Province, China. *Heritage Science*. 2022;10:1. https://doi.org/10.1186/s40494-021-00642-w

44. Ling X.-X., Schmädicke E., Li Q.-L., et al. Age determination of nephrite by in-situ SIMS U-Pb dating syngenetic titanite: A case study of the nephrite deposit from Luanchuan, Henan, China. *Lithos*. 2015;220–223:289–299. https://doi.org/10.1016/j.lithos.2015.02.019

45. Bai B., Du J., Li J., Jiang B. Mineralogy, geochemistry, and petrogenesis of green nephrite from Dahua, Guangxi, Southern China. *Ore Geology Reviews*. 2020;118:103362. https://doi.org/10.1016/j.oregeorev.2020.103362

46. Yin Z., Jiang C., Santosh M., et al. Nephrite jade from Guangxi province, China. *Gems and Gemology*. 2014;50(3):228–235. https://doi.org/10.5741/GEMS.50.3.228

47. Zhong Q., Liao Z., Qi L., Zhou Zh. Black nephrite jade from Guangxi, Southern China. *Gems and Gemology*. 2019;55(2):198–215. https://doi.org/10.5741/GEMS.55.2.198

48. Wang W., Liao Z., Zhou Z., et al. Gemmological and mineralogical characteristics of nephrite from Longxi, Sichuang Province. *Journal of Gems & Gemmology*. 2022;24(1):20–27. (In Chinese). https://doi.org/10.15964/j.cnki.027jgg. 2022.01.003

49. Wang L., Lin J.H., Ye T.P., et al. Discussing the coloration mechanism of Luodian Jade from Guizhou. *Open Access Library Journal*. 2020;7:e6364. https://doi.org/10.4236/oalib.1106364

50. Feng Y., He X., Jing Y. A new model for the formation of nephrite deposits: A case study of the Chuncheon nephrite deposit, South Korea. *Ore Geology Reviews*. 2022;141:104655. https://doi.org/10.1016/j.oregeorev.2021.104655

51. Yui T.-F., Kwon S.-T. Origin of a dolomite-related jade deposit at Chuncheon, Korea. *Economic Geology*. 2002;97(3):593–601. https://doi.org/10.2113/gsecongeo.97.3.593

52. Nichol D. Two contrasting nephrite jade types. *The Journal of Gemmology*. 2000;27(4):193–200.

53. Tan T.L., Ng N.N., Lim N.C. Studies on nephrite and jadeite jades by Fourier transform infarred (FTIR) and Raman spectroscopic techniques. *Cosmos*. 2013;9(1):47–56. https://doi.org/10.1142/S0219607713500031

54. Adamo I., Bocchio R. Nephrite jade from Val Malenco, Italy: Review and Update. *Gems and Gemology*. 2013;49(2):98–106. https://doi.org/10.5741/GEMS.49.2.98

55. Korybska-Sadło I., Gil G., Gunia P., et al. Raman and FTIR spectra of nephrites from the Złoty Stok and Jordanów Śląski (the Sudetes and Fore-Sudetic Block, SW Poland). *Journal of Molecular Structure*. 2018;1166:40–47. https://doi.org/10.1016/j.molstruc.2018.04.020

56. Gil G., Barnes J.D., Boschi C. Nephrite from Złoty stok (Sudetes, SW Poland): petrological, geochemical, and isotopic evidence for a dolomite-related origin. *The Canadian Mineralogist*. 2015;53:533–556. https://doi.org/10.3749/canmin.1500018

57. Gil G., Bagiński B., Gunia P., et al. Comparative Fe and Sr isotope study of nephrite deposits hosted in dolomitic marbles and serpentinites from the Sudetes, SW Poland: Implications for Fe-As-Au-bearing skarn formation and post-obduction evolution of the oceanic lithosphere. *Ore Geology Reviews*. 2020;118:103335. https://doi.org/10.1016/j.oregeorev.2020.103335

58. Platonov A.N., Taran M.N., Balitsky V.S. *The nature of the color of gems*. Moscow: Nedra Publ. House; 1984. 196 p. (In Russ.)

59. Sviridov D.T., Sviridova R.K., Smirnov Yu.F. *Optical spectra of transition metal ions in crystals*. Moscow: Nauka Publ. House; 1976. 266 p. (In Russ.)

Information about the authors

Evgeniy V. Kislov – Cand. Sci. (Geol. and Min.), Associate Professor, Leading Researcher, Dobretsov Geological Institute of Siberian Branch of the Russian Academy of Sciences, Ulan-Ude, Russian Federation; ORCID 0000-0003-2266-0942; e-mail evg-kislov@ya.ru

Liudmila I. Khudyakova – Dr. Sci. (Eng.), Leading Researcher, Baikal Institute of Nature Management of the Siberian Branch of the Russian Academy of Sciences, Ulan-Ude, Russian Federation; ORCID 0000-0003-1423-410X; e-mail lkhud@binm.ru

Anatoly G. Nikolaev – Cand. Sci. (Geol. and Min.), Associate Professor, Kazan (Volga Region) Federal University, Kazan, Russian Federation; ORCID 0000-0002-8082-6536, ResearcherID F-7024-2017

Received 24.01.2023
Revised 15.02.2023
Accepted 14.03.2023

MINING SCIENCE AND TECHNOLOGY (RUSSIA)
ГОРНЫЕ НАУКИ И ТЕХНОЛОГИИ
2023;8(3):207–214

eISSN 2500-0632
https://mst.misis.ru/

MINING ROCK PROPERTIES. ROCK MECHANICS AND GEOPHYSICS

Research paper

https://doi.org/10.17073/2500-0632-2023-04-105
UDC 536:24:622.413

Absolute heat sources as a method to check the accuracy of temperature prediction in underground structures within cryolithozone

A.F. Galkin[1] ✉, **V.Yu. Pankov**[2]

[1] *P.I. Melnikov Geocryology Institute, Siberian Branch of the Russian Academy of Sciences, Yakutsk, Russian Federation*
[2] *North-Eastern Federal University named after M.K. Ammosov, Yakutsk, Russian Federation*
✉ *afgalkin@mail.ru*

Abstract
Forecasting the thermal regime of mine workings and the surrounding rock mass is a necessary element of the design of underground structures in cryolithic zone. This is particularly necessary when substantiating and selecting reliable methods and means of rock supporting, in order to ensure safe operation of underground structures during the entire standard service life. Changes in the temperature of discontinuous permafrost rocks in the range of negative values (below the ice point in the rock) can lead to a decrease in their strength characteristics, and consequently to a decrease in the stability of workings. The aim of the research was to compare two ways of considering absolute heat sources (point sources and sources uniformly distributed along the length of a mine working) when forecasting the thermal regime in mine workings of underground structures. The dependencies used to determine temperature differences in various methods of considering absolute heat sources were established. For the sake of generality, the dependencies were produced in dimensionless (criterial) form. The variants were calculated, and the results are presented in the form of graphs. The aim is to visually present the influence of the method of heat sources when considering the accuracy of air temperature prediction in an underground facility. Key qualitative and quantitative features of the formation of thermal regime in workings at different methods of considering absolute heat sources were established. It was shown in particular that during the transition from a negative temperature in a working to a positive one, incorrect consideration of the action of absolute heat sources can lead to an almost 30 % (1.26 times) difference (i.e., error) in the calculated depth of thawing of discontinuous rocks.
It was also established that at a positive temperature, when the initial air temperature in a structure is more than 7.5 °C, there is no fundamental difference in engineering calculations results depending on the method of considering of absolute heat sources.

Keywords
underground structure, cryolithozone, safety, thermal regime, forecast, heat source, method of considering, temperature

For citation
Galkin A.F., Pankov V.Yu. Absolute heat sources as a method to check the accuracy of temperature prediction in underground structures within cryolithozone. *Mining Science and Technology* (*Russia*). 2023;8(3):207–214. https://doi.org/10.17073/2500-0632-2023-04-105

СВОЙСТВА ГОРНЫХ ПОРОД. ГЕОМЕХАНИКА И ГЕОФИЗИКА

Научная статья

Влияние способа учета абсолютных источников тепла на точность прогноза температуры в подземных сооружениях криолитозоны

А.Ф. Галкин[1] ✉, **В.Ю. Панков**[2]

[1] *Институт мерзлотоведения им. П.И. Мельникова СО РАН, г. Якутск, Российская Федерация*
[2] *Северо-Восточный федеральный университет им. М.К. Аммосова, г. Якутск, Российская Федерация*
✉ *afgalkin@mail.ru*

Аннотация
Прогноз теплового режима выработок и окружающего их массива горных пород является необходимым элементом проектирования подземных сооружений криолитозоны, в частности, при обосновании и выборе надежных способов и средств крепления породных обнажений, обеспечиваю-

щих безопасную эксплуатацию подземных сооружений в течение всего нормативного срока. Даже изменение температуры дисперсных мерзлых пород в диапазоне отрицательных значений (ниже температуры плавления льда в породе) приводит к уменьшению их прочностных характеристик, а следовательно, и к снижению устойчивости выработок. Целью исследований было сравнение двух способов учета абсолютных источников тепла (как точечных источников и как равномерно распределенных по длине выработки источников) при прогнозе теплового режима в горных выработках подземных сооружений. Получены расчетные зависимости для определения температурных отклонений при различных способах учета абсолютных источников. Для общности анализа расчётные зависимости получены в безразмерном (критериальном) виде. Проведены вариантные расчеты, результаты которых представлены в виде графиков, позволяющих наглядно оценить влияние способа учета источников тепла на точность прогноза температуры воздуха в подземном сооружении. Установлены основные качественные и количественные особенности формирования теплового режима в выработках при различных способах учета абсолютных источников тепла. В частности, показано, что при переходе от отрицательного теплового режима в выработке к положительному неправильный учет действия абсолютных источников тепла может привести к изменению глубины оттаивания дисперсных пород почти на 30 % (в 1,26 раза). В то же время установлено, что при положительном тепловом режиме для начальной температуры воздуха в сооружении больше 7,5 °С принципиальной разности для инженерных расчетов в способе учета абсолютных источников тепла нет.

Ключевые слова
подземное сооружение, криолитозона, безопасность, тепловой режим, прогноз, источник тепла, способ учета, температура

Для цитирования
Galkin A.F., Pankov V.Yu. Absolute heat sources as a method to check the accuracy of temperature prediction in underground structures within cryolithozone. *Mining Science and Technology* (*Russia*). 2023;8(3):207–214. https://doi.org/10.17073/2500-0632-2023-04-105

Introduction

The reliability and safety of engineering structures in cryolithozone (permafrost zone) are largely determined by climatic conditions, and the variability of the properties of soils and rocks under the influence of external factors, natural [1–3] and anthropogenic [4–6] ones. This applies to both aboveground [7–9] and underground engineering structures [10–12]. The scientific community, engaged in research of the processes of interaction between engineering structures and frozen soils, have already established that the main technical and technological parameters determining the safe operation of underground structures in the cryolithozone (both mining and non-mining related) directly depend on the thermal regime of workings during their construction [13–15] and operation [16–18]. First of all, this can be explained by the temperature dependence of the strength characteristics of most frozen sedimentary host rocks [19–21]. Even changes in the temperature of frozen rocks in the negative value range (below the ice point in the rock, $T \le T_{\mathrm{melt}}$) can lead to a decrease in their strength characteristics. This can consequently lead to a decrease in the stability of workings [22–24]. Many types of discontinuous rocks, such as ice-saturated sandstones, have zero strength at positive temperatures [13, 16, 17]. Therefore, predicting the thermal regime of mine workings and the surrounding rock mass is necessary for the design of underground structures in cryolithic zone. This is the case, in particular, when substantiating and selecting reliable methods and means of rock supporting, thus ensuring safe operation of underground structures during the entire standard service life [14, 25, 26]. The thermal regime of mines and underground structures is determined by the action of two groups of heat sources: absolute and relative [13, 17, 27]. In this case, it would be appropriate to present a qualitative characterization of the groups of these sources, as given by A.F. Voropaev [17]. "The first group includes absolute heat sources that release heat, and heat and air by the same value at the same amount of released heat regardless of the actual air temperature. The second group includes relative heat sources, heat transfer and heating of air due to temperature difference – temperature head". Relative heat sources include such sources as: the surface of mine workings; pipelines of various purposes; and transported minerals, inter alia. The group of absolute heat sources includes: energy losses in power grids; lighting devices; working machines and mechanisms, among others. A sufficient number of scientific studies consider various aspects of the influence of absolute heat sources [28–30], including diesel vehicles [29, 31, 32], on the formation of the thermal regime in underground structures of various purposes. In the construction of mathematical models for predicting the thermal regime in underground structures/workings, absolute heat sources as a rule are considered either as point sources, or as evenly distributed along the length of a working.

The aim of the research was to compare two ways of considering absolute heat release sources when predicting the thermal regime of mine workings in underground structures: a) as point sources; b) as sources uniformly distributed along the length of a working.

Research techniques

Taking into account the dependencies [17, 27, 33] previously obtained for the prediction of air temperature in mine workings of various purposes using the concept of unsteady heat transfer coefficient [34–36], the initial formulas for calculations can be written in the following form:

Temperature difference at the end point with different methods of considering absolute heat sources

$$\Delta t = t_{k1} - t_{k2} = Q_2[Z(Kr+1)-1], \quad Z = \exp(-Kr). \tag{1}$$

Temperature at the end of a working when a heat source is distributed along the whole length

$$t_{k1} = T_e + (t_0 - T_e + Q_1)Z. \tag{2}$$

Temperature at the end of a working under the action of a point heat source

$$t_{k2} = T_e + Q_2 + (t_0 - T_e + Q_2)Z. \tag{3}$$

The parameters included in formulas (1)–(3) are determined using the following dependencies:

$$Q_1 = \frac{q}{GC_p}; \quad Q_2 = \frac{q}{FK_\tau}; \quad \mathrm{Kr} = \frac{FK_\tau}{GC_p}, \tag{4}$$

where t_{k1}, t_{k2} – air temperature in the end of a mine working at the distributed (1) and point (2) heat source, °C; T_e – natural temperature of rocks, °C; t_0 – initial (at the entrance to a working) air temperature, °C; q – heat source power, W; G – mass flow rate of air in a working, kg/s; C_p – specific heat capacity of moist air, J/kgK; F – a working surface area, m²; K_τ – unsteady heat transfer coefficient, W/m²K; Kr – Kremnev criterion.

An unsteady heat transfer coefficient for mine workings of different symmetry can be determined using expressions familiar to mining thermal physics and given in [17, 27].

The formula for calculating the relative error that can arise in temperature prediction is as follows:

$$e = \left(1 - \frac{t_{k1}}{t_{k2}}\right) 100\ \%. \tag{5}$$

Following the known postulates for engineering calculations, we assume that if the condition $e \le 10\ \%$ is met, then the method of considering absolute heat sources in mine workings when predicting thermal regime is not crucial.

Findings Discussion

Analysis of the dependencies shows that, when using the first method (a point source), we formally change the initial temperature of the air supplied into a working. Considering absolute sources as uniformly distributed along the length of a structure (the second method) in the mathematical model is equivalent to a change in the natural temperature of rocks. The objective is to assess the degree of influence of the natural rock temperature and the initial air temperature in the structure on the accuracy of the temperature prediction at the end of a working. A simple comparison of formulas (2) and (3) allows an obvious conclusion to be drawn: the equality of temperature values at the end of a working, using different methods of considering the action of absolute sources, is possible only if the source power is zero. Therefore, the lower the source power, the lower the unknown difference in air temperature at the end of a working. Quantitative analysis should answer the following question: "At what power of absolute sources does the method of considering them in temperature predictions result in an error greater than the acceptable error in engineering practice?" In order to answer this question using the above formulas, variant calculations were carried out. The results are presented as 2D and 3D graphs in Figs. 1–4. Fig. 1 shows the temperature difference at the end of the calculation section of a working. This is taken as a function of Kremnev criterion Kr at different methods of considering absolute heat sources and at different reduced power of a source Q2.

The graphs show that the temperature difference in the considered range of initial data does not exceed 1.5 °C. Note that the following pattern is observed: the lower the source power and the value of Kremnev criterion, the lower the difference in air temperatures at the end of a working. Thus, the dependence of the final result on the method of considering absolute heat sources becomes weaker with lowering the source power.

Fig. 2 presents 3D graphs of the temperature difference at the end of the calculation section of a working. This is a function of Kremnev criterion Kr and reduced power of a source Q2 at different methods of considering absolute heat sources.

The graphs in the Figure show that when we consider a heat source as distributed along the length, we always underestimate the air temperature at the end of a mine working. Note that this does not depend on the value of power of the sources Q2 operating in a working, or the conditions of heat exchange of air with rocks. Thus, the error cannot be attributed to the calculation features (design margin). The absolute value of the temperature difference (Fig. 3) is relatively low on the whole when considered (typical for underground structures in cryolithozone) range of variation of the initial parameters of the thermal regime simulation.

The graphs show that for the characteristic operating conditions of underground structures in cryolithic zone, the temperature difference does not exceed 1.6 °C. This value could be considered quite acceptable, since it is within the accuracy of the engineering forecast. However, it should be notes that this difference may not always be attributed to the calculation features. For example, when selecting the method and means for working supports, one of the key design parameters is the depth of rock thawing. Thawing depth and air temperature are related to

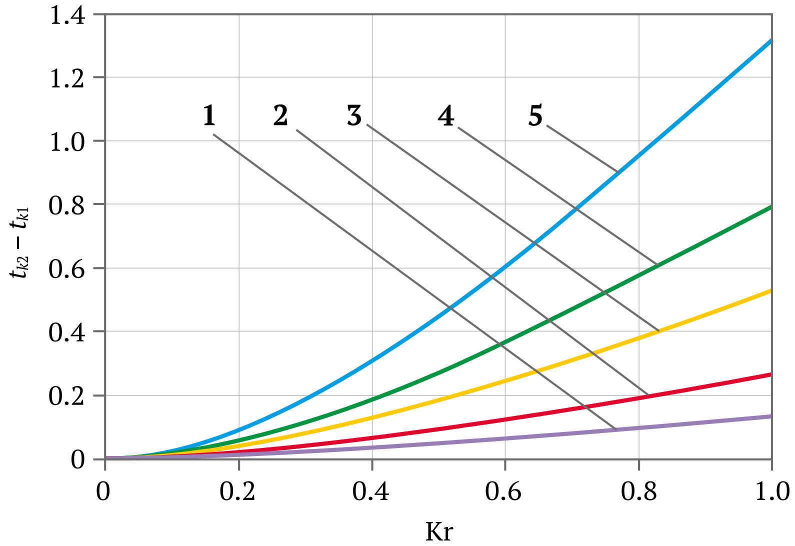

Fig. 1. The temperature difference (°C) at the end of the calculation section of a working as a function of Kremnev criterion Kr at different methods of considering absolute heat sources and at different reduced power of a source Q2: *1* – 0.5; *2* – 1.0; *3* – 2.0; *4* – 3.0; *5* – 5.0

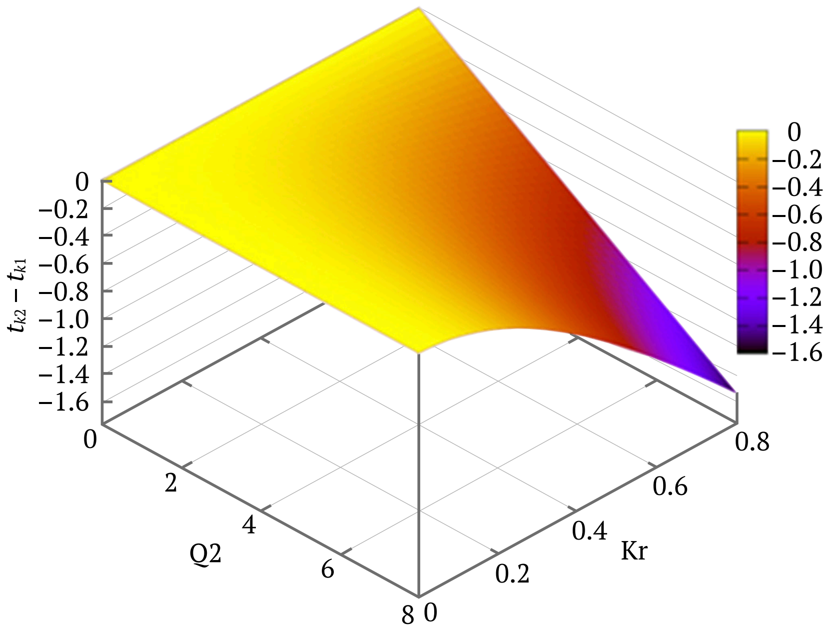

Fig. 2. The difference in air temperature (°C) at the end of the calculation section of a working as a function of Kremnev criterion Kr and reduced power of a source Q2 at different methods of considering absolute heat sources

each other by a relationship close to a quadratic. For example, when temperature positive-going zero crossing in an underground structure due to the action of absolute heat sources happens, the change in air temperature in the structure by 1.6 °C (all other conditions being equal) will lead to an increase in the thawing depth by 1.26 times. This exceeds the allowable value of 10 % in engineering practice. Therefore, in such cases, it is necessary to rely on the calculated value obtained by modeling absolute sources as point sources. In this case, the choice of the method of considering sources is decisive for obtaining a correct and reliable final result of the calculation of the design parameter. Naturally, everything referred to above depends on the initial air temperature in an underground structure. Fig. 4 shows the area of initial temperatures, at which the error in calculating the thawing depth will not exceed the permissible value (highlighted in blue in the figure).

If the initial air temperature in a structure is less than or equal to about 7.5 °C, then the method of considering absolute sources is important for the accuracy of the temperature prediction. Otherwise, the method is not important.

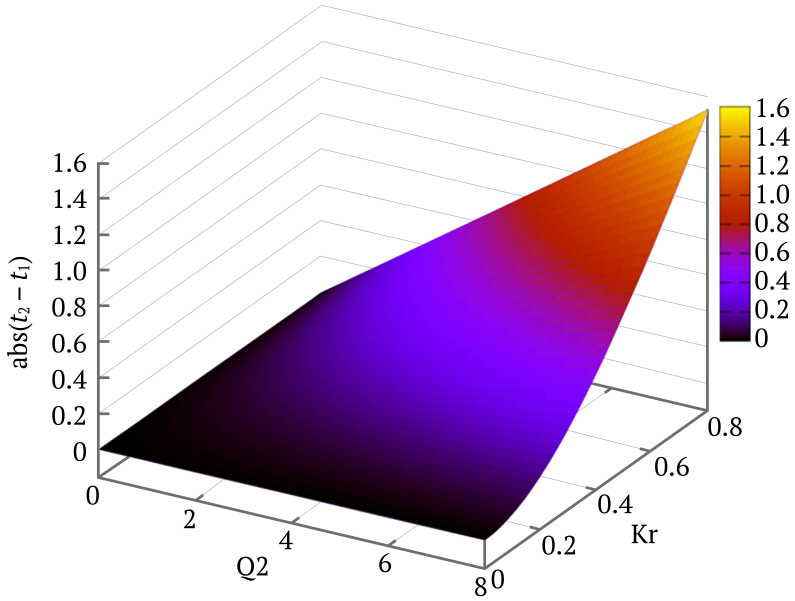

Fig. 3. Absolute value of the air temperature difference (°C) at the end of the calculated section of a working as a function of Kremnev criterion Kr and reduced power of a heat source Q2

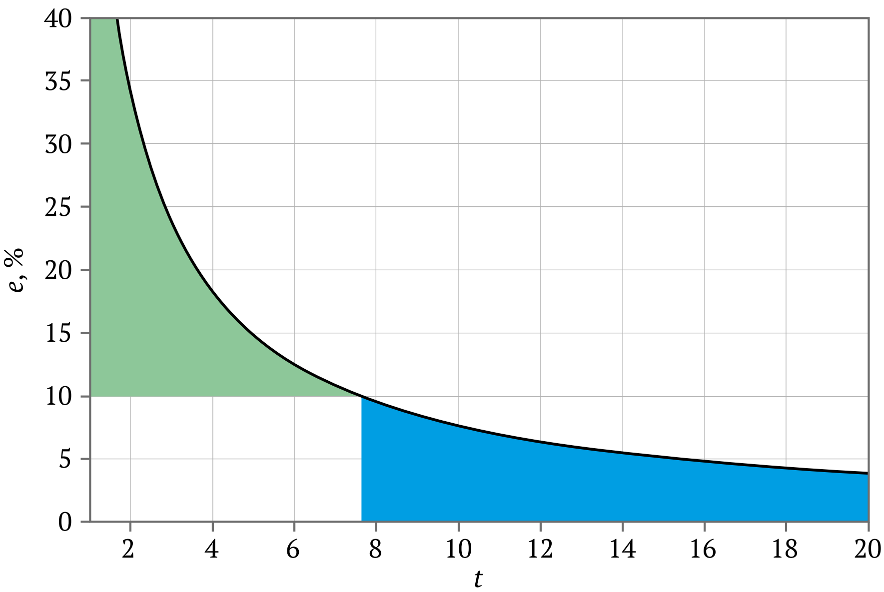

Fig. 4. Error in determining the depth of thawing of frozen rocks around an underground structure as a function of initial air temperature t, °C

Conclusion

Key conclusions, practical significance of the study, and the area of future research. Qualitative and quantitative assessment was undertaken of the effect of the method of considering absolute heat sources on predicted air temperature in mine workings when forecasting the thermal regime of underground structures in cryolithozone. Two possible ways were considered of taking into account absolute heat sources in the mathematical modeling of heat processes in mine workings: point sources, and sources uniformly distributed along the length of a working. The study presents formulae for determining the air temperature at the end of a mine working depending on the method of considering absolute heat sources. For the sake of generality of the analysis, the calculation formulas are presented in the form of functional dependences on Kremnev criterion and the reduced total power of absolute heat sources. Qualitative analysis of the dependencies obtained showed that using the first method of considering (as a point source) is equivalent to the change in the initial temperature of the air supplied into a working. Considering absolute sources as uniformly distributed along the length of a structure (the second method of considering) in the mathematical model is equivalent to a change in the natural temperature of rocks. Quantitative analysis showed, in particular, that the lower the source power and the value of Kremnev criterion, the smaller the dependence of the final result (air temperature at the end of a mine working) on the method of taking into account absolute heat sources when predicting thermal regime. As an example, we considered the influence of the method of absolute sources on the accuracy of predicting the depth of thawing of discontinuous frozen rocks around a working. It was shown that during the transition from a negative temperature in a working to a positive one, incorrect consideration of the action of absolute heat sources can lead to an almost 30% (1.26 times) difference (i.e., error) in the calculated depth of thawing of discontinuous rocks. This can produce a significant impact on the selection of support parameters of mine workings driven in discontinuous frozen rocks, which (the selection) directly depends on the temperature regime of the rocks. It was also found that at a positive temperature, when the initial air temperature in a structure is more than 7.5 °C, there is no fundamental difference in engineering calculations results depending on the method of considering absolute heat sources. On the whole, it was found that for the characteristic conditions of construction and operation of underground structures in cryolithozone, such as underground gold mines, there is no fundamental difference in the methods of considering absolute heat sources when predicting the thermal regime. The differences in the values of air temperature at the end of a mine working obtained using different methods of consideration, as a rule, do not exceed the values allowed in engineering practice.

References

1. Zhirkov A., Permyakov P., Wen Z., Kirillin A. Influence of rainfall changes on the temperature regime of permafrost in Central Yakutia. *Land*. 2021;10(11):1230. https://doi.org/10.3390/land10111230

2. Stanilovskaya Yu.V., Merzlyakov V.P., Sergeev D.O., Khimenkov A.N. Ice wedge hazard assessment for linear objects. *Geoekologiya. Inzheneraya Geologiya, Gidrogeologiya, Geokriologiya*. 2014;(4):367–378. (In Russ.)

3. Eppelbaum L.V., Kutasov I.M. Well drilling in permafrost regions: Dynamics of the thawed zone. *Polar Research*. 2019;38(2):3351. https://doi.org/10.33265/polar.v38.3351

4. Gao Q., Wen Z., Feng W. et al. Effect of a ventilated open structure on the stability of bored piles in permafrost regions of the Tibetan plateau. *Cold Regions Science and Technology*. 2020;178:103–116. https://doi.org/10.1016/j.coldregions.2020.103116

5. Zheleznyak M., Kirillin A., Zhirkov A. et al. Permafrost distribution and temperature in the Elkon Horst, Russia. *Sciences in Cold and Arid Regions*. 2021;13(2):107–122. https://doi.org/10.3724/SP.J.1226.2021.20027

6. Wen Z., Wang D., Ma W. et al. Thermal interaction between a thermokarst lake and a nearby embankment in permafrost regions. *Cold Regions Science and Technology*. 2018;155:214–224. https://doi.org/10.1016/j.coldregions.2018.08.010

7. Permyakov P.P., Zhirkov A.F., Varlamov S.P. Numerical modeling of railway embankment deformations in permafrost regions, Central Yakutia. In: Petriaev A., Konon A. (eds.) *Transportation Soil Engineering in Cold Regions, Volume 2. Lecture Notes in Civil Engineering, Vol. 50*. Singapore: Springer; 2020. Pp. 93–103. https://doi.org/10.1007/978-981-15-0454-9_11

8. Zhirkov A., Zheleznyak M., Shats M., Sivtsev M. Numerical simulation change permafrost conditions of the runway airport Olekminsk. *Mine Surveying and Subsurface Use*. 2021;(5):22–32. (In Russ.)

9. Permyakov P.P., Zhirkov A.F., Zheleznyak M.N. Account for the process of underground condensation in modeling heat and moisture exchange in frozen soils. *Journal of Engineering Physics and Thermophysics*.

2021;94(5):1232–1241. https://doi.org/10.1007/s10891-021-02404-8 (Orig. ver.: Permyakov P.P., Zhirkov A.F., Zheleznyak M.N. Account for the process of underground condensation in modeling heat and moisture exchange in frozen soils. *Inzhenerno-Fizicheskiy Zhurnal*. 2021;94(5):1260–1270. (In Russ.))

10. Kutasov I.M., Eppelbaum L.V. The effect of thermal properties changing (at ice-water transition) on the radius of permafrost thawing. *Cold Regions Science and Technology*. 2018;151:156–158.

11. Zheleznyak M.N., Shatz M.M. Teplofizical conditions of diamond deposit of the Aikhal (Yakutia). *Nedropol'zovaniye XXI Vek*. 2022;(1):98–103. (In Russ.) URL: https://nedra21.ru/archive/160/2864/

12. Nikolaeva M.V., Struchkova G.P. Forecasting the thermal interaction of underground pipeline with ice grounds. *Tekhnologii Nefti i Gaza*. 2018;(4):56–60. (In Russ.)

13. Dyadkin Yu.D. *Fundamentals of mining thermal physics*. Moscow: Nedra Publ.; 1968. 256 p. (In Russ.)

14. Skuba V.N. *Study of mine workings stability in permafrost conditions*. Novosibirsk: Nauka Publ.; 1974. 118 p. (In Russ.)

15. Sherstov V.A. *Improving stability of mine workings at placer mines in the North*. Novosibirsk: Nauka Publ.; 1980. 56 p. (In Russ.)

16. Kuzmin G.P. *Underground structures in cryolithozone*. Novosibirsk: Nauka Publ.; 2002. 176 p. (In Russ.)

17. Voropaev A.F. *Theory of heat exchange of mine air and rocks in deep mines*. Moscow: Nedra Publ.; 1968. 249 p. (In Russ.)

18. Vernigor V.M., Morozov K.V., Bobrovnikov V.N. On approaches to designing of thermal regime at ore mines under permafrost conditions. *Journal of Mining Institute*. 2013;205:139–140. (In Russ.) URL: https://pmi.spmi.ru/index.php/pmi/article/view/5508?setLocale=en_US

19. Zhang S., Teng J., He Z. et al. Canopy effect caused by vapour transfer in covered freezing soils. *Géotechnique*. 2016;66(11):927–940. https://doi.org/10.1680/jgeot.16.P.016

20. Teng J., Shan F., He Z. et al. Experimental study of ice accumulation in unsaturated clean sand. *Géotechnique*. 2019;69(3):251–259. https://doi.org/10.1680/jgeot.17.P.208

21. Xu G., Qi J., Wu W. Temperature Effect on the compressive strength of frozen soils: a review. recent advances in geotechnical research. In: Wu, W. (eds.) *Recent Advances in Geotechnical Research. Springer Series in Geomechanics and Geoengineering*. Springer, Cham; 2019. https://doi.org/10.1007/978-3-319-89671-7_19

22. Niu F., Li A., Luo J. et al. Soil moisture, ground temperatures, and deformation of a high-speed railway embankment in Northeast China. *Cold Regions Science and Technology*. 2017;133:7–14. https://doi.org/10.1016/j.coldregions.2016.10.007

23. Khimenkov A.N., Gagarin V.E. Approaches to the study of deformations in permafrost soils. *Arctic and Antarctica*. 2022;(2):36–65. https://doi.org/10.7256/2453-8922.2022.2.38229

24. Vakhrin I.S., Kuzmin G.P., Spektr V.V. Haw deformation characteristics of undisturbed soils. *Advances in Current Natural Sciences*. 2020;(8):37–42. (In Russ.) https://doi.org/10.17513/use.37455

25. Galkin A.F. Increase of stability of mine workings in the permafrost zone. *Journal of Mining Institute*. 2014;207:99–102. (In Russ.) URL: https://pmi.spmi.ru/index.php/pmi/article/view/5392

26. Galkin A.F., Pankov V.Yu. Formation of thermal regime in a permafrost area mine. In: Beskopylny A., Shamtsyan M. (eds) *XIV International Scientific Conference "INTERAGROMASH 2021". Lecture Notes in Networks and Systems, Vol. 247.* Springer, Cham; 2022. Pp. 205–213. https://doi.org/10.1007/978-3-030-80946-1_21

27. Shcherban A.N., Kremnev O.A. *Scientific basis for calculating and regulating thermal regime of deep mines*. Kyiv: Academy of Sciences of the Ukrainian SSR; 1959. 430 p. (In Russ.)

28. Kazakov B., Zaytsev A., Shalimov A. Influence of backfill operations on the formation of thermal conditions of mine workings in OJSC MMC "Norilsk Nickel". *Bulletin of the Perm National Research Polytechnic University. Geology. Oil and Gas and Mining*. 2012;(2):110–114. (In Russ.)

29. Kurilko A.S., Khokholov Yu.A., Soloviev D.E. Features of formation of temperature conditions in placer mines equipped with self-propelled machines in permafrost zone. *Gornyi Zhurnal*. 2015;(4):29–32. (In Russ.) https://doi.org/10.17580/gzh.2015.04.06

30. Kazakov B.P., Zaitsev A.V. Study of the formation of thermal regimes in deep mines. *Bulletin of the Perm National Research Polytechnic University. Geology. Oil and Gas and Mining*. 2014;(10):91–97. (In Russ.)

31. Galkin A.F., Dormidontov A.V., Kurta I.V., Korotkova K.B. Influence of diesel vehicles on the temperature regime of mine workings. *Estestvennye i Tekhnicheskie Nauki*. 2018;(5):84–86. (In Russ.)

32. Galkin A., Pankov V.Y., Fedorov Y.V. Temperature Change in the Chambers of Underground Structures when operating Diesel Units. *Security Issues*. 2022;(4):27–33. https://doi.org/10.25136/2409-7543.2022.4.38938

33. Chernyak V.P., Shcherban A.N. Methods for predicting thermal regime of deep mines. *Fiziko-Texhnicheskiye Problemy Razrabbotki Poleznykh Iskopaemykh*. 1977;(2):88–92 (In Russ.)

34. Shcherban A.N., Chernyak V.P., Braicheva N.A. Solution of a system of differential equations with variable coefficients to calculate the temperature of mine air. *Doklady Akademii nauk Ukrainskoy SSR. Seriya A: Fiziko-Matematicheskie i Tekhnicheskie Nauki*. 1975;(9):843–847 (In Russ.)

35. Dobryansky Yu.P. *Computations of heat and humidity regimes of underground workings*. Kyiv: Naukova Dumka Publ.; 1991. 122 p. (In Russ.)

36. Galkin A.F., Pankov V.Yu. Forecasting of thermal regime in an oil mine. In: Mottaeva A. (eds.) *Technological Advancements in Construction. Lecture Notes in Civil Engineering, Vol. 180.* Springer, Cham; 2022. Pp. 39–46. https://doi.org/10.1007/978-3-030-83917-8_4

Information about the authors

Alexander F. Galkin – Dr. Sci. (Eng.), Chief Researcher of the Laboratory of Geothermal Permafrost, Melnikov Permafrost Institute of the Siberian Branch of the Russian Academy of Science, Yakutsk, Russian Federation; ORCID 0000-0002-5924-876X, Scopus ID 56559565600; e-mail afgalkin@mail.ru

Vladimir Yu. Pankov – Cand. Sci. (Geol. and Miner.), Associate Professor of the Department of Automobile Roads and Airfields, M.K. Ammosov North-Eastern Federal University, Yakutsk, Russian Federation; ORCID 0000-0003-4933-0265, Scopus ID 57216812632; e-mail pankov1956@inbox.ru

Received 01.04.2023
Revised 19.06.2023
Accepted 20.06.2023

BENEFICIATION AND PROCESSING OF NATURAL AND TECHNOGENIC RAW MATERIALS

Research paper

https://doi.org/10.17073/2500-0632-2023-04-112
UDK 622.7

Enrichment of Algerian kaolin using froth flotation method

M. Laraba ✉
Echahid Cheikh Larbi Tebessi University, Tébessa, Algeria
✉ *larabamd@univ-tebessa.dz*

Abstract

The objective of this research is to study the removal of coloring impurities from Algerian kaolin ore (Tamazert kaolin, TK) located in the eastern region of Algeria, utilizing froth flotation process. The results obtained from XRF, SEM, and XRD characterization demonstrate that this local material is an alumino-silicate containing kaolinite, along with impurities such as Fe_2O_3 (> 2.7 % by weight) and TiO_2 (0.28 % by weight) which contribute to its coloring. After homogenization, crushing and milling, several froth flotation tests were conducted on TK. The results revealed that Tamazert kaolin exhibits favorable performance with froth flotation, in order to improve its properties. Based on the results obtained, it can be concluded that all fractions can be treated effectively using froth flotation with an optimal mass yield (weight recovery) of 79.84 % in concentrate for the fraction of 20–40 μm. Iron and titanium, the main coloring impurities in Tamazert kaolin, were reduced from 2.7 % to 0.08 % by weight for Fe_2O_3 in the fraction 20-40 μm, and from 0.28 % to 0.04 % by weight for TiO_2 in the same fraction, as determined by the optimum test. The significant reduction in coloring impurities (Fe_2O_3 and TiO_2) achieved through the flotation process confirms that iron is present in a free state in Tamazert kaolin. It can be ultimately confirmed that the froth flotation process can be a potentially effective process to improve the quality of Tamazert kaolin ore by removing Fe_2O_3 and TiO_2 with satisfactory results which meet the requirements of local companies.

Keywords

Tamazert kaolin, froth flotation, coloring impurities, Fe_2O_3, TiO_2

Acknowledgements

The author expresses his gratitude to Professor Juan Maria Menendez-Aguado at Mining Exploitation & Prospecting Dept., Mineral Raw Processing Material Laboratory, Polytechnic School of Mieres, University of Oviedo, Asturias, Spain, for the technical support of this research work.

For citation

Laraba M. Enrichment of Algerian kaolin using froth flotation method. *Mining Science and Technology* (*Russia*). 2023;8(3):215–222. https://doi.org/10.17073/2500-0632-2023-04-112

ОБОГАЩЕНИЕ, ПЕРЕРАБОТКА МИНЕРАЛЬНОГО И ТЕХНОГЕННОГО СЫРЬЯ

Научная статья

Обогащение каолиновой руды месторождения Тамазерт (Алжир) методом пенной флотации

М. Лараба ✉
Университет Эхахида Шейха Ларби Тебеси, г. Тебесса, Алжир
✉ *larabamd@univ-tebessa.dz*

Аннотация

Целью данного исследования является изучение процесса удаления окрашивающих примесей из каолиновой руды месторождения Тамазерт (тамазертский каолин, ТК), расположенного в восточном регионе Алжира, с использованием процесса пенной флотации. Исследования методами рентгенофлуоресцентной спектрометрии, сканирующей растровой электронной микроскопии и рентгенофазового анализа показали, что данный местный материал представляет собой алюмосиликат, содержащий каолинит, а также примеси Fe_2O_3 (> 2,7 % по весу) и TiO_2 (0,28 % по весу), которые способствуют его окрашиванию. После гомогенизации, дробления и измельчения ТК был подвергнут серии испытаний по пенной флотации. Результаты показали, что тамазертский каолин приобретает благоприятные характеристики после применения пенной флотации для улучшения его свойств. На основании полученных результатов можно сделать вывод, что все фракции могут быть эффективно обогащены методом пенной флотации с оптимальным массовым выходом по весу (извлечением по весу) 79,84 % в концентрат для фракции 20–40 мкм. Содержания железа и титана, являющихся основными окрашивающими примесями в тамазертском каолине, были снижены посредством флотационной обработки с 2,7 до 0,08 % по весу для Fe_2O_3 во фракции 20–40 мкм и с 0,28 до 0,04 % по весу для TiO_2 в той же фракции, что было показано в оптимальном испытании. Значительное снижение содержаний окрашивающих примесей (Fe_2O_3 и TiO_2), достигнутое в процессе флотации, подтверждает, что железо присутствует в тамазертском каолине в свободном состоянии. В итоге можно утверждать, что процесс пенной флотации может быть потенциально эффективным способом улучшения качества каолиновой руды Тамазерта путем удаления Fe_2O_3 и TiO_2 с удовлетворительными результатами, отвечающими требованиям местных компаний.

Ключевые слова
тамазертский каолин, пенная флотация, окрашивающие примеси, Fe_2O_3, TiO_2

Благодарности
Автор выражает благодарность профессору Хуану Марии Менендес-Агуадо из отдела горных работ и разведки лаборатории обогащения полезных ископаемых Политехнического института Миереса Университета Овьедо, Астурия, Испания, за техническую поддержку данной исследовательской работы.

Для цитирования
Laraba M. Enrichment of Algerian kaolin using froth flotation method. *Mining Science and Technology* (*Russia*). 2023;8(3):215–222. https://doi.org/10.17073/2500-0632-2023-04-112

Introduction

Kaolin is a finely granulated rock, usually white and chemically inert. It is widely used in many industrial fields [1, 2] due to its favorable properties such as natural whiteness, fine particle size, plasticity, non-abrasiveness and chemical stability. The main impurities associated with commercial kaolin are quartz, feldspar, muscovite, biotite, titanium oxides and iron oxides or hydroxides, such as goethite, hematite and magnetite [3, 4].

There are many techniques for the beneficiation of kaolin ore. These include selective flocculation, magnetic separation, bleaching and flotation to remove colored impurities. The presence of iron oxides in kaolin has a deleterious effect on the color of the clay which declines in brightness with increasing iron content [2, 5, 6].

Flotation is undoubtedly the most important and versatile mineral separation technique, and both its use and application are continually being expanded to treat greater tonnages and to cover new areas [7].

Flotation is a separation process which exploits natural and induced differences in surface properties of the minerals, whether the surface is easily wetted by water, i.e. hydrophilic, or repels water, i.e. hydrophobic. If hydrophobic, the mineral particle can attach to air bubbles and be floated. The system is complex, involving three phases (solids, water, and air) and the interaction of chemical and physical variables [7].

The success of flotation processes is dependent primarily on the tendency of surface-active species to concentrate at the water-fluid interface, and on their capability to make selected non-surface-active materials hydrophobic by means of adsorption or association [8]

Froth flotation is the dominating mineral beneficiation technique and has achieved great commercial success [9]. In froth flotation, first a pulp of crushed and ground particles in water is conditioned with the desired flotation reagents including pH modifiers and surfactants. Then it is agitated in a cell in the presence of air sucked or fed into the impeller zone where the air is well dispersed due to intense agitation in that zone. The air bubbles collide with particles and are attached to those that are hydrophobic or have acquired hydrophobicity. The bubble-particle aggregates rise to the top of the cell and are removed by skimming [8].

In froth flotation, the parameters that can affect the efficiency of the separation are as follows [10]: the nature of the ore, dose of reagents, particle size, pulp density, conditioning time, pH...etc.). The optimum size range of froth flotation varies with the flotation process parameters and flotation machine types. Too coarse or fine sizes are not suitable for flotation, thus, the suitable flotation size is subject to upper and lower limits [11].

Flotation is a process used for the removal of TiO_2, especially when this mineral is colored by iron [12].

Kaolinite is hydrophilic. Thus with the addition of a small amount of chemical dispersant to negate the edge charges due to broken bonds, it will disperse readily in water. Ionic and/or polar non-ionic surfactants can be applied to the surfaces of the kaolinite to modify them to produce particles which have hydrophobic ororganophilic characteristics [13].

Flotation [13–15] is also used to improve the whiteness of kaolin intended for the paper industry.

The purpose of the present study is to improve (if possible) the quality of kaolin ore from the Tamazert deposit (Fig. 1) using the froth flotation technique based on the recovery of iron. A consequent objective is to improve the whiteness and the brightness level wished by the most industrial applications.

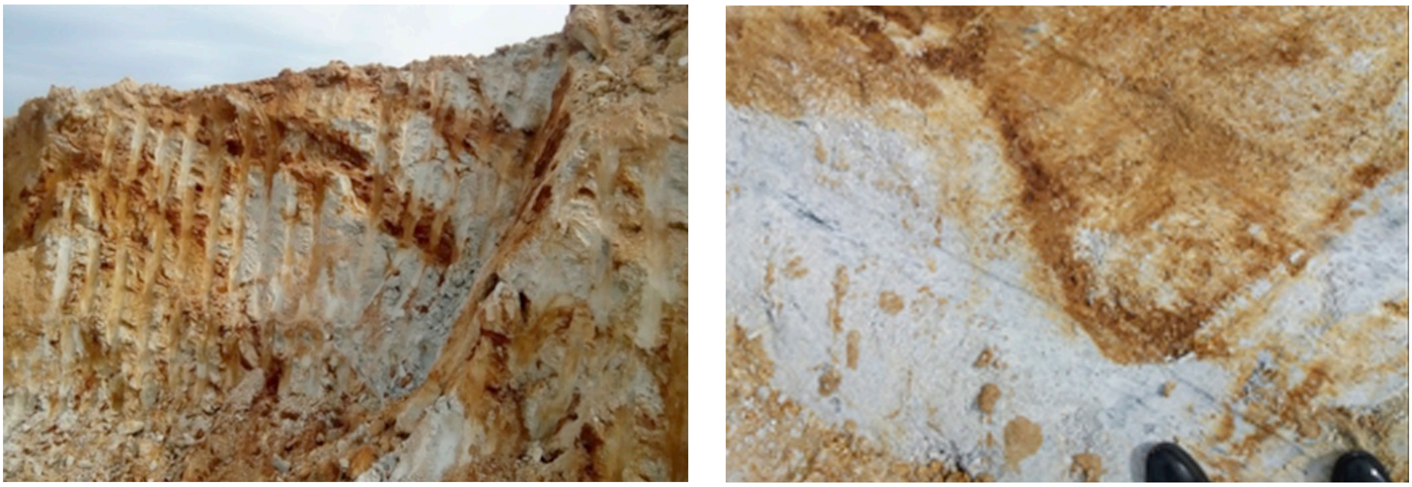

Fig. 1. Kaolin deposit of Tamazert

Materials and experimental methods

Characterization of Tamazert kaolin

In this study, the representative sample of kaolin ore was collected from Tamazert mine situated in Jijel city, East of Algeria and studied using X-Ray Fluorescence (XRF), X Ray Diffraction (XRD) and Scanning Electron Microscope (SEM) coupled with EDX.

The X-Ray Fluorescence (XRF) was realized with a Thermo Niton XL3t XRF Analyzer. The Scanning Electron Microscopy (SEM-EDX) was performed using JEOL JSM-5600. The surface of the thin section of sample was metallized (Au). The X-ray diffraction (XRD) was performed using PHILIPS-X'Pert MPD System diffractometer equipped with Cu-Kα (λ = 1.54 Å) radiation which was generated at 40mA. 45kV generator settings were performed to characterize the kaolin sample.

Scanning electron microscopy (SEM) was used to observe the morphology of Tamazert kaolin. The XRD was used to determine the mineralogical composition, while the XRF was used to determine the chemical composition.

Used Materials

The samples were milled using Retsch RS 100 laboratory miller, and then sieved to obtain five fractions: (0–20, 20–40, 40–80, 80–100 and 100–120 μm). For the test, the most commonly used materials are:

Flotation cell (KHD HUMBOLDT WEDAG AG) with a volume of the tank is 1.5 liters), pH-meter, Electronic balance, Magnetic agitator and Oven.

Used reagents

Most minerals are not water-repellent in their natural state and flotation reagents must be added to the pulp. The most important reagents are collectors which adsorb on mineral surfaces, rendering them hydrophobic and facilitating bubble attachment. Regulators are used to control the flotation process. These either activate or depress mineral attachment to air bubbles and are also used to control particle dispersion and the pH of the system. Frothers enable producing fine bubbles required to increase collision rates and allow maintaining a reasonably stable froth [7]. The chemical reagents used to carry out the flotation tests are presented in Table 1. All reagents were supplied by the laboratory of mineral processing, polytechnic school on Mieres, university of Oviedo, Spain.

Table 1

Used reagents in froth flotation of TK

Reagent	Formula	Role
Oleic acid	$C_{18}H_{34}O_2$	Collector
Methyl Isobutyl Carbinol (MIBC)	$C_6H_{14}O$	Frother
Sodium Metasilicate (pentahydrate)	$Na_2SiO_3 \cdot 5H_2O$ $Na_2SiO \cdot 5H_2O$	Depressor
Kerosene	$C_{10}H_{22}$	Activator
Sodium Hydroxide	NaOH	pH regulator

Experimental procedure of flotation

Each kaolin sample powder (**250 g**) was introduced in the flotation cell with 1000 g (1L) of water to form a pulp (slurry) which contains 25% of solid by weight. The diluted Sodium Hydroxide was added prudently to adjust the flotation pulp at 9.5. The machine is left running and 9 ml of Sodium Meta-Silicate added for about 5 minutes, then 4 droplets (≈0.84 g) of Kerosene to render our useful mineral (kaolin) hydrophobic for duration of 2 minutes. 13 droplets of Oleic

Acid (≈0.338 g) are carefully added to the cell and conditioned for 5 minutes; Oleic Acid plays the role of a collector. Ultimately, 3 droplets of Methyl Isobutyl Carbinol (MIBC) are added and the suspension was conditioned for 2 minutes. Then the air tap is opened to create the foam (air bubbles) required for flotation (Fernando Pita, 2017). This operation is known as bubbling. All tests were performed at room temperature and the flotation machine was adjusted to a rotational speed of 450 rpm for the all tests. Flotation tests were carried out in a KHD HUMBOLDT WEDAG AG flotation machine.

The zeta-potential of kaolinite is negative in a wide range of pH values and kaolin can be floated by amine collectors in acidic and alkaline medium [16–18]. The dried concentrates and tailings were analyzed. The results obtained are used to calculate grade, yields and recovery rates.

The concentrates and tailing obtained after the flotation operations were dried in an oven at 105°C during 24 hours. All these steps are summarized in Fig. 2.

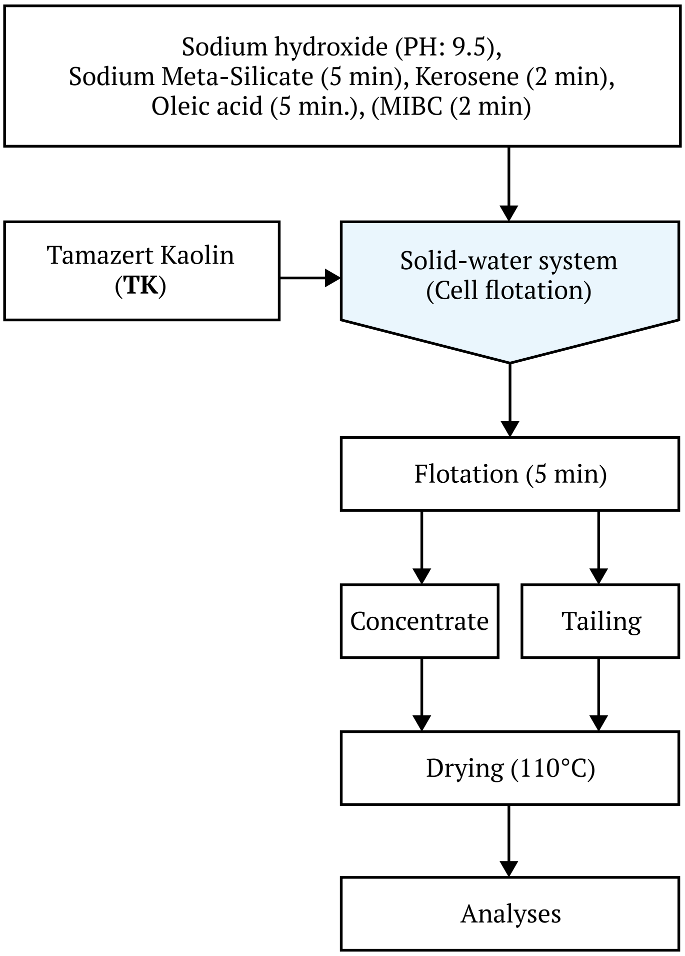

Fig. 2. A flowchart summarizing the steps of the kaolin flotation (TK)

Results and discussions

Characterization results

X-Ray fluorescence (XRF)

The chemical analyses of the kaolin sample are listed in Table 2. The kaolin sample was rich in SiO_2 at 46.70% and Al_2O_3 at 32.67%. The SiO_2/Al_2O_3 ratio of this sample was equal to 1.43. SiO_2/Al_2O_3 ratio in kaolinite mineral is usually 1.18[1] (Kaolinite Mineral Data). X-ray fluorescence measurements to determine the oxide composition of kaolin were carried out using Thermo Niton XL3t XRF Analyzer.

Chemical analyzes reveal that Tamazert kaolin has a high content of Fe_2O_3 (2.70 %), SiO_2 (46.70 %) and K_2O (2.58 %). TiO_2 content is low, 0.28 %.

The loss on ignition of TK is relatively low (9.36 %). It is less than the value of the loss on ignition of pure kaolinite [19], indicating the low presence of organic matter. This may be due to the presence of micas.

The value of the SiO_2/Al_2O_3 ratio (1.27) of TK is differs from the corresponding value of ideal kaolinite (1.18). This may be connected with the presence of alumina in this kaolin.

The presence of Fe_2O_3 produces the brownish color and decreases brightness and whiteness. The low content of TiO_2 makes the TK kaolin a very attractive raw material for a number of industries.

Scanning Electron Microscopy (SEM-EDX)

Figure 3 presents the SEM micrographs of the Tamazert kaolin (TK). The chemical elements proportion of kaolin was established by the Energy Dispersive X-ray (EDX) method. The Scanning Electron Microscopy (SEM-EDX) analysis was used to determine the morphology and composition of kaolin using JEOL-JSM 6610-LV coupled with an OXFORD INCA-ENERGY microanalyser.

In general terms, the morphology of kaolin presents hexagonal shaped kaolinite plates. According to the results of scanning electron microscopy (SEM-EDS), Fig. 3, A, the micrograph presented an imperfect structure of kaolinite. It thus shows that the particles have irregular and flat platelet shapes. There are also quartz particles surrounding the kaolinite particles. According to Amigo et al., 1994 [20], Tamazert kaolin has more or less low crystallinity. Fig. 3, B shows the presence of Hematite as impurity (Fe_2O_3) in this kaolin.

X-ray diffraction (XRD)

X-ray diffraction (XRD) analysis was performed using PHILIPS-X'Pert MPD System diffractometer with CuKα radiation adjusted at 40 mA and 45 kV generators. Fig. 4 shows that the mineral components of Tamazert kaolin were mainly kaolinite, quartz, muscovite and illite.

---

[1] Kaolinite Mineral Data. Available online: http://www.webmineral.com/data//Kaolinite.shtml#.W1CcIfZuLIU

Flotation test results

The products obtained from flotation tests (froth and tailing) were dried in an oven at 105 °C for 24 hours. The foam composed of kaolin particles (hydrophobic) is recovered by overflow of the scum on the surface of the flotation cell, while the tailing (hydrophilic) remains in the bottom of the cell and consists of mainly iron and titanium. Controlling the airflow to the flotation cell during the initial flotation period was found to be very crucial both for loading air bubbles with minerals, as well as for detachment. In addition, a foaming time of 5 minutes or more is necessary for the satisfactory formation of the foamy layer.

The results of the material balance and yields of flotation for each test are reported in Table 3. The chemical analysis of the concentrates products of flotation process are reported in Table 4.

Table 2

Chemical composition (wt %) of kaolin ore (TK)

Sample	SiO_2	Al_2O_3	Fe_2O_3	MnO	MgO	CaO	Na_2O	K_2O	TiO_2	P_2O_5	LOI	SiO_2/Al_2O_3
TK	46.70	36.67	2.70	0.02	0.21	0.12	0.19	2.58	0.28	0	9.36	1.27
Kaolin: KGa-1b, (low-defect)	44.20	39.70	0.21	0	0.03	0	0.013	0.05	1.39	0	13.49	1.11
Ideal kaolinite*	46.55	39.50	–	–	–	–	–	–	–	–	–	1.18

LOI: measured at 1000 °C.

ORIGIN: Tuscaloosa formation , County of Washington, State of Georgia, USA

Ideal kaolin: Refers to a high-purity, fine-grained, absence of impurities, high whiteness and brightness, with excellent plasticity, thermal stability, and other specific properties suited to its intended application, such as ceramics, paper, paint, or pharmaceuticals productions.

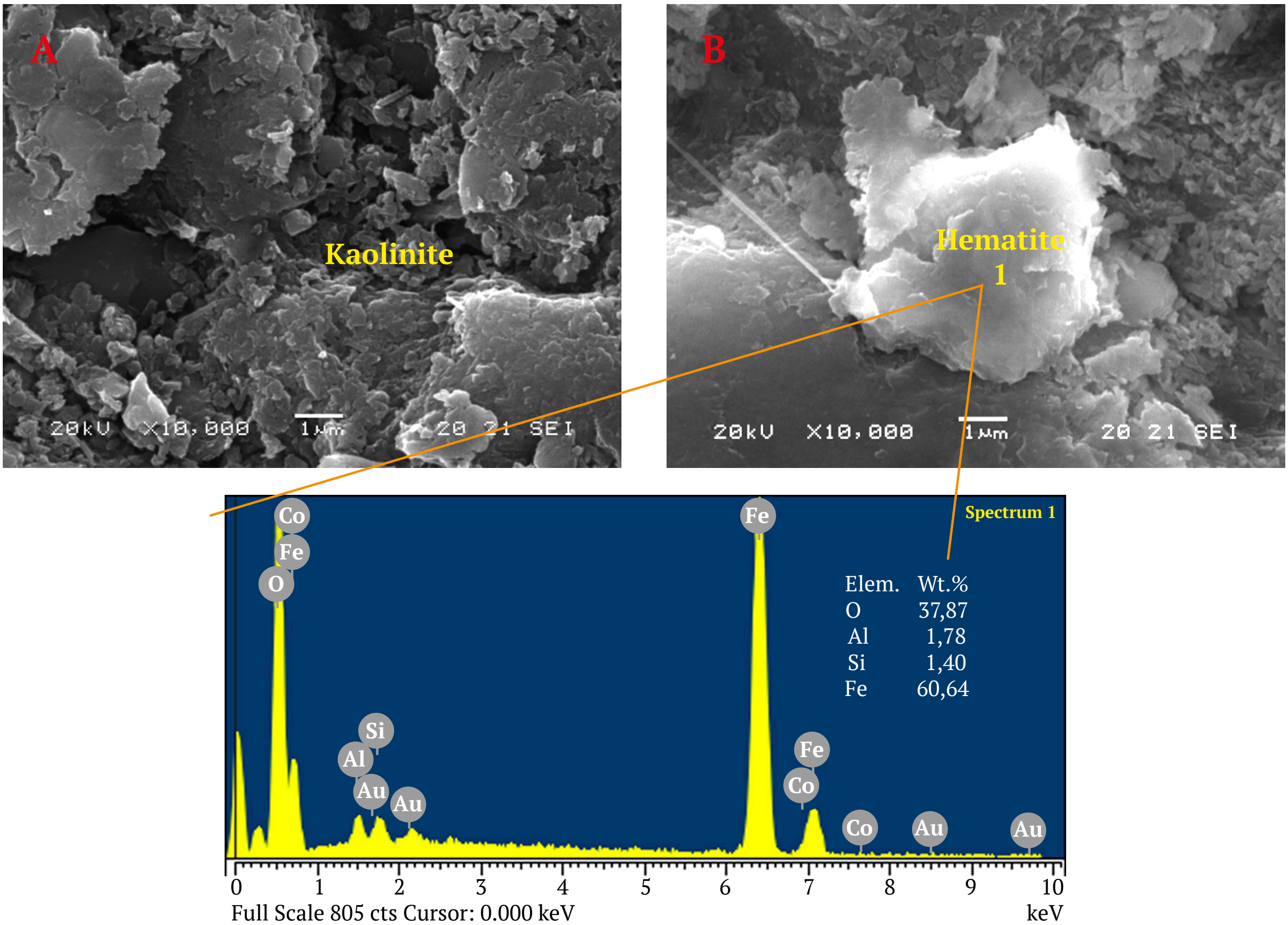

Fig. 3. SEM-EDX of Tamazert kaolin (TK)

eISSN 2500-0632
https://mst.misis.ru/

Calculation of technological indicators

Each separation product can be characterized by qualitative and quantitative indices. For this reason, several equations were used [21]:

– material balance equation for separation products:

$$Q_f = Q_c + Q_t; \tag{1}$$

– balance equation for yields, %:

$$\gamma_f = \gamma_c + \gamma_t; \tag{2}$$

– yield of concentrate, %

$$\gamma_c = \frac{Q_c}{Q_f} \cdot 100; \tag{3}$$

– yield of tailings, %:

$$\gamma_t = \frac{Q_t}{Q_f} \cdot 100, \tag{4}$$

Q_f – masse of feed, t; Q_c – masse of concentrate, t; Q_t – masse of tails, t ; γ_f – yield of feed, %; γ_c – yield of concentrate, %; γ_t – yield of tailings, %.

Tamazert kaolin shows a good flotation performance. The yields and the contents results of the concentrates and tails of Tamazert kaolin (TK) after flotation process are illustrated in Figs. 5 and 6. The optimum yield value is in the fraction between 20 and 40 µm with 79.84 wt. % and 19.92 % by wt.% for the concentrate and the tailing respectively.

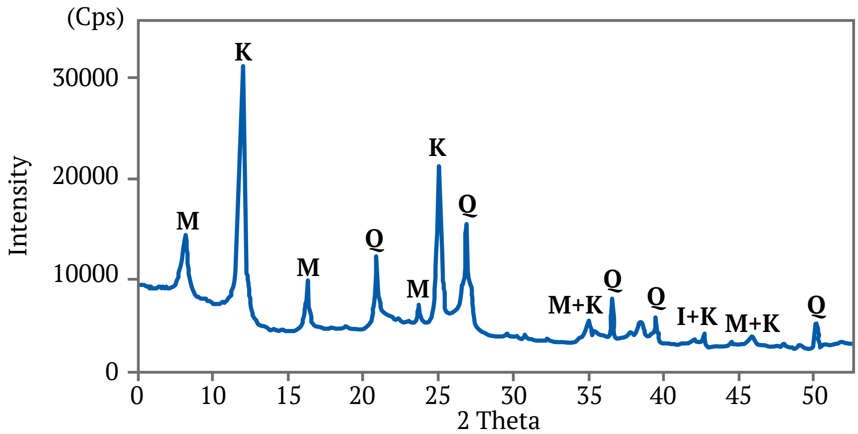

K: Kaolinite **Q**: Quartz **M**: Muscouvite **I**: Illite

Fig. 4. XRD pattern of Tamazert kaolin (TK)

Table 3

Material balance and yields of the flotation tests

Test N°	1		2		3		4		5	
Fraction, µm	0–20		20–40		40–80		80–100		100–120	
Material balance, g	Q_{c1}	Q_{t1}	Q_{c2}	Q_{t2}	Q_{c3}	Q_{t3}	Q_{c4}	Q_{t4}	Q_{c5}	Q_{t5}
	190.5	58.9	199.6	49.8	185.6	63.7	162.5	85.7	148.6	100.5
Q_F, g	249.4		249.6		249.5		249.2		249.5	
Yields, %	γ_{c1}	γ_{t1}	γ_{c2}	γ_{t2}	γ_{c3}	γ_{t3}	γ_{c4}	γ_{t4}	γ_{c5}	γ_{t5}
	76.25	23.30	79.84	19.92	74.24	25.26	65	34.28	59.44	40.20

Table 4

Material balance and yields of the flotation tests

Fraction, µm	**Oxide, wt.%**											
	SiO_2	**Al_2O_3**	**Fe_2O_3**	**TiO_2**	**MgO**	**CaO**	**Na_2O**	**K_2O**	**MnO**	**P_2O_5**	**LOI**	**SiO_2/Al_2O_3**
0–20	49.13	38.81	0.15	0.05	0.10	0.06	0.07	1.05	00	00	10.58	1.26
20–40	49.38	38.97	0.08	0.04	0.11	0.06	0.09	1.11	00	00	10.19	1.27
40–80	48.95	38.79	0.13	0.09	0.12	0.08	0.11	1.23	00	00	10.42	1.26
80–100	48.14	36.85	0.19	0.12	0.15	0.10	0.12	1.28	00	00	12.98	1.30
100–120	47.31	36.72	0.28	0.20	0.19	0.10	0.16	1.41	00	00	13.59	1.29

It can be seen from Table 3, Figs. 5 and 6 that, on the whole, the yield of concentrate decreases with increasing kaolin particle sizes. There is general agreement: flotation efficiency decreases with increasing particle size [22].

The content of K_2O decreased from 2.58 to 1.05 wt. % in the fraction < 20 μm; this indicate a significant removal of illite and/or muscovite.

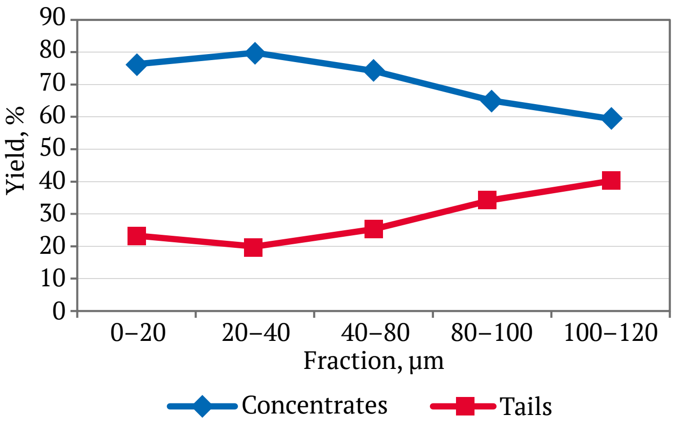

Fig. 5. Yields of the concentrates and tailings of Tamazert kaolin (TK)

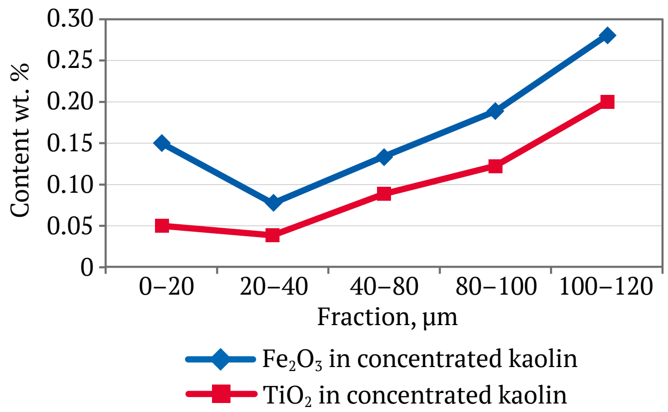

Fig. 6. Fe_2O_3 and TiO_2 contents in concentrated Tamazert kaolin after flotation process

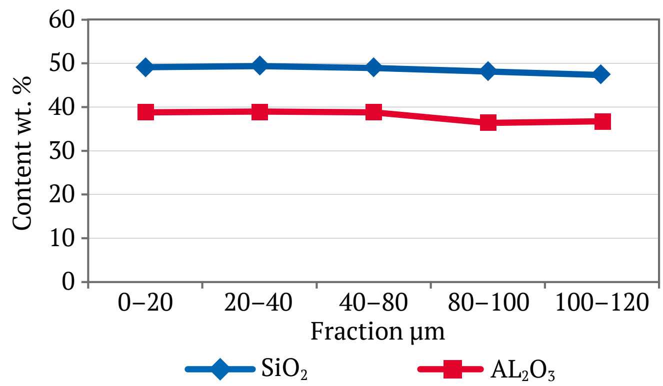

Fig. 7. Al_2O_3 and SiO_2 contents in concentrated of Tamazert kaolin after flotation process

The chemical results (Table 1 and Table 4) and Figure 7 show that the SiO_2 and Al_2O_3 contents of the analyzed sample increased from 46.70 to 49.38 wt.% and 36.67 to 38.97 wt.%, respectively, in the fraction of 20–40 μm. This means logically that the kaolinite content will increase and the whiteness also will be increased.

All these analyses show that the dimensions of particles have a significant influence on the enrichment of Tamazert kaolin (TK) situated between 0 to 40μm.

Comparing the chemical analysis of ideal and Georgian kaolin (KGa-1b) and chemical analysis of processed Tamazert kaolin (TK) can confirm that the flotation beneficiation gives satisfactory results.

Conclusion

Most commonly, the presence of Fe_2O_3 and TiO_2 are the first impurities that cause the coloring of kaolin and reduce its commercial value and industrial utilization. Several tests were performed on the Tamazert kaolin sample using froth flotation process, in order to meet commercial specifications.

The chemical analysis showed that Tamazert kaolin (TK) is an alumino-silicate with contents of 46.70 % SiO_2 and 36.67% Al_2O_3. The impurities as Fe_2O_3 and TiO_2 with 2.7% and 0.28%, respectively, give the brownish color to Tamazert kaolin (low quality) which is not suitable for many industries.

The results obtained using froth flotation are very encouraging. The test results showed that after the enrichment of samples, iron and titanium (the main coloring impurities in Tamazert kaolin) were removed from 2.7 to 0.08 wt.% for Fe_2O_3 in the fraction of 20–40 μm and from 0.28 to 0.04 wt.% for TiO_2 in the same fraction as the optimum test. These results confirm that iron is not substituted in the structure of kaolin and that it is in the free-state.

The contents of SiO_2 and Al_2O_3 after froth flotation of the samples analyzed were increased from 46.70 to 49.38 wt.% and 36.67 to 38.97 wt.%, respectively, in the fraction of 20–40 μm. This means logically that the kaolinite content will increase and the whiteness and brightness will also increase.

Moreover, this study highlighted the importance of dimensional distribution, and has a significant influence on beneficiation of Tamazert kaolin (TK) using froth flotation process. The best results were obtained in the fraction from 0 to 40μm.

Comparing the chemical analysis of Georgian kaolin (KGa-1b) and ideal and treated Tamazert kaolin (TK) confirmed that the froth flotation process can be a potentially effective process to remove Fe_2O_3 and TiO_2 with satisfactory results.

References

1. Bundy W.M. The diverse industrial applications of kaolin. In: Murray H.H., Bundy W., Harvey C. (Eds.) *Kaolin, Genesis and Utilization*. Special Publication 1. Boulder, Colorado: The Clay Mineral Society; 1993. Pp. 43–73.

2. Murray H.H., Keller W. Kaolins, kaolins, and kaolins. In: Murray H. H., Bundy W., Harvey C. (Eds.) *Kaolin, Genesis and Utilization*. Special Publication 1. Boulder, Colorado: The Clay Mineral Society; 1993. Pp. 1–24.

3. Muller J.P., Calas G. Genetic significance of paramagnetic centers in kaolinites. In: In: Murray H.H., Bundy W., Harvey C. (Eds.) *Kaolin, Genesis and Utilization*. Special Publication 1. Boulder, Colorado: The Clay Mineral Society; 1993. Pp. 261–290.

4. Clozel B., Allard T., Muller J.P. Nature and stability of radiation-induced defects in natural kaolinites: new results and a reappraisal of published works. *Clays and Clay Minerals*. 1994;42:657–666. https://doi.org/10.1346/CCMN.1994.0420601

5. Grimshaw R.W. *The chemistry and physics of clays and other ceramic materials*. 4th ed. London: Ernest Benn; 1971.

6. Grim R.E. *Clay mineralogy*. 2nd ed. New York: McGraw-Hill Book Company, International Series in the Earth and Planetary Sciences; 1968. P. 596.

7. Wills B.A., Finch J. *Wills' mineral processing technology. An introduction to the practical aspects of ore treatment and mineral recovery*. 8th ed. Butterworth-Heinemann; 2015. Pp. 266–268.

8. Rousseau R.W. *Handbook of separation process technology*. NY, USA: John Wiley & Sons, Inc.; 1987. 775 p.

9. Tao D. Role of bubble size in flotation of coarse and fine particles – A review. *Separation, Science and Technology*. 2005;39(4):741–760. https://doi.org/10.1081/SS-120028444

10. Blazy P. *La valorisation des minerais*. Presses Universitaires de France; 1970. 415 p. (In French)

11. Zhengchang Sh. *Principles and Technologies of Flotation Machines*. Beijing General Research Institute of Mining and Metallurgy (BGRIMM), Beijing, China; 2021. https://doi.org/10.1007/978-981-16-0332-7

12. Young R.H., Morris H.H. *Method of treating clay to improve its whiteness*. U.S Patent. 1985. No. 4,492,628.

13. Öster R., Schreck B., Rybinski W., Dobiás B. New reagent systems for the flotation of kaolinite. *Minerals Engineering*. 1992;5(3–5):445–456.

14. Yoon R.H., Nagaraj D.R., Wang S.S., Hildebrand T.M. Benefication of kaolin clay by froth flotation using hydroxamate collectors. *Minerals Engineering*. 1992;5(3–5):457–467.

15. Murray H.H. Major Kaolin Processing Developments. *International Journal of Mineral Processing*. 1980;7:263–274.

16. Fuerstenau M.C., Miller J.D., Kuhn M.C. *Chemistry of flotation*. New York: American Institute of Mining, Metallurgical and Petroleum Engineers, Inc.; 1985. P. 132.

17. Köster R., Schreck B., von Rybinski W., Dobias B. New reagent systems for the flotation of kaolinite. *Minerals Engineering*. 1992;5(3–5):445–56. https://doi.org/10.1016/0892-6875(92)90224-W

18. Jiang H., Sun Z., Xu L., Hu Y., Huang K., Zhu S. A comparison study of the flotation and adsorption behaviors of diaspore and kaolinite with quaternary ammonium collectors. *Minerals Engineering*. 2014;65:124–129. https://doi.org/10.1016/j.mineng.2014.05.023

19. Castelein O. *Influence de la vitesse de traitement thermique sur le comportement du kaolin bio: application au frittage rapide*. Thèse de doctorat de l'université de Limoges. 2000. (In French)

20. Amigo J.M., Bastida M., Sanz J. et al. Crystallinity of Lower Cretaceous kaolinites of Teruel (Spain). *Applied Clay Science*. 1994;9:51–69. https://doi.org/10.1016/0169-1317(94)90014-0

21. Pilov P.I., Petrova O.V. *Procédés et machines de traitement des minéraux utiles*. Le manuel. Université Nationale des Mines; 2013.

22. Trahar W.J., Warren L.J. The floatability of very fine particles – A review. *International Journal of Mineral Processing*. 1976;3:103–131. https://doi.org/10.1016/0301-7516(76)90029-6

Information about the author

Mohammed Laraba – Dr. Sci., Lecturer, Department of Mines & Geotechnology, Institute of Mining, Echahid Cheikh Larbi Tebessi University, Tébessa, Algeria; ORCID 0000-0003-1479-7092, Scopus ID 14034384200, ResearcherID M-9255-2018; e-mail larabamd@univ-tebessa.dz

Received 14.04.2023
Revised 19.05.2023
Accepted 30.05.2023

SAFETY IN MINING AND PROCESSING INDUSTRY AND ENVIRONMENTAL PROTECTION

Research paper

https://doi.org/10.17073/2500-0632-2023-01-73
УДК 502.132

Establishment of an erosion-control plant cover in a sand pit under Arctic conditions using sewage sludge

A.V. Lusis[1,2], L.A. Ivanova[2,3], T.T. Gorbachyova[3] SC, A.V. Rumyantseva[4]

[1] *SC Evoblast, Moscow, Russian Federation*

[2] *Polar-Alpine Botanical Garden-Institute of N.A. Avrorin, KSC RAS, Kirovsk, Russian Federation*

[3] *Institute of North Industrial Ecology Problems, KSC RAS, Apatity, Russian Federation*

[4] *Cherepovets State University, Cherepovets, Russian Federation*

adeliysrab@gmail.com

Abstract

This paper presents the findings of a prolonged field studies that aimed to assess the feasibility of using the sewage sludges (SS) form a regional water and wastewater services enterprise to expedite the establishment of a resilient erosion-control plant cover in sand pits located in the Arctic region of the Russian Federation. The study confirms the beneficial impact of the SS on the seed germination, subsequent growth, and development of plants. The study shows that SS can be used in two ways: first, by applying a continuous layer measuring 5 to 10 cm thick on the soil surface or by fragmentarily applying a layer 2–3 cm thick. Second, through early-winter sowing of seeds directly on the soil surface (under the SS layer) or on top of the sewage sludge. In both cases, an annual enhancement of the qualitative and quantitative parameters of the artificially formed stand of grass was observed. This included a significant increase in its height and density, biomass, foliage cover, and thickness of the formed sod, in contrast to the reference sample. The present study investigates the characteristics of the floristic composition of the phytocenoses formed in a sand pit. The findings demonstrate that the use of sewage sludge (SS), regardless of the quantity and application method, accelerates the restorative succession in the sand pit. The thick stand in the experimental variants, resulting from the attraction of pioneer vegetation, promotes the complexity of its structure and species composition, rapid vegetation of inner bare areas, and the emergence of natural phytocenoses elements that are specific to the zonal type of vegetation. Additionally, the use of SS stabilizes erosion processes in the study area. Consequently, the plant community formed in the experiment using SS can be classified as ecologically sustainable, with the potential for independent existence and further development. These results can serve as a foundation for monitoring efforts and the development of measures to optimize the vegetation of such ecotopes.

Keywords

sand pit, phytoremediation, sewage sludge (SS), ameliorant, grass mixture, plant cover

Acknowledgements

This research received funding from the Russian Foundation for Basic Research and the Ministry of Education and Science of the Murmansk Region. The project, titled “Dephosphorization of municipal wastewater under the conditions of reduced water consumption” (Project 17-45-510205), was conducted between 2017 and 2019.

For citation

Lusis A.V., Ivanova L.A., Gorbachyova T.T., Rumyantseva A.V. Establishment of an erosion-control plant cover in a sand pit under Arctic conditions using sewage sludge. *Mining Science and Technology* (*Russia*). 2023;8(3):223–231. https://doi.org/10.17073/2500-0632-2023-01-73

MINING SCIENCE AND TECHNOLOGY (RUSSIA)
ГОРНЫЕ НАУКИ И ТЕХНОЛОГИИ
2023;8(3):223–231
eISSN 2500-0632
https://mst.misis.ru/

ТЕХНОЛОГИЧЕСКАЯ БЕЗОПАСНОСТЬ В МИНЕРАЛЬНО-СЫРЬЕВОМ КОМПЛЕКСЕ И ОХРАНА ОКРУЖАЮЩЕЙ СРЕДЫ

Научная статья

Формирование противоэрозионного растительного покрова на песчаном карьере в условиях Арктики с помощью осадка сточных вод

А.В. Лусис[1,2], **Л.А. Иванова**[2,3], **Т.Т. Горбачева**[3], **А.В. Румянцева**[4]

[1] ГК «Эвобласт», г. Москва, Российская Федерация

[2] Полярно-альпийский ботанический сад-институт им. Н.А. Аврорина Федерального исследовательского центра «Кольский научный центр Российской академии наук» (ПАБСИ КНЦ РАН), г. Кировск, Российская Федерация

[3] Институт проблем промышленной экологии Севера Федерального исследовательского центра «Кольский научный центр Российской академии наук» (ИППЭС КНЦ РАН), г. Апатиты, Российская Федерация

[4] Череповецкий государственный университет, г. Череповец, Российская Федерация

adeliysrab@gmail.com

Аннотация

В настоящей работе представлены результаты многолетних полевых исследований по оценке возможности применения ОСВ регионального предприятия водопроводно-канализационного хозяйства для ускоренного формирования устойчивого противоэрозионного растительного покрова на песчаных карьерах в Арктической зоне РФ с подтверждением оказания им стимулирующего эффекта на прорастание семян, дальнейший рост и развитие растений. Показано, что ОСВ может применяться двумя способами: нанесением на поверхность грунта сплошным слоем высотой от 5 до 10 см, и фрагментарно – слоем 2–3 см, а подзимний посев семян – непосредственно по поверхности грунта (под слой ОСВ) либо поверх осадка сточных вод. В обоих случаях отмечено ежегодное улучшение качественных и количественных показателей искусственно созданного травостоя – многократное, по сравнению с контролем, увеличение его высоты и плотности, биомассы, проективного покрытия и мощности сформированной дернины. Исследованы особенности формирования флористического состава созданных в песчаном карьере фитоценозов. Установлено, что независимо от количества и способа нанесения применение ОСВ способствует ускорению восстановительной сукцессии на песчаном карьере, а мощный травостой опытных вариантов путем привлечения пионерной растительности – усложнению его структуры и видового состава, быстрому зарастанию внутренних оголенных участков и возникновению элементов естественных фитоценозов, свойственных зональному типу растительности, а также стабилизации процессов эрозии на объекте исследования. Все это позволяет характеризовать сформированное в эксперименте с помощью ОСВ растительное сообщество как экологически устойчивое, имеющее перспективы к самостоятельному существованию и дальнейшему развитию. Результаты таких исследований могут послужить основой для организации мониторинга и разработки мероприятий по оптимизации растительности подобных экотопов.

Ключевые слова

песчаный карьер, фиторекультивация, осадок сточных вод (ОСВ), мелиорант, травосмесь, растительный покров

Благодарности

Проведенные исследования были поддержаны грантом РФФИ и Министерства образования и науки Мурманской области. Проект 17-45-510205: «Дефосфотация коммунальных стоков в условиях снижения водопотребления» в 2017–2019 гг.

Для цитирования

Lusis A.V., Ivanova L.A., Gorbachyova T.T., Rumyantseva A.V. Establishment of an erosion-control plant cover in a sand pit under Arctic conditions using sewage sludge. *Mining Science and Technology* (*Russia*). 2023;8(3):223–231. https://doi.org/10.17073/2500-0632-2023-01-73

Introduction

The annual increase in mineral resource utilization, exploration and construction activities by mining companies for oil, gas and ore, as well as the construction of roads, power lines and other works, has resulted in the disturbance of natural ecosystems. These activities lead to the destruction of soil, plant cover and reduction of biodiversity, resulting in the emergence of new man-made forms of the landscape [1].

In the Murmansk Region, one of the most common forms of man-made change in the Arctic landscapes are pits that emerge after the removal of sand for construction and other purposes. Restoration of these areas requires measures to transform the disturbed lands into a state suitable for further use and prevent adverse impact on the environment [2].

One of way to rehabilitate such areas is to allocate a portion of them for self-organized vegetation [3]. However, due to the unfavorable forecast for natural vegetation and the complexity of revegetation on sand deposits due to individual and regional specifics, reclamation works are necessary to restore the productivity of disturbed lands by creating new, purposefully synthesized, artificial biogeocenoses [4][1].

When implementing reclamation measures to form a plant cover on sandy soil, one of the determining factors is the nutritive conditions of its surface layer. The structurelessness of such substrate, low water-holding capacity, lack of organic matter of biogenic origin (humus), and insufficient nutrient provision make it necessary to invest in expensive mineral fertilizers annually [5]. Sewage sludge (SS) treatment, a byproduct of regional municipal wastewater, can play a positive role in solving the problem of the low NPK status of sandy soils, creating a plant cover on them, and maintaining its stability [6–8]. SS has potentially useful properties due to its high content of easily accessible organic matter for microbiota [9], as well as the lability of nitrogen, phosphorus and potassium, which determines their rapid assimilation by plants [10, 11]. Although SS has a positive effect on the physical properties of sandy soils, optimizing the density and aggregation, it may contain a set of heavy metals and pathogens. Therefore, it is necessary to study each sediment in specific conditions of reclaimed areas [12].

The purpose of the study is to assess the feasibility of utilizing SS from a regional water and wastewater services (WWS) enterprise Apatityvodokanal JSC to expedite the development of a sustainable and effective erosion-control plant cover in sand pits located in the Arctic zone of the Russian Federation.

Research objectives:

1. To investigate the effects of SS on plant growth and quality of artificially formed seeded phytocenoses.

2. To evaluate the effectiveness of different methods of applying SS onto the surface of the sand pit soil during reclamation activities.

Objects and methods of research

The research was conducted between October 7, 2017, and October 10, 2020, in the Murmansk Region (Kola Peninsula, Russian Federation) on a local disturbed territory, which is a sand pit owned by Apatityvodokanal JSC.

The pit's depth ranges from 3 to 5 meters and is located in the northern taiga coniferous forests subzone, which has about 250 species of vascular plants [13]. Based on the research findings, the model site was identified as a secondary ecotope with a little number of plant germs in the soil surface layer. Examination of the plant communities growing in the pit area revealed the presence of small microgroups consisting of one, two and perennial pioneer plant species with a low degree of surface coverage. Surrounding the pit, the plant cover comprises natural forest communities, primarily birch, lichen-grass and lichen-grass-moss fir wood, and meadow plants in open areas. In total, 56 species characteristics of dry and barren soils were recorded within the pit and its immediate vicinity. Under favorable growing conditions, these species could contribute to the natural vegetation of the pit's sandy soil, promoting biodiversity and the formation of a much more sustainable artificial phytocenosis [14].

The pit area shows clear indications of wind and water erosion, including soil sliding and rounded hilltops. The model site itself is was a 30° sandy slope facing northwest, with an area of 200 m^2 that has been cleared of vegetation, and prepared with surface flattening, terracing and levelling[2].

The objective of this study was to investigate sandy pit soil with an admixture of gravel and small boulders, which is classified as medium-grained according to State Standard 25100–2011[3], with a low proportion of clay particles.

[1] GOST R 57446–2017. Best available techniques. Disturbed lands reclamation. Restoration of biological diversity. Moscow: Standartinform; 2017.

[2] GOST 17.5.3.0483 (ST SEV 5302–85). Nature protection. Lands. Reclamation general requirements. Moscow: Standardinform; 1984.

[3] GOST 25100–2011. Interstate standard. Soils. Classification. 2013-01-01. Moscow: Standartinform; 2011.

Table 1

Diagram of field experiment

Variant	SS application technique
Variant 1 (*n* = 6)	SS was applied to the soil surface in a fragmentary manner, with a layer 2–3 cm high. The seeds were then sown directly on the soil surface, underneath the layer of SS
Variant 2 (*n* = 6)	SS was applied to the soil surface in a continuous layer, with a height of 5–10 cm. The seeds were then sown on top of the layer of SS
Variant 3 (*n* = 6)	No sludge was applied to the soil surface. The seeds were directly sown on the soil surface

The objective of this study was to investigate sandy pit soil with an admixture of gravel and small boulders, which is classified as medium-grained according to State Standard 25100-2011, with a low proportion of clay particles. To enhance the biogenesity of the soil, sludge from wastewater treatment plant (WTP-3) in Apatity (Murmansk Region) was used as an ameliorant. The sludge is a moist, plasticine-like mass with a black-brown color and a pungent specific smell. The sludge is classified as hazardous class V waste according to GOST R 54534–2011, and its total content of heavy metals is well below the standards [12] established by this regulation[4], At the WTP-3, sludge treatment involves drying and aging on sludge beds for three or more years[5].

The field experiment was designed with three variants, each with six replications, for a total of 18 experimental plots measuring 1×1 m and spaced 0.5 m apart at the model site. The experimental variants involved the application of sludge to the soil surface in two ways: fragmentarily and as a continuous layer, while the reference site did not receive any sludge application. The diagram of the field experiment is presented in Table 1.

No covering of the sandy surface with a fertile soil layer or additional fertilization of plants with mineral fertilizers was carried out during the experiment.

A complex sowing phytocenosis was formed using the early-winter method of direct sowing of the grass mixture, developed on the basis of biological characteristics of perennial herb species. The grass mixture comprised three species of grasses (red fescue (*Festuca rubra* L.), European dune wild ruttishness (*Leymus arenarius Hochst.*), and couch (*Elymus repens* (L.) *Gould*) and two species of legumes (*Washington lupine (Lupinus polyphyllus Lindl.*) and sweet vetch (Hedysarum alpinum L.) taken in the ratio of 5:1:1:0.1:0.1 (vol.), with a seed rate of 27.5 g/m^2. In variant 1, seeds were sown directly on the soil surface (under the sludge layer), and in variant 2, they were sown on top of a continuous layer of sludge. Additionally, six seeds of Scots pine (*Pinus sylvestris L.*) were sown separately from the grass mixture in the lower right corner of each plot.

Subsequent fieldwork involved regular monitoring of plant growth and development, as well as the formation of the grass stand. The effect of the ameliorant on the quality of the resulting phytocenosis was evaluated based on various parameters, such as plant height in the grass stand (cm), foliage cover (%) on the plots, changes in the structure and species composition of the phytocenosis [15, 16], and, at the end of the experiment, the sod thickness (cm), grass stand density (number of shoots per 1 m^2), and accumulation of raw biomass (g/m^2). Biometric measurements were taken simultaneously in all replications, and the biomass was determined in the laboratory using analytical scales.

The Latin names of plants are given according to the common international names of World Flora Online[6].

The collected data were processed using one-way analysis of variance (one-way ANOVA) in Excel.

Research results

2018. The first sprouts of seeded plants were observed in all three variants of the experiment simultaneously after the snow cover melted in May. However, the most vigorous and high-quality sprouts were noted in the variants with the use of SS (Table 2), which led to the assumption of a stimulating effect of this ameliorant on the seed germination process.

Over the next 1.5 months, primitive (one-tier) plant communities were formed on the experimental sites (Table 2), consisting of only two sown species – red fescue and couch as of July 2018. The quality of the grass stand on the experimental plots was significantly different from the reference plots. In both experimental variants, a dense and well-developed grass stand with high foliage cover of bright emerald green color was observed. The foliage cover was 100 % in plots with continuous application of SS

[4] GOST R 54534–2011. Resources saving. Sewage sludge. Requirements for recultivation of disturbed lands (official edition). Moscow: Standartinform, 2012.

[5] GOST R 54534–2011. Resources saving. Sewage sludge. Requirements for recultivation of disturbed lands. Moscow: Standartinform; 2013.

[6] The WFO Plant List. Snapshots of the taxonomy. URL: https://wfoplantlist.org/plant-list

and top sowing of the grass mixture (variant 2), and 87 % in the plots with fragmentary application of SS (variant 1). Seed germination was mainly observed in the areas of experimental plots free of the SS layer, and to a lesser extent in the areas covered with an ameliorant layer. In the reference area (without application of SS), the grass stand formed was sparse, yellow-red in color, covering only 15 % of the plot area. Plants within it were in a depressed state, and by the end of the growing season, they practically did not increase in height.

In the first vegetation period, an increase (up to five species) in the composition of the phytocenoses formed was observed only on the experimental plots (Table 2) due to the introduction of three new species from the nearby territories. These were native pioneer and weed plants – foalfoot (*Tussilago farfara* L.), fireweed (*Epilobium angustifolium* L.) and field sorrel (*Rumex acetosella* L.).

In **2019**, the grass stand at the reference sites remained low and sparse with the foliage cover of only 20 %, and the resulting community remained one-tiered (Table 2, Figure 1). The experimental plots were characterized by a dense grass stand of complex two-tier structure, with a height 4–5 times exceeding the height of plants at the reference site.

While the plants at the reference sites were only in the vegetative stage, the plants at the experimental sites had already entered the flowering phase. All six sown species, including Scots Pine seedlings, were only observed at the experimental plots. During this period, the species composition of the created plant community was augmented with four species from the main sowing grass mixture, namely European dune wild ruttishness (*Leymus arenarius Hochst.*), Washington lupine (*Lupinus polyphyllus Lindl.*), sweet vetch (*Hedysarum alpinum* L.) and Scots pine. Colonization of experimental plots, as well as their

Table 2

Average indicators of artificial phytocenosis in 2018–2019 in the sand pit of Apatityvodokanal JSC

Indicator	Variant and method of SS application					
	2018			2019		
	1*	2**	3 (reference)	1*	2**	3 (reference)
Number of tiers, pcs.	1	1	1	2	2	1
Average plant height (by dominant species), cm	27.4±1.5	35.3±1.2	8.1±0.3	56.9±1.7	69.7±1.9	12.8±0.5
Average number of species from the number of sown ones, pcs.	2	2	2	4.5	5.6	4,0
Average number of invaded species, pcs.	3	3	–	3.8	3.8	2.3
Foliage cover, %	87	100	15	100	100	20

* – fragmentary application of SS;
** – application of SS as a continuous layer.

Variant 1 *Variant 2* *Reference variant*

Fig. 1. Appearance of experimental plots in 2019

perimeter, continued with six new species of native plants: subarctic astragalus (*Astragalus norvegicus Grauer*), tufted hair grass (*Deschampsia caespitosa* (L.), *P. Beauv.*), marsh cress (*Rorippa palustris Besser*), fall dandelion (*Scorzoneroides autumnalis* (L.) *Moench*), colonial bent grass (*Agrostis capillaris* L.), and mountain sorrel (*Oxyria digyna Hill.*). At the reference sites, European dune wild ruttishness or Scots Pine were often not detected in the grass stand, which may be attributed to the quality of seeds collected from natural conditions and their low volume ratio during planting. Although Washington lupine is usually found in habitats with sandy soils and can thrive on nutrient-poor substrates [17], this species was only observed at experimental plots where sewage sludge was present.

2020. Over the course of three vegetation periods, plant communities with vigorous growth and development were formed on the model slope of the pit that lacked plant and soil cover, without the use of earthing or fertilizers, due to the application of SS. These communities were dominated by two species that determined their height: red fescue and couch.

The height of plants in the experimental variants reached 95.2 ± 1.4 cm (variant 2) and 86.7 ± 3.3 (variant 1), whereas at the reference sites, this measurement was six times lower (Table 3). In contrast to the reference sites, plants in the experimental variants retained an intense green color and a shiny surface of leaves and stems. The grass stand density in the experimental variants 1.7–4.4 times higher than the reference one. Only the experimental variants showed a 100 % foliage cover, whereas the reference site had an indicator of only 10 %, which was 5–10 % lower than the first and second vegetation periods. The roots of plants in the experimental variants effectively utilized the

Table 3

Results of variance analysis of the impact of SS application technique on the main qualitative indicators of artificial phytocenosis (2020)

Variant, sources of variation	Indicator		
	Height of plants (by dominant species), cm	Density of grass stand, number of stems/1 m^2	Green biomass, g/m^2
1	86.7 ± 3.3	12 830 ± 123.14	2952 ± 52.5
2	95.2 ± 1.4	32 589.7±546.7	5632 ± 28.9
3	13.7 ± 0.9	7431.7 ± 20.9	100 ± 3.2
SS	120 538	2 105 022 787	76 295 880.9
df	2	2	2
MS	60 269	1 052 511 394	38 147 940.5
F	13 452.6	10 040	39 119.4
p-value	< 0.001	< 0.001	< 0.001
*F critical**	7.4	3.7	3.9

* Critical *F* is a tabular value of the criterion of the adopted level – the reliability of differences between the variants was taken at the values of $p < 0.05$ ($n = 6$). Variants were considered unreliable at $p > 0.05$.

Table 4

Effect of SS application technique on qualitative indicators of artificial phytocenosis (2020)

Indicator	Variant		
	1*	2**	3 (reference)
Number of tiers, pcs.	2	3	1
Average number of species from the number of sown ones, pcs.	6,0	6,0	4,5
Average number of invaded species, pcs.	11.7	12.0	3.0
Foliage cover, %	100	100	10
Sod thickness (by core, $n = 3$), cm	3.6 ± 0.03	9.6 ± 0.02	2.6 ± 0.2

* – fragmentary application of SS;
** – application of SS as a continuous layer.

sandy substratum and formed a dense grass sod with a thickness of 3.6±0.03 cm (variant 1) and 9.6±0.02 cm (variant 2). In comparison this indicator was 1.4 and 3.7 times lower, respectively, at the reference site (Table 4). The high foliage cover and density of the grass stand in the variants with the use of SS resulted in a significant accumulation of biomass, which is notable for the northwest region of the Russian Federation [18]. The experimental variant 1 accumulated 2952.0±52.5 g/m^2, and in variant 2, it was 5632.0±28.9 g/m^2 (29 and 56.3 t/ha), which was 29 and 56 times higher than the reference site, which only accumulated 100.7±3.2 g/m^2) (1 t/ha) (Table 3).

The present study investigated the impact of SS on the qualitative indicators of the vegetation cover created over three vegetation periods (Table 3). The results demonstrated statistically significant differences ($p < 0.05$) in the average values of the three main quality indicators of the artificial phytocenosis. The calculated F statistic was greater than the critical F value, leading us to reject the null hypothesis that height, accumulation of green plant biomass, and grass stand density are not dependent on the use of SS. Instead, we accepted the alternative hypothesis that the main quality indicators are statistically influenced by the use of SS. These findings suggest that there is a 95 % probability that the use of SS has a positive effect on the quality indicators of the plant cover formed in the sand pit during the three vegetation periods.

The grass stand that formed at the experimental plots exhibited a complex two- and three-tiered structure, in contrast to the primitive, sparse, one-tiered structure of the reference site (Table 4). In 2020, two additional native plants, tea-leaved willow (*Salix phylicifolia* L.) and Kentucky bluegrass (*Poa pratensis* L.), were incorporated into the plant community; which accelerated the vegetation of bare inter-plot areas and the perimeter of the sites by pioneer plants, hastening the restoration succession of the pit. The total number of species at the model site, adapted to the specific conditions, increased to 21 in 2020, with seven of them completing a full cycle of development. The appearance of natural phytocenoses elements, typical of the zonal type of plant cover, allowed for the artificial plant community to be classified as ecologically sustainable, with potential for independent existence and further development [19].

Practical application

The value of research results for practice is evidenced by the proposal of an innovative and cost-effective method of creating high quality rehabilitative phytocenoses for environmental purposes.

This method is based on the use of a widely available and ow-cost high-absorbency component, which is also an additional source of nutrients from the product of regional municipal wastewater treatment – SS. This approach can play a positive role in addressing the problem of low productivity of sandy man-made soils. The proposed measures in this study could contribute to the growth of profit of wastewater treatment enterprises due to the reduction of penalties for the excessive waste discharge and the possibility of improving processes. Furthermore, it could allow for the involvement of a large volume of waste requiring utilization in the economic turnover, leading to a significant reduction of their adverse impact on the environment. The resulting economic effect of environmental protection is challenging to evaluate [20, 21].

Directions for future research

The results of this study require verification when implemented at the objects of accumulated environmental damage, specifically for fixing dusty surfaces of different types of tailings ponds in the Murmansk Region. This verification aims to recognize the proposed method as an alternative to traditional methods of reclamation of man-made soils.

Conclusion

Long-term field research was conducted to develop practical bases for an innovative method of bioreclamation of sandy soils without peating or earthing, and without use of mineral and organic fertilizers.

This method is based on the field observations of experimental irrigation of the man-made soil in a sand pit with the product of the regional municipal wastewater (SS) treatment, which confirmed the stimulating effect of its use on seed germination, further growth and development of plants, and improvement of the quality of artificially created sowing phytocenoses. This approach could partially contribute to the solution of important environmental problems such as the sound use of SS of regional WWS enterprises in the restoration of objects with accumulated environmental damage and environmental enhancement in the Extreme North.

The study showed that SS can be applied in two ways: as a continuous and fragmentary layer 2 to 10 cm thick on the man-made soil, and early-winter sowing of seeds – directly on the soil surface (under the SS layer) or on top of the sediment.

The method of ameliorant application significantly affects the quality of the sowing phytocenosis formed. Fragmentary application of SS on the soil surface increases the plant height in the created phytocenosis by 6.3 times, the grass stand density by 1.7 times, the biomass by 29.3 times, the foliage cover by 10 times, and the turf thickness by 1.4 times compared to the reference site (the variant without SS application). When applying the sediment as a continuous layer, these indicators increase even more compared to the reference site: the height of plants by 6.9 times, the density of the grass stand by 4.4 times, the biomass by 55.9 times, and the sod thickness by 3.7 times.

Regardless of the method of application, the application of SS contributes to the acceleration of restoration succession and an increase in biodiversity in a sand pit. A thick grass stand promotes the colonization of pioneer species, rapid vegetation of inner bare areas, the appearance of elements of natural phytocenoses typical of the vegetation zonal type, fixing, as well as stabilization of erosion processes.

References

1. Kapelkina L.P. Natural revegetation and remediation of disturbed lands of the north. *Advances in Current Natural Sciences*. 2012;(11):98–102. (In Russ.) URL: https://s.natural-sciences.ru/pdf/2012/11-1/29.pdf

2. Pevzner E.M., Kostovetsky V.P. *Ecology of mining*. Moscow: Nedra; 1990. 235 p. (In Russ.)

3. Kondratyuk E.N., Tarabrin V.P., Baklanov V.I., et al. *Industrial botany*. Kyiv: Naukova Dumka; 260 p. (In Russ.)

4. Kapelkina L.P. *Ecological aspects of optimization of man-made landscapes*. Moscow: Nauka; St. Petersburg: PROPO; 1993. 191 p. (In Russ.)

5. Evdokymova G.A., Pereverzev V.N., Zenkova I.V., et al. *Evolution of technogenic landscapes (on the example of waste from the apatite industry)*. Apatity: Publ. House of the Kola National Center of the Russian Academy of Sciences; 2010. 146 p. (In Russ.)

6. Koptsik G.N., Koptsik S.V., Smirnova I.E. Alternative technologies for remediation of technogenic barrens in the kola subarctic. *Eurasian Soil Science*. 2016;49(11):1294–1309. https://doi.org/10.1134/S1064229316090088 (Orig. ver.: Koptsik G.N., Koptsik S.V., Smirnova I.E. Alternative technologies for remediation of technogenic barrens in the kola subarctic. *Pochvovedenie*. 2016;(11):1375–1391. (In Russ.) https://doi.org/10.7868/S0032180X16090082)

7. Koptsik G.N., Smirnova I.E., Koptsik S.V., et al. Efficiency of remediation of technogenic barrens around the "Severonikel" works in the Kola peninsula. *Vestnik Moskovskogo Universiteta. Seriya 17: Pochvovedenie*. 2015;(2):42–48. (In Russ.)

8. Chen W., Wu L., Frankenberger W.T., Chang A.C. Soil enzyme activities of long term reclaimed wastewater-irrigated soils. *Journal of Environmental Quality*. 2008;37(5):36–42. https://doi.org/10.2134/jeq2007.0315

9. Kuypers M.M.M., Marchant H.K., Kartul B. The microbial nitrogen-cycling network. *Nature Review Microbiology*. 2018;16:263–276. https://doi.org/10.1038/nrmicro.2018.9

10. Jones D.L. Organic acids in the rhizosphere – a critical review. *Plant and Soil*. 1998;205:25–44. https://doi.org/10.1023/A:1004356007312

11. Gorbacheva T.T., Lusis A.V., Ivanova L.A. Chemical amelioration of nepheline sands using sewage sludge from a regional wastewater treatment plant. *Vestnik of MSTU*. 2021;24(1):88–96. (In Russ.) https://doi.org/10.21443/1560-9278-2021-24-1-88-96

12. Petrova T.A., Rudzisha E. Utilization of sewage sludge as an ameliorant for reclamation of technogenically disturbed lands. *Journal of Mining Institute*. 2021;251:767–776. https://doi.org/10.31897/PMI.2021.5.16

13. Ramenskaya M.L. *Analysis of the flora of the Murmansk region*. Leningrad: Nauka; 1983. 216 p.

14. McGill B.J. Towards a unification of unified theories of biodiversity. *Ecology Letters*. 2010;13(5):627–642. https://doi.org/10.1111/j.1461-0248.2010.01449.x

15. Lavrenko E.M., Korchagin A.A. (eds.) *Field geobotany*. Moscow-Leningrad: Nauka Publ. House; 1964. 530 p. (In Russ.)

16. Tikhodeeva M.Yu., Lebedeva T.Kh. *Practical geobotany (analysis of the composition of plant communities)*. St. Petersburg: Saint Petersburg University Publ. House; 2015. 166 p. (In Russ.)

17. Skvortsov V.E. *Atlas-determiner of vascular plants of the taiga zone of European Russia*. Moscow: Greenpeace of Russia; 2000. 587 p. (In Russ.)

18. Vikhman M.I., Kislykh E.E., Liseenko L.A. Yield and quality of fodder grasses depending on meteorological factors under controlled soil fertility. In: *Proceedings of the 40th International Scientific*

Conference "Agrochemical Methods for Increasing Soil Fertility and Productivity of Agricultural Crops in Adaptive Landscape Farming Systems" of All-Russian Research Institute of Agrochemistry named after D. N. Pryanishnikov. Moscow: Publishing house VNIIA; 2006. Pp. 127–129. (In Russ.)

19. Tretyakova A.S., Mukhyn V.A. *Synanthropic flora of the Middle Urals*. Yekaterinburg; 2001. 147 p. (In Russ.)

20. Harder R., Peters G.M., Svanström M., et al. Estimating human toxicity potential of land application of sewage sludge: the effect of modeling choices. *International Journal of Life Cycle Assess*. 2017;22(5):731–743. https://doi.org/10.1007/s11367-016-1182-x

21. Zema D.A., Bombino G., Andiloro S., Zimbone S.M. Irrigation of energy crops with urban wastewater: effects on biomass yields, soils and heating values. *Agricultural Water Management*. 2012;115:55–65. https://doi.org/10.1016/j.agwat.2012.08.009

Information about the authors

Adelina V. Lusis – Specialist, Evoblast Group, Moscow, Russian Federation; Leading Specialist in Labor Protection, Industrial Safety and Environmental Protection, Polar-Alpine Botanical Garden-Institute named after N. A. Avrorin of the Federal Research Center "Kola Scientific Center of the Russian Academy of Sciences, Kirovsk, Russian Federation; ORCID 0009-0004-0114-5372; e-mail adeliysrab@gmail.com

Lubov A. Ivanova – Dr. Sci. (Biol.), head of the laboratory of decorative floriculture and landscaping, Polar-Alpine Botanical Garden-Institute named after N. A. Avrorin of the Federal Research Center "Kola Scientific Center of the Russian Academy of Sciences, Kirovsk, Russian Federation; Leading Researcher, Institute for Problems of Industrial Ecology of the North of the Federal Research Center "Kola Scientific Center of the Russian Academy of Sciences", Apatity, Russian Federation; ORCID 0000-0002-7994-5431; e-mail ivanova_la@inbox.ru

Tamara T. Gorbacheva – Cand. Sci. (Biol.), Leading Researcher, Institute for Problems of Industrial Ecology of the North of the Federal Research Center "Kola Scientific Center of the Russian Academy of Sciences", Apatity, Russian Federation; ORCID 0000-0001-5014-4385, Scopus ID 6602532642; e-mail podzol_gorby@mail.ru

Anzhella V. Rumyantseva – Cand. Sci. (Biol.), Associate Professor, Department of Biology, Cherepovets State University, Cherepovets, Russian Federation; ORCID 0000-0002-7918-1857; e-mail a-v-rum@yandex.ru

Received 12.01.2023
Revised 17.02.2023
Accepted 09.03.2023

POWER ENGINEERING, AUTOMATION, AND ENERGY PERFORMANCE

Research paper

https://doi.org/10.17073/2500-0632-2023-03-100
UDC 622:621.31

Internal and cross sectional benchmarking of electrical energy use in opencast coal mine

S.A. Topno[1,2], B.S. Umre[2], M.V. Aware[2], L.K. Sahoo[1]

[1] CSIR-Central Institute of Mining & Fuel Research, Nagpur Research Centre, Nagpur, India
[2] Visvesvaraya National Institute of Technology, Nagpur, India
✉ *seematopno@rediffmail.com*

Abstract
Electrical energy consumption in the opencast coal mine is very high. Electric shovels, pumps and coal handling plants consume 75% of the total electricity consumption of an opencast coal mine. In this paper, a modelling framework has been developed for electrical energy use benchmarking (internal as well as cross-sectional) of the mine. To develop a mine specific model for benchmarking electrical energy use statistical approach (linear regression method) has been applied. Specific power consumption (SPC) is used as a benchmarking index to assess the operating energy performance of a specific mine and multiple coal mines of India based on the field studies. Seasonal analysis of the electrical energy usage has also been analysed. Our results show the benchmark SPC as 0.50 kWh/t and the energy-saving potential as 10.7% for a single mine and the benchmark SPC of multiple coal mines as 0.52 kWh/t. The result concludes that SPC widely depends on its capacity and mining method and the developed model are useful for benchmarking and targeting for efficient electrical energy use in opencast mine.

Keywords
electrical, benchmarking, internal , cross sectional, specific power consumption, energy use, opencast mine

Acknowledgements
The authors duly acknowledge to the Director, CIMFR for permitting to publish this paper. The authors also extend their thanks to Head of the research group and other scientific staff of CSIR-CIMFR, Nagpur Research Centre (Fuel science group) for their support. We are extremely and sincerely thankful to Dr A.K. Soni, Chief Scientist, CSIR-CIMFR, Nagpur Research Centre (Mining technology group) for his valuable inputs and suggestions to improve the text and language content of this paper. Our thanks and acknowledgement are also due to the Department of Electronics and Information Technology and HOD, Electrical Department of VNIT; All mine authorities of SECL, BCCL and WCL mines from where relevant data have been collected during energy efficiency and benchmarking studies.

For citation
Topno S.A., Umre B.S., Aware M.V., Sahoo L.K. Internal and cross sectional benchmarking of electrical energy use in opencast coal mine. *Mining Science and Technology* (*Russia*). 2023;8(3):232–244. https://doi.org/10.17073/2500-0632-2023-03-100

ЭНЕРГЕТИКА, АВТОМАТИЗАЦИЯ И ЭНЕРГОЭФФЕКТИВНОСТЬ

Научная статья

Внутренний и перекрестный сопоставительный анализ потребления электроэнергии на угольных разрезах

С.А. Топно[1,2], Б.С. Умре[2], М.В. Аваре[2], Л.К. Саху[1]

[1] CSIR – Центральный институт горного дела и научно-исследовательских работ по изучению и использованию топлива, Исследовательский центр Нагпура, г. Нагпур, Индия
[2] Национальный институт технологии им. М. Висвесарая, г. Нагпур, Индия
✉ *seematopno@rediffmail.com*

Аннотация
На угольных разрезах потребляется большое количество электроэнергии. Электрические экскаваторы, насосы и установки для перегрузки угля потребляют 75 % от общего объема электроэнергии. В данной работе представлена схема моделирования для проведения сопоставительного анализа (как внутреннего, так и перекрестного) потребления электроэнергии на предприятии. Для разра-

ботки модели сопоставительного анализа потребления электроэнергии на конкретном предприятии был применен статистический подход (метод линейной регрессии). Удельное потребление электроэнергии (УПЭ) используется в качестве контрольного показателя оценки энергоэффективности конкретного предприятия и нескольких угольных предприятий в Индии на основе полевых исследований. Также проведен сезонный анализ потребления электроэнергии. Согласно полученным результатам контрольный показатель УПЭ составляет 0,50 кВт-ч/т, а потенциал энергосбережения для одного предприятия – 10,7 %. Для нескольких угольных предприятий контрольный показатель УПЭ составляет 0,52 кВт-ч/т. Сделан вывод о том, что УПЭ в значительной степени зависит от производственной мощности, а разработанные метод и модель горных работ позволяют выполнить сопоставительный анализ и достичь эффективного энергопотребления на разрезах.

Ключевые слова

электрический, сопоставительный анализ, внутренний анализ, перекрестный анализ, удельное энергопотребление, потребление энергии, разрез

Благодарности

Авторы выражают благодарность директору Центрального института горного дела и научно-исследовательских работ по изучению и использованию топлива за разрешение опубликовать данную работу. Авторы также выражают благодарность руководителю исследовательской группы и научным сотрудникам Исследовательского центра Нагпур Центрального института горного дела и научно-исследовательских работ по изучению и использованию топлива (группа топливоведения) за оказанную поддержку. Мы искренне благодарны д-ру А.К. Сони, главному научному сотруднику Исследовательского центра Нагпур Центрального института горного дела и научно-исследовательских работ по изучению и использованию топлива (группа геотехнологий), за ценные замечания и предложения по редактированию текста данной статьи. Мы также благодарим факультет электроники и информационных технологий и заведующего кафедрой электротехники Национального института технологии им. М. Висвесарая, все руководство предприятий SECL, BCCL и WCL, у которых были получены соответствующие данные в ходе исследований энергоэффективности и сопоставительного анализа.

Для цитирования

Topno S.A., Umre B.S., Aware M.V., Sahoo L.K. Internal and cross sectional benchmarking of electrical energy use in opencast coal mine. *Mining Science and Technology* (*Russia*). 2023;8(3):232–244. https://doi.org/10.17073/2500-0632-2023-03-100

Nomenclature

SPC	Specific power consumption, kWh/t
SPC_{BM}	Benchmark SPC, kWh/t
$SPC_{\mathrm{mine},BM}$	Mine Benchmark SPC, kWh/t
$SPC_{\min}$	Minimum SPC, kWh/t
E_c	Annual energy consumption, kWh
E_s	Energy-saving potential, %
Q_t	Annual composite production, t /y
Q_{coal}	Annual coal production, t/y
Q_{ob}	Overburden handled, t/y
ρ_{ob}	Bulk density of overburden, t/cu.m.
V_{ob}	Volume of overburden, cu.m./y

Subscripts and superscripts

a, *e*, *p*	Aggregate, equipment, progressive
i, *j*, *k*, *r*	month, year, equipment, mine

Abbreviations

Tr	Transformer
SECL	South Eastern Coalfields Ltd
BCCL	Bharat Coking Coal Limited
WCL	Western Coalfields Limited
CIMFR	Central Institute of Mining & Fuel Research
CSIR	Council of Scientific and Industrial Research

Introduction

Coal production is an energy-intensive operation in an opencast mine. Coal production in India accounts for 78 per cent of total mineral sector production. India produced 730.87 MT (million tons) of coal during 2019–2020[1] mined from both underground as well as surface mining methods. In India, about 94 % of the total coal production comes from opencast mining[2]. According to our review of data, it was found that the Specific Energy Consumption (SEC) of best practices opencast positive gradient mine in India is 123 MJ/t [1]. The Specific energy consumption of three large opencast mines of China when compared varies from 90–225 MJ/t [2]. Similarly, SEC for total operation for seven Canadian opencast mines varies from 97–256 MJ/t[3]. In India, the energy consumption in mining and quarrying consumes about 2.39 % of

[1] Ministry of Coal, Government of India. URL: https://coal.gov.in/index.php/major-statistics/production-and-supplies

[2] I bid.

[3] Canadian Industry Program for Energy Conservation (CIPEC). Benchmarking the energy consumption of Canadian open-pit mine. Report No. 2005. URL: https://www.nrcan.gc.ca/sites/www.nrcan.gc.ca/files/oee/pdf/publications/industrial/mining/open-pit/Open-Pit-Mines-1939B-Eng.pdf

industrial energy usage[4] and the US mining industry consumes about 12 % of total industrial energy consumption[5].

As the energy consumption in opencast mines is high involving energy-intensive operations such as drilling, loading, hauling, pumping, coal handling etc., its energy monitoring and performance evaluation is of paramount importance. Energy benchmarking is a powerful tool to assess the energy performance targeted towards a process, plant, commercial buildings etc. Benchmarking can be done by comparing the energy performance of similar plants including best practices in the specific sectors against one another also termed 'cross-sectional benchmarking'. Benchmarking is also feasible internally by time series analysis. The statistical approach has been applied by Boyd et al. for benchmarking energy in industrial sectors [3]. Cooke and Randal used a statistical method to establish an energy use benchmark by calculating energy consumption and production [4]. These approaches are defined as 'statistical energy benchmarking'. Model-based energy benchmarking for glass industries has been discussed by Sardeshpande et al. [5]. Beerkens et al. compared the specific energy consumption of glass furnaces for benchmarking the energy efficiency of glass furnaces [6]. Tan et al. developed an energy efficiency benchmarking methodology for the manufacturing industry [7]. Internal benchmarking of the industry has been done using linear Regression analysis of monthly energy consumption and production. Similarly benchmarking based on the best practices in terms of energy efficiency has been done for shopping centres in Gulf Coast region by Juaidi et al., [8]. From the above-mentioned review, it is learnt that there is a need for internal benchmarking as well as cross-sectional benchmarking to be applied for energy savings and enhancing energy efficiency. This fact has been supported by Wang et al. who revealed that there is no literature available on energy efficiency and benchmarking of mines [9]. Our attempt has been focused on Indian Coal mines. Techniques such as time series analysis, internal and cross-sectional benchmarking have been tried considering 4–5 years of field data.

Further, an analysis about mines indicates that Sahoo et. al [10, 11] has evaluated the energy efficiency of dump trucks in opencast mine. SEC have been used as an energy efficiency indicator for assessing the energy performance of mine dewatering systems [12], and for benchmarking energy efficiency of energy intensive industries in Taiwan [13]. Topno et al. used SPC as a performance indicator for benchmarking electrical energy consumption in a coal mine [14, 15]. In the present paper, benchmarking electrical energy use of opencast coal mine has been attempted by comparison method to know the performance of mine in different periods (yearly). The principal objective is to evaluate its best operational practices and set targets for the coming year. Energy performance during different operational conditions, round the year, has also been studied to get the practical benchmark for the opencast mine. A modelling framework has been developed for benchmarking using a statistical approach that remains applicable for mine. The model is extended further for electric energy usage in similar opencast mines in India. The model is tested in a large opencast coal mine of India using time series data by a statistical approach. Aggregate annualized data, as well as equipment wise data, have been analyzed to predict the benchmark SPC. The benchmark so obtained gave us the minimum power required for the mining process, which is the best practice followed within the mine during the past years. Energy-saving potential (plant) has been assessed that leads to continuous improvement and increased efficiency. The present paper is an extended work of energy efficiency benchmarking of power consumption in opencast mine by Topno et al. [14]. Apart from benchmarking in a mine, cross sectional benchmarking has been included.

1. Mining processes and energy usage

The mining process in an opencast mine includes drilling, blasting, excavation, transportation, crushing and sizing of the coal (Fig. 1). The coal extraction process from the mine could be either conventional, manual or mechanized. The major operating equipment in large opencast mine include high capacity electric rope shovels for loading operations, high capacity dump trucks for transportation of ore, diesel excavators, dozers and electric pumps for dewatering. The coal handling plant in opencast mine use crushers and vibrating screens to get sized coal as per the requirement of user. It is evident that to perform all major unit operations, input energy is needed. For bulky and heavy-duty mining operations in opencast coal mines, electrical power and diesel power (used as fuel in machines) are the major energy sources. The electricity consumption in shovel-dumper operated opencast mine accounts for 52 % of total energy supplied to the mine.

[4] Government of India, Ministry of Statistics and Programme Implementation, Energy statistics 2018: Central statistics office. URL: http://mospi.nic.in/publication/energy-statistics-2018

[5] US Energy information and administration, US Industrial sector energy consumption by type of Industry. URL: https://www.eia.gov/energyexplained/use-of-energy/industry.php

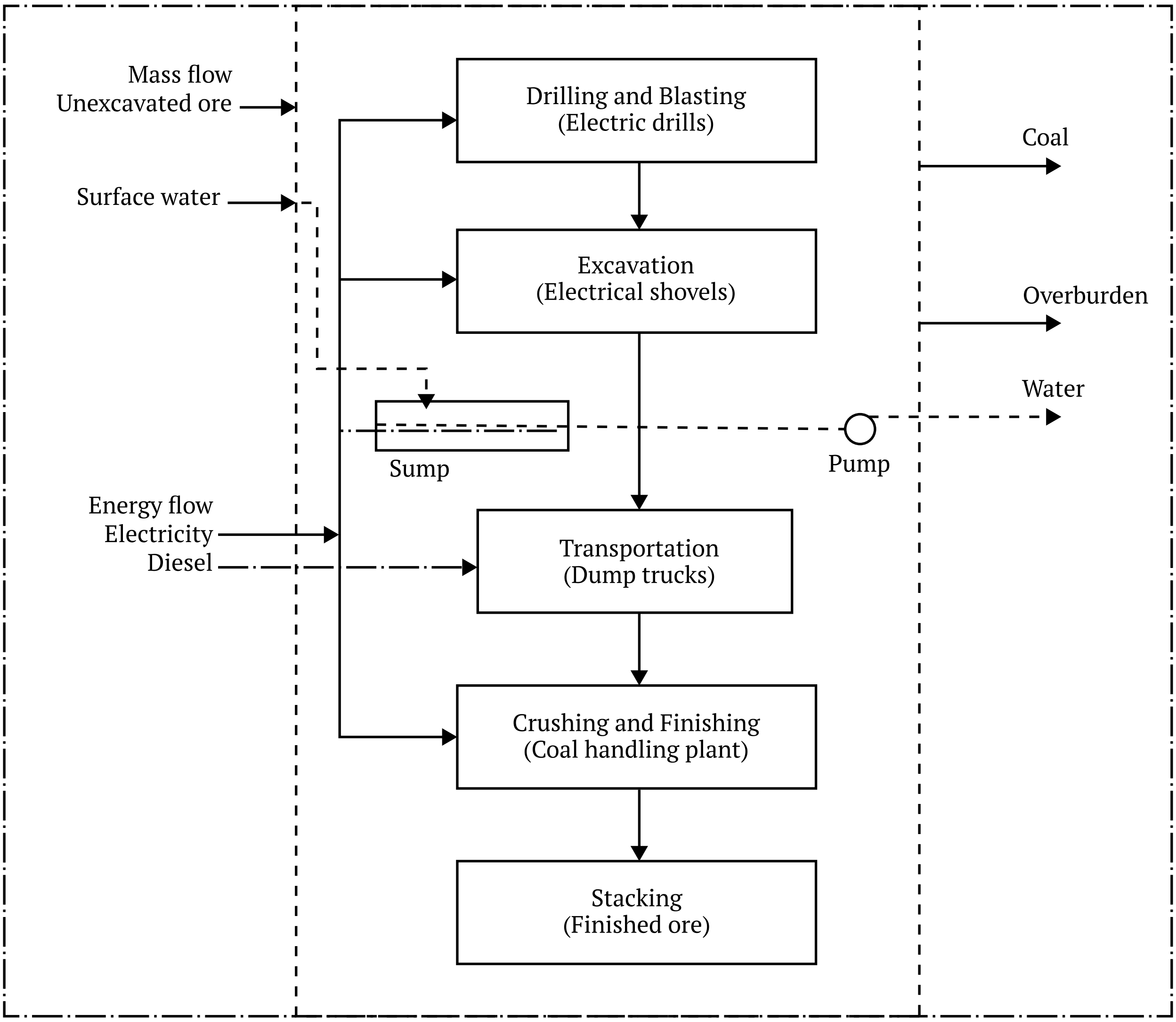

Fig. 1. Mining process of an opencast mine [14]

1.1. Electrical energy usage in opencast mine

As said above, energy input to the mine is diesel and electricity. Because of mobility, most or all HEMM's has Diesel as energy input mainly for operation whereas the electrical equipment, to which we targeted our study, are cables shovels, drills, crushers and coal handling plant (CHP) pumps and mine lighting. The energy consumption profile of an opencast coal mine (shovel-dumper combination) having a Coal Handling Plant (CHP) in terms of percentage has been depicted in Fig. 2. The share of electric operated shovels and CHPs is highest (more than 50 % of the total electrical energy input of the mine). Pumps contribute to 18 % of energy share, thus affecting the specific power consumption of the mine. This energy consumption is further linked with the rainfall that occurred in the mine area and pump usage i.e. running hours of the pump (s).

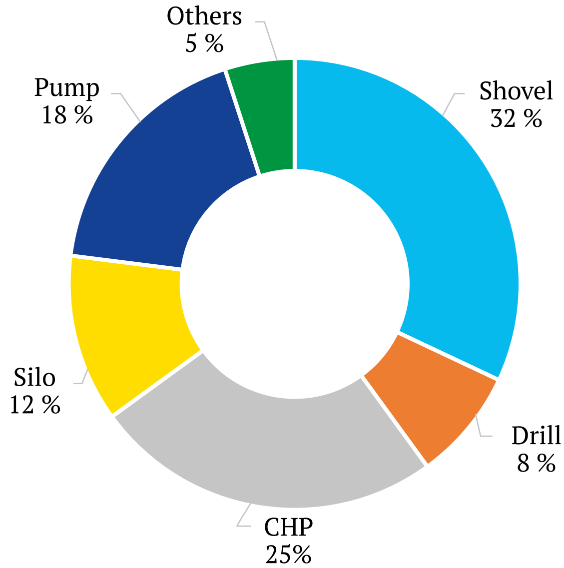

Fig. 2. Energy profile

1.2. Electrical energy distribution

Like the energy usages, the distribution of electrical energy has equal importance. 'High voltage' and 'Medium voltage transmission systems, are the two most important electrical distribution systems in nearly all the surface mines (an open-pit mine). High-voltage distribution line feeds most quarries since the electrical loads are generally located far from distribution mains. In the present case electrical power is supplied from 132/33 kV grid substation through step-down transformers (2 Nos. @ 36 MVA each). Primary voltage of 33 kV is common for mining equipment like electric shovels and drills. Coal handling plant, pumps and lightings are fed through medium/low lines of 6.6 kV/3.3 kV/440V. The single line diagram of the electrical distribution is shown in Fig. 3.

2. Methodology

Benchmarking for power consumption of open-cast coal mines has been done using a 'statistical approach'. Following two methods have been used:

1. Internal benchmarking (within the mine).
2. Cross-sectional benchmarking.

2.1. Internal Benchmarking

A statistical model is developed for specific power consumption (SPC) benchmarking from past data of power consumption and composite production. A flow diagram of the methodology (Fig. 4) shows the steps involved and the stages of model is described in Fig. 5. This is significant to note here that the energy has been used for handling both overburden and coal (a mineral). A composite production is considered for energy performance assessment and internal benchmarking i.e. within the mine.

The formula used for the specific power consumption (SPC) and monthly/yearly progressive consumption of process, equipment or a mine is described in the following paragraphs using equations 1 to 8 for detailed understanding further.

Progressive SPC of each process/equipment

The specific power consumption (SPC) for each progressive year (j = 1, 2...4) of all equipment/processes (drills, electric shovels, coal handling (CHP), pumps) is calculated using Eq. (1)

$$SPC_{j,k} = \frac{\sum_{k=1}^{n} E_{c,j,k}}{Q_{t,j}} \quad (j = 1, 2, 3...), \tag{1}$$

where each equipment (k) is noted for shovels ($k = 1$), drills ($k = 2$), CHP ($k = 3$), Silo pumps and other miscellaneous equipment and E_c is the total yearly energy consumption for each equipment/process $k = 1, 2; ..., n$; Q_t is total composite production (the sum of coal production (Q_{coal}) and overburden handled (Q_{ob})) for $j = 1, 2...4$ and (Q_t):

$$Q_t = Q_{coal} + Q_{ob}, \tag{2}$$

where

$$Q_{ob} = \rho_{ob} V_{ob}. \tag{3}$$

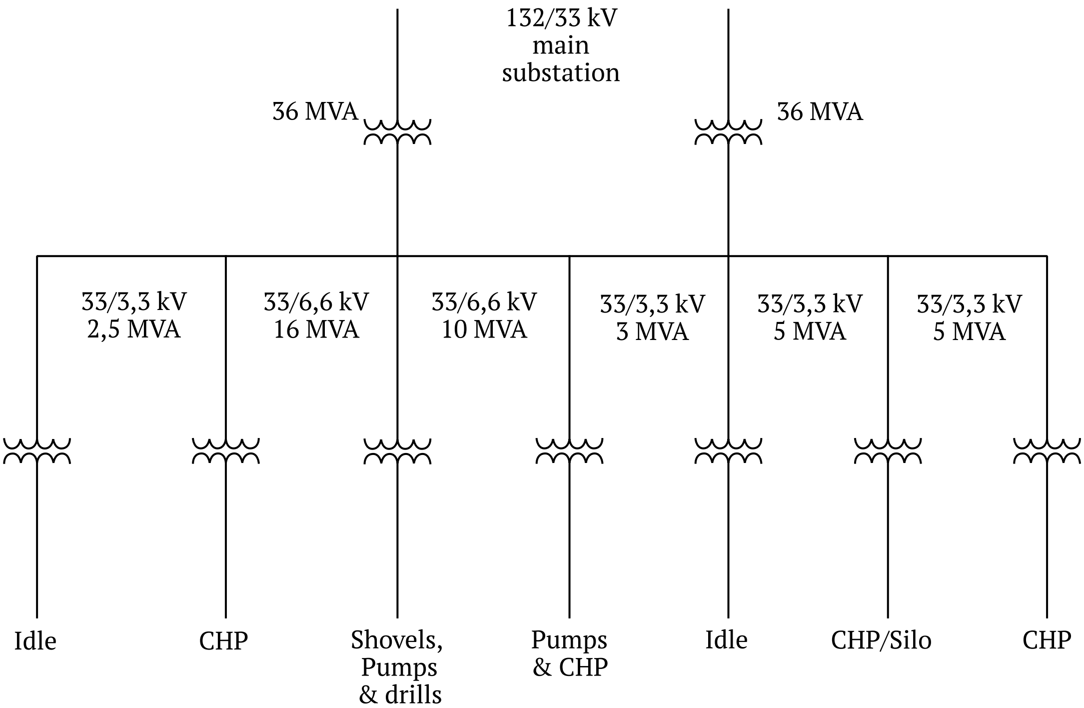

Fig. 3. Electrical distribution of an opencast coal mine

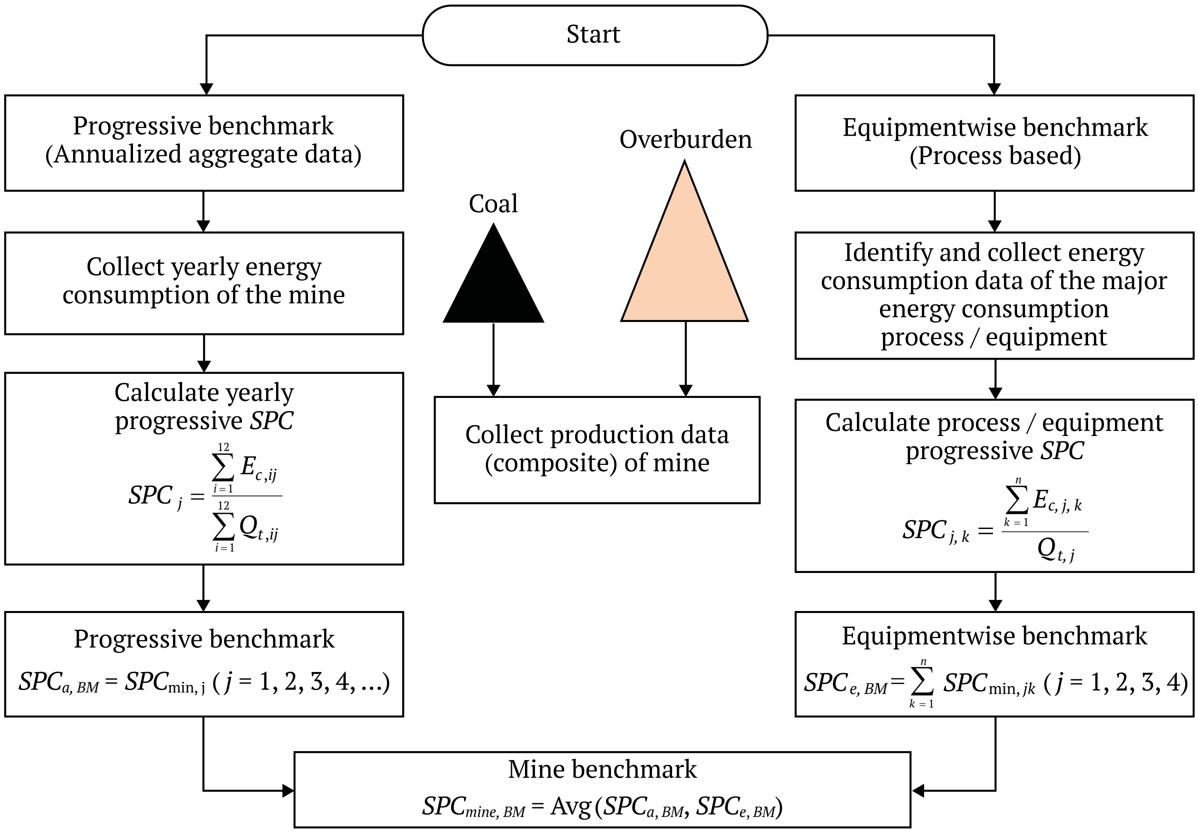

Fig. 4. Benchmarking methodology

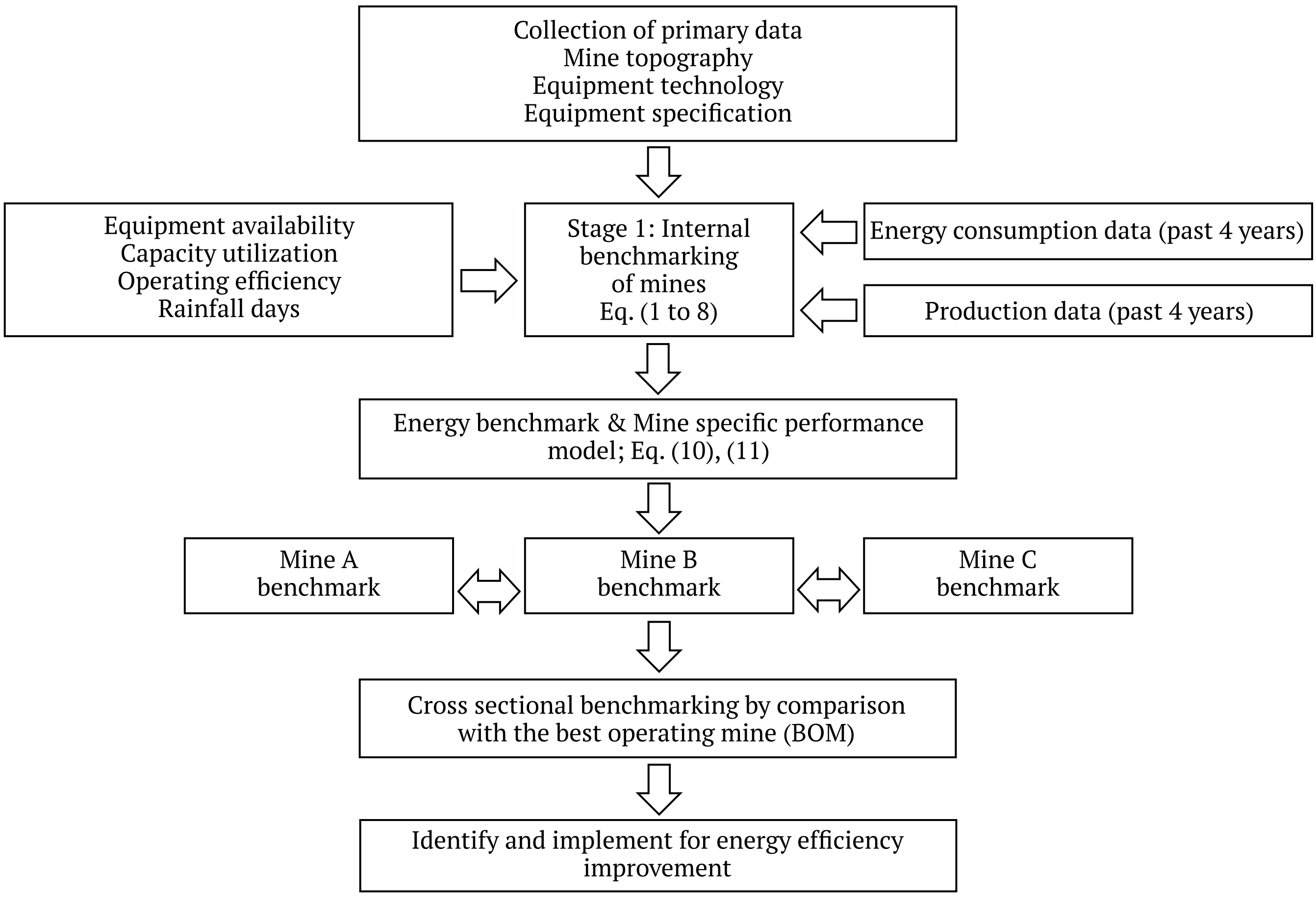

Fig. 5. Steps and the stages of the statistical model

Monthly and Yearly Progressive SPC of mine

SPC in kWh/t is defined as the ratio of total electrical consumption (E_c) to the composite production (Q_t) of a specific month/year. It has been evaluated using aggregated data of monthly/yearly energy consumption and composite production. Both, monthly as well as annual progressive SPC i.e. SPC_i & SPC_j has been studied to analyze the variations.

The monthly SPC is given as:

$$SPC_i = \frac{E_{c,i}}{Q_{t,i}} \quad (i = 1, 2, 3, ..., 12), \tag{4}$$

where $E_{c,\,i}$ – the energy consumption for ith month of the year and $Q_{t,\,i}$ – the composite production for the corresponding month.

The yearly progressive SPC (SPC_j) of j^{th} year is given as:

$$SPC_j = \frac{\sum_{i=1}^{12} E_{c,ij}}{\sum_{i=1}^{12} Q_{t,ij}} \quad (j = 1, 2...4). \tag{5}$$

Mine Benchmark

The benchmark SPC of the mine ($SPC_{\min\, e,\, BM}$) for the upcoming year is calculated from the average of the benchmark obtained from the Progressive SPC of each process/equipment and that obtained from the yearly progressive SPC of the mine.

The progressive SPC benchmark of equipment/process ($SPC_{e,\, BM}$) is estimated as

$$SPC_{e,\,BM} = \sum_{k=1}^{n} SPC_{\min,\,jk} \quad (j = 1, 2...4). \tag{6}$$

Yearly benchmark SPC for the mine is obtained by comparing progressive SPC of past 4 years and is obtained as:

$$SPC_{a,\,BM} = SPC_{\min,\,j}\,(j = 1, 2, 3, 4). \tag{7}$$

Hence, the overall benchmark of the mine is given as Eq. (9).

$$SPC_{mine,\,BM} = \mathrm{Avg}\,(SPC_{e,\,BM}, SPC_{a,\,BM}). \tag{8}$$

2.2. Cross-sectional benchmarking

The cross-sectional benchmarking, for SPC, can be calculated or modelled using Eq. (9). This remains applicable for similar coal mines having shovel-dumper combination only and gets affected with the methodology of extraction (mining), equipment used, coal/ore/material handled and operational practices of the electric equipment:

$$SPC_{BM} = SPC_{\min,\,r}\,(r = 1, 2, 3, ..., m). \tag{9}$$

3. Case study

The statistical approach of benchmarking has been applied for evaluating a large opencast coal mine named, *Dipka Opencast Coal Mine*, located at Korba in the Chhattisgarh state of India. The mine is owned by M/s South Eastern Coalfields Ltd (SECL) – A Government Public Sector Company and is considered as an important and productive colliery of India. The input data of energy consumption, production (material handled by the mining equipment and utilities) was collected as primary data from the field visit of the *Dipka mine* during different periods of this study. The connected electric load of the mine is 38.49 MW that includes, 6.6 kV electric shovels of 42 m³ & 10 m³ bucket capacity; 3.3 kV/440 V pumps; Coal handling plant; Silos, and other electrical loads. The annual power consumption of the mine is 49 GWh (2014–2015). The installed production capacity of the mine is 25 MTPA and has an average stripping ratio of 1 : 1 which means one cubic meter volume of coal extraction will require 1 cubic meter overburden removal.

3.1. Energy performance

Dipka mine deploy different equipment in coal production. The equipment-wise SPC has been calculated from the electrical energy consumption of individual equipment operating in the mine using Eq. 1. given in the previous section. Fig. 6 shows the yearly variation of average SPC for each equipment. The average SPC has been considered for benchmarking due to the seasonal variation of electrical load. The minimum, maximum and average SPC of shovel, drill, pumps and CHP for the mine is analysed and the SPC band for mine equipment is shown in Fig. 7. The equipment operating and its energy characteristics is given as Table 1.

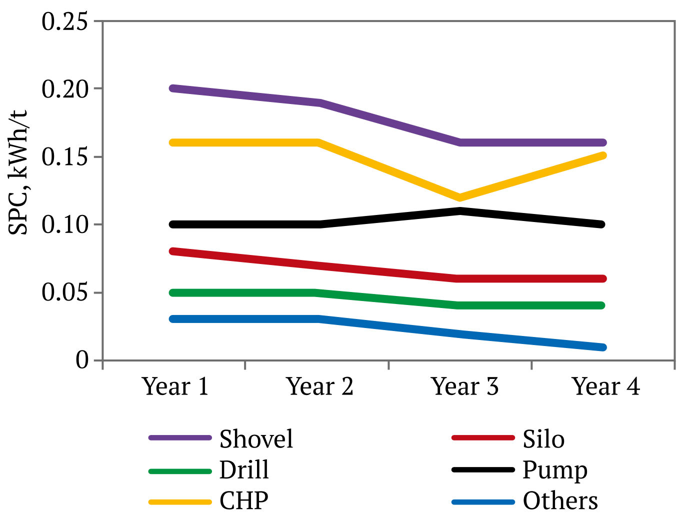

Fig. 6. Equipment-wise analysis of progressive SPC

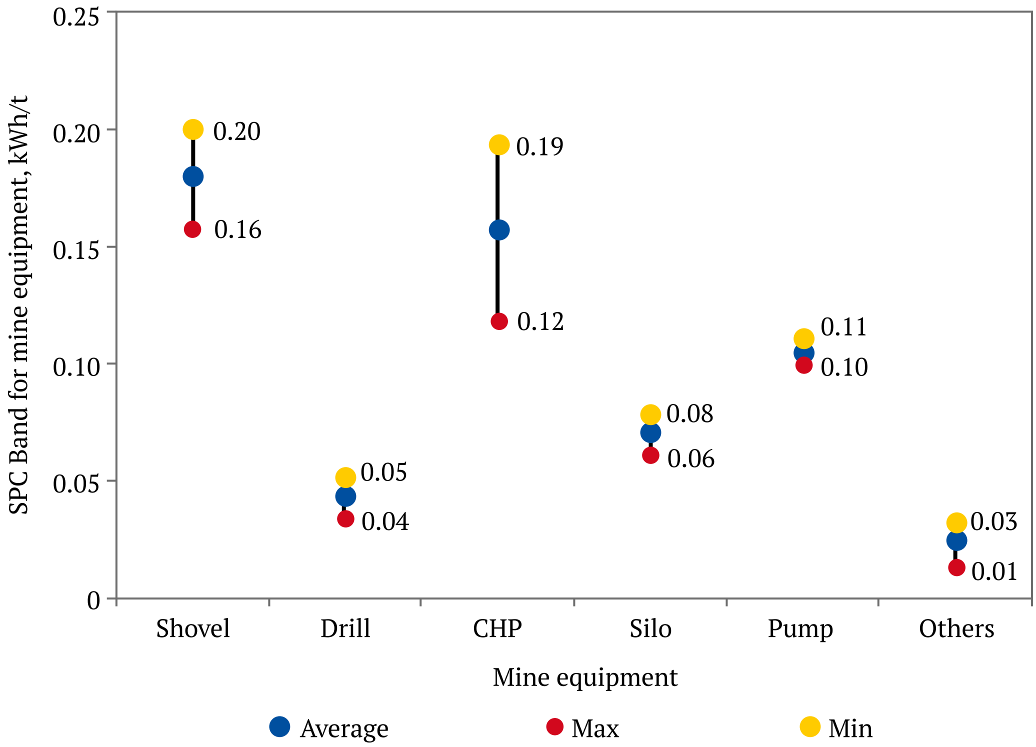

Fig. 7. SPC Band for mining equipment

Table 1

Equipment and energy characteristics of opencast mine (Case study)

Name of equipment	Process	Capacity	Make	Energy input	Energy usage, MUs/Kl/year*
Electric rope shovels	Excavation	42 cu.m	P &H and Bucyrus	Electricity (6.6 kV)	16
Electric shovel		5–10 cu.m			
Hydraulic shovels	Excavation	4,3 cu.m	BEML BE 1000	Diesel	1005
Payloader		0.96–10 cu.m			
Electric Rock drills	Drilling	–	–	Electricity (6.6 kV)	3
Hydraulic Rock drills	Drilling	6.3 inch dia, 8 m depth	IDM 30	Diesel	380
Large mining dump trucks	Transportation	240 t, 120 t, 100 t	BEML / Caterpillar / Terex	Diesel	6715
Large Dozers	Transportation	320 hp / 410 hp / 850hp	BH-35-II CAT834B Komatsu	Diesel	2899
Coal handling plant (CHP) and Silos	Crushing and sizing of coal	–	–	Electricity	20
Pumps	Pumping of mine water	2775 LPS	–	Electricity	10
Total energy consumption		–	–	–	49 MU

* MU = kWh in case of electricity consumption); Kl/year – in case of diesel consumption).

Table 2

Analysis of annual progressive SPC of coal mine

Year	Total Units consumed, kWh · 10^6	Coal, Mt	OB, Mt	Composite Production, Mt	SPC Composite, kWh/t
2011–2012	34.87	25.00	31.10	56.10	0.62
2012–2013	37.49	29.13	33.59	62.72	0.60
2013–2014	40.24	29.18	49.10	78.28	0.51
2014–2015	49.30	31.00	63.73	94.73	0.52
Average	40.48	28.58	44.38	72.96	0.56

Table 3

Analysis of annual progressive SPC of coal mine

Mines studied*	Annual energy, kWh · 10^6	Coal production, Mt	OB production, Mt	Composite production, Mt	SPC Composite, kWh/t
A	49	31	63.73	94.73	0.517
B	118	41	61.085	102.09	1.156
C	50	18.75	61.46	80.21	0.623
D	16.5	2.51	11.81	14.32	1.15
E	18	2.59	4.0145	6.60	2.727
F	8	1.34	2.077	3.42	2.339

* Means: Operating mines, Similar to the mine studied with different production capacity.

From Fig.7 it is clear that the minimum SPC of an electric shovel is 0.16 kWh/t and that of CHP is 0.12 kWh/t; for the pump is 0.10 kWh/t . The benchmark SPC of the mine based on the mining equipment and other utilities is 0.49 kWh/t. The SPC band for CHP is very wide due to variations in flow of coal input to the crushers and conveyors. For shovels, the SPC band is also high due to variations in operational practices and materials handled in the mine. The benchmark SPC by equipment-wise analysis is calculated as 0.49 kWh/t by comparing specific energy consumption data of all equipment.

3.2. Benchmark SPC within the mine

Progressive SPC of the mine is calculated from the annualized electrical energy consumption in the mine and the corresponding composite production. Analysis of annual progressive SPC of coal mining is given in Table 2. The average progressive SPC is 0.56 kWh/t of composite production whereas the minimum SPC is 0.51 kWh/t. Using Eq. (9) the benchmark SPC of the mine is estimated as 0.50 kWh/t.

3.3. Benchmark SPC for similar mines

The cross-sectional benchmarking of six operating mines (Mine – A, B, C, D, E, F) has been done by comparing the specific power consumption (Table 3)[6]. All these opencast mines of different capacities are the coal mines having similar features comparable with the mine, studied here.

4. Results and discussions

The estimated benchmark SPC for the case study is 0.50 kWh/t. However, the monthly SPC has wide variation throughout the year due to monsoon and the average minimum SPC for the off-rainy season is 0.43 kWh/t and for the rainy season, it is 0.52 kWh/t. The average progressive SPC is 0.56 kWh/t. Comparing the benchmark SPC and average SPC, the electrical energy saving potential is calculated as 10.7 %. The energy-saving areas can be identified by a detailed investigation based on a field trial of equipment operating in the mine using sophisticated energy audit instruments. A performance trial was conducted on P&H electric shovel operating in Dipka opencast mine and the SPC was calculated from the actual material handled and energy consumption for validation of the result. The SPC of an electric shovel alone is calculated as 0.18 kWh/t and accounts for 36 % of the total electricity consumption.

[6] CIMFR studies and technical communications on energy efficiency and benchmarking in Opencast mines. 2015.

MINING SCIENCE AND TECHNOLOGY (RUSSIA)
ГОРНЫЕ НАУКИ И ТЕХНОЛОГИИ
eISSN 2500-0632
https://mst.misis.ru/
2023;8(3):232–244

4.1. Mine-specific energy performance model

The linear regression method has been used to obtain the correlation between specific power consumption (*SPC*) and composite production (*Q*) and the analysis results are summarized (Fig. 8). The variations of SPC with the composite production have been plotted. The scatter plot shows the relationship between the yearly aggregated progressive specific power consumption (SPC_a) and composite production (Q_t) and is given as Eq. (10) (the R^2 value of linear regression is 0.791):

$$SPC_a = -0.002Q_t + 0.771. \qquad (10)$$

The linear trend has a negative slope and indicates that SPC decreases with an increase in composite production. The above linear model can be used for the prediction of SPC with an increase or decrease in production rate. From Fig. 9 it is clear that energy consumption increases with the increase in composite production whereas SPC decreases due to optimum utilization of the mining equipment deployed at the mine. The model can be used to predict the SPC of the mine for varying material handling rates. A modelling framework was developed by Topno et al. [15] for assessing energy performance of electric shovel operating in the same opencast mine and the results obtained for *SPC* is 0.12 kWh/cu.m.

For another mine specific model given as Eq (11); a linear regression model from the actual aggregated past data of specific power consumption and composite production for a mine of different topography, equipment and energy characteristics as given in Table 4.

$$SPC_a = -6 \times 10^{-8}Q_t + 1.8995. \qquad (11)$$

Fig. 10 shows the linear model with different x-coefficient and constant. The constant and x-coefficient changes from mine to mine depending on both mine topography, equipment and their energy characteristics.

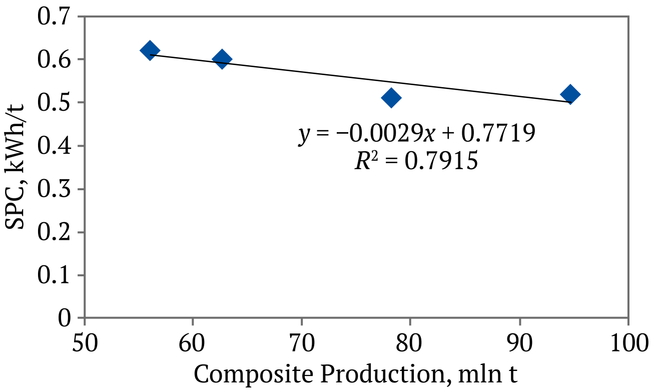

Fig. 8. Variation of SPC with production

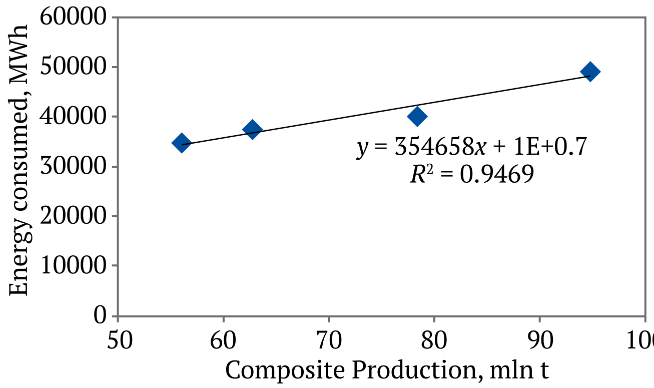

Fig. 9. Variation of electrical energy consumption

Table 4

Mine equipment and energy characteristics of Mine D

Name of equipment	Process	Capacity	Energy input	Energy usage (MUs)/Kl/year
Electric shovel	Excavation	2.4 Cu.m / 5 Cu.m / 10 Cu.m	Electricity (3.3 kV & 6.6 kV)	16.5 MU
Electric Rock drills	Drilling	160 mm		
Coal handling plant (CHP) and Silos	Crushing and sizing of coal	–		
Pumps	Pumping of mine water	732 lps.	Electricity 3.3 kV / 415 V	
Hydraulic shovels Payloader)	Excavation	3.5 Cu.m	Diesel	1557.6
Hydraulic Rock drills	Drilling	160 mm	Diesel	871.6
Medium mining dump trucks Scania dumpers	Transportation	(60 t, 50 t, 35 t)	Diesel	3106.6
Dozers	Transportation	320 hp/BD155 410 HP/BD355	Diesel	978.1

* MU = Million units (Million kWh in case of electricity consumption); Kl/year = kilo litres/year (in case of diesel consumption).

The specific power consumption in the present models given in Eq (10) and Eq (11) shows its variation at different composite production for two opencast mines of different capacity, equipment characteristics as well as their energy consumption profiles. The equipment and energy characteristics affect the energy performance of the mine.

4.2. Seasonal analysis of SPC

A time-series data of monthly SPC has been plotted in Fig. 11. The analysis shows that the specific power consumption is higher during the month of July-October than the period between November-June. The composite production during these months is lower due to the effect of monsoon on mining operation and poor capacity utilization of electric shovels, drills etc. Further, the SPC is higher due to the increased load of pumps used for dewatering. The monthly minimum SPC of the off-rainy season and the rainy season plot (Fig. 12) shows that the average SPC varies from 0.43 kWh/t to 0.52 kWh/t. The seasonal analysis of SPC helps the mine management to prepare a monsoon plan to reduce energy consumption by optimizing the pump and machine operation schedule.

4.3. Benchmarking of similar coal mines

The results obtained by comparison of different opencast coal mines, studied by CSIR-CIMFR[7] for different energy efficiency projects are presented in Table 3, Fig. 13.

The aggregated SPC of similar coal mines varies between 0.52 kWh/t to 1.15 kWh/t, minimum being 0.52 kWh/t. As large mines (production capacity more than 30 Mt) makes use of high capacity electric shovel which are the major electrical consuming equipment (36 %). In smaller mines, producing 1.3 Mt to 2.6 Mt of coal, the SPC varies between 1.15 to 2.72 kWh/t.

4.4. Energy-saving potential

Estimation of the electrical energy saving potential, by comparing the progressive benchmark SPC ($SPC_{p,\ BM}$) and annualized average ($SPC_{a,\ Avg}$) is possible for a coal mine and this calculation is done using Eq. 12 given below.

[7] CIMFR studies and technical communications on energy efficiency and benchmarking in Opencast mines. 2015.

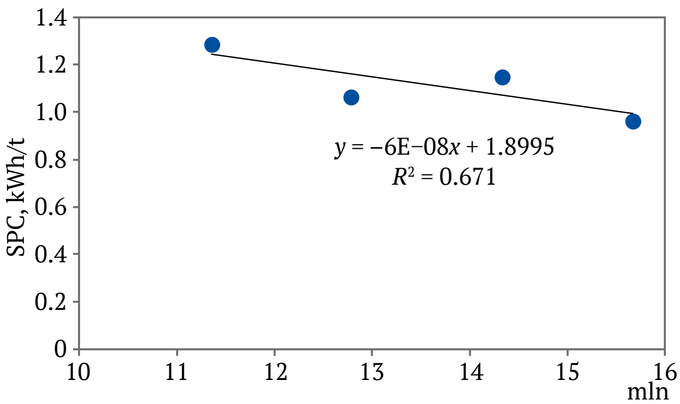

Fig. 10. The linear model with different x-coefficient and constant

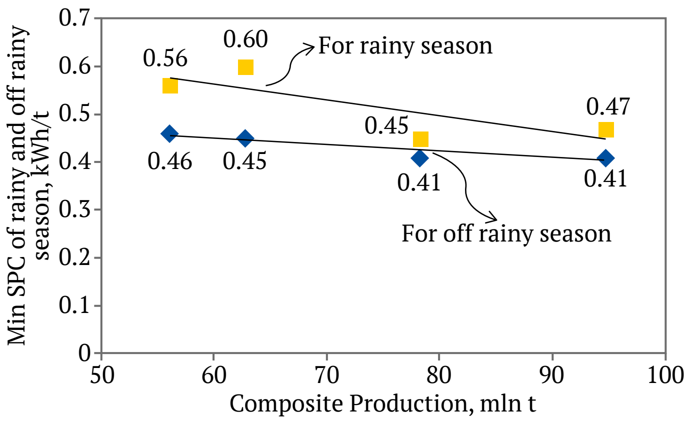

Fig. 12. Monthly SPC for the off-rainy and rainy season

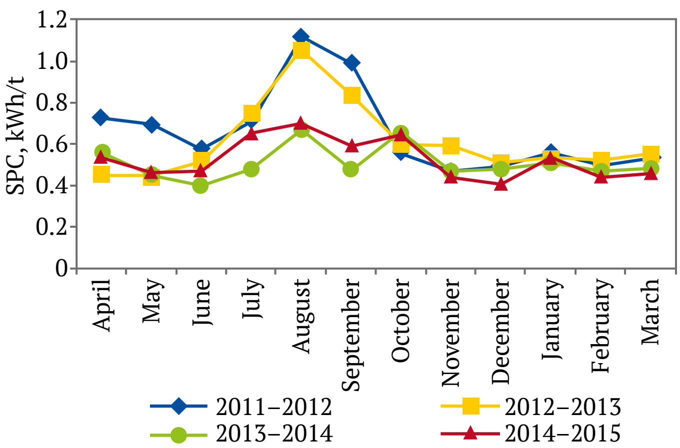

Fig. 11. Seasonal analysis of SPC

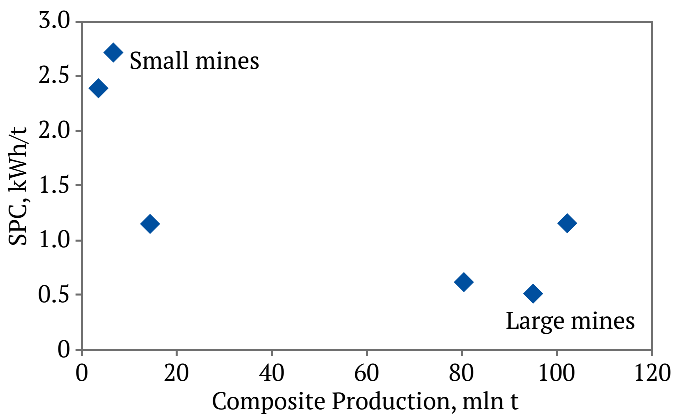

Fig. 13. The results obtained by comparison of different opencast coal mines

$$E_s = \frac{(SPC_{a,\,Avg} - SPC_{p,\,BM}) \cdot 100}{SPC_{a,\,Avg}}, \qquad (12)$$

where ($SPC_{a,\,Avg}$) is the average of annual progressive SPC and is given by Eq. (13)

$$SPC_{a,\,Avg} = \frac{\sum_{j=1}^{4} SPC_j}{4}. \qquad (13)$$

As per Eq. (12), the energy-saving potential of the mine is 10.7 % for the studied mine, which vary on each progressive year, based on the analysis of four years of data and the actual operating condition of the mine.

Conclusions

Benchmarking energy consumption is an effective tool to assess and compare the energy performance of the mines. Opencast surface mines, producing coal (or other minerals) are the industrial beneficiaries of the benchmarking. Both, internal benchmarking and cross-sectional benchmarking can be used by the mine management to identify the key areas that require performance improvement to reduce energy consumption and set up targets for the mining sector, to reduce industrial energy consumption. In this research paper, benchmarking work of the electrical energy usage for a large opencast mine of India has been done and the progressive benchmark SPC is estimated as 0.50kWh/t.

A new method of comparison and modelling using past operating data for each process as well as aggregated data of composite production and energy consumption, have been applied for various surface coal mines of both small size and large size. Linear regression methods have been used for solving the present mine specific data. Especially, coal mines of the Indian mining industry are targeted to predict the benchmark SPC. The benchmark obtained by internal benchmarking is useful to assess the energy efficiency of a specific mine and the SPC obtained by cross-sectional benchmarking is useful to assess the best performing mines with the best practices. The energy-saving potential of the mine has also been assessed.

In brief, it is concluded that the energy performance evaluation of a specific mine or a group of mine is feasible by benchmarking models suggested in this paper for mining sector and benefits by assessing and implementing the energy saving potential.

References

1. Sahoo L.K., Bandyopadhyay S., Banerjee R. Benchmarking energy efficiency of opencast mining in India. In: *Proceedings of the 4th International Conference on Advances in Energy Research (ICAER-2013)*. 10–12 December 2013, Mumbai, India. Pp. 1684–1692.

2. Shuzhao C., Qingxian C., Cangyan X., Wang H. Energy consumption comparison and energy-saving measures of open pit development. In: *Proceedings of International Conference on Computer Distributed Control and Intelligent Environmental Monitoring (CDCIEM)*. 19–20 February 2011, Changsha, China. Pp. 712–715, https://doi.org/10.1109/CDCIEM.2011.64

3. Boyd G., Dutrow E., Tunnessen W. The evolution of the ENERGY STAR® energy performance indicator for benchmarking industrial plant manufacturing energy use. *Journal of Cleaner Production*. 2008;16(6):709–715. https://doi.org/10.1016/j.jclepro.2007.02.024

4. Cooke D., Randall C. Energy use benchmarks for open cut coal mines. In: Proceedings of The AusIMM annual conference. 23–26 March 1995, Newcastle, Australia. URL: https://old.decoa.com.au/HTMLobj-480/Energy_Use_Benchmarks_Coal_Mines.pdf

5. Sardeshpande V., Gaitonde U.N., Banerjee R. Model-based energy benchmarking for glass furnace. *Energy Conversion and Management*. 2007;48(10):2718–2738. https://doi.org/10.1016/j.enconman.2007.04.013

6. Beerkens R.G.C., Limpt J.V. Chapter 7. Energy efficiency benchmarking of glass furnaces. In: Kieffer J. (ed.) *62nd Conference on Glass Problems: Ceramic Engineering and Science Proceedings, Vol. 23*. The American Ceramics Society; 2008. Pp. 93–105. https://doi.org/10.1002/9780470294727.ch7

7. Tan Y.S., Tjandra T.B., Song B. Energy efficiency benchmarking methodology for mass and high-mix low-volume productions. *Procedia CIRP*. 2015;29:120–125. https://doi.org/10.1016/j.procir.2015.02.200

8. Juaidi A., AlFaris F., Montoya F.G., Agugliaro F.M. Energy benchmarking for shopping centres in the Gulf Coast region. *Energy Policy*. 2016;91: 247–255. https://doi.org/10.1016/j.enpol.2016.01.012

9. Wang N., Wena Z., Liu M., Guo J. Constructing an energy efficiency benchmarking system for coal production. *Applied Energy*. 2016;169:301–308. https://doi.org/10.1016/j.apenergy.2016.02.030

10. Sahoo L.K., Bandyopadhyay S., Banerjee R. Benchmarking energy consumption of dump trucks in mines. *Applied Energy*. 2014;113:1382–1396. https://doi.org/10.1016/j.apenergy.2013.08.058

11. Sahoo L.K., Bandyopadhyay S., Banerjee R . Benchmarking energy consumption of truck haulage. In: Awuah-Offei K. (eds.) *Energy Efficiency in the Minerals Industry. Green Energy and Technology.* Springer, Cham; 2018. https://doi.org/10.1007/978-3-319-54199-0_9

12. Sahoo L.K., Bandyopadhyay S., Banerjee R. Water and energy assessment for dewatering in opencast mines. *Journal of Cleaner Production*. 2014;84:736–745. https://doi.org/10.1016/j.jclepro.2014.07.072

13. Chan D.Y.L., Huang C.F., Lin W.C., Hong G.B. Energy efficiency benchmarking of energy-intensive industries in Taiwan. *Energy Conversion and Management*. 2014;77:216–220. https://doi.org/10.1016/j.enconman.2013.09.027

14. Topno S.A., Sahoo L.K., Umre B.S., Jhungare A.S. Energy efficiency benchmarking of power consumption for an opencast coal mine. In: *Efficiency, Cost, Optimisation, Simulation and Environmental Impact of Energy Systems (ECOS 2017)*. 2–6 July 2017, San Diego, California, USA.

15. Topno S.A., Sahoo L.K., Umre B.S. Energy efficiency assessment of electric shovel operating in opencast mine. *Energy*. 2021;230:120703. https://doi.org/10.1016/j.energy.2021.120703

Information about the authors

Seema Ashishan Topno – Principal Investigator, CSIR-Central Institute of Mining & Fuel Research, Nagpur Research Centre, Nagpur, India; Visvesvaraya National Institute of Technology, Department of Electrical Engineering, Nagpur, India; ORCID 0000-0003-2941-3047, Scopus ID 57202512585; e-mail seematopno@rediffmail.com

Bhimrao Sitaram Umre – Ph. D. (Electrical Engineering), Professor, Department of Electrical Engineering, Visvesvaraya National Institute of Technology, Nagpur, India; ORCID 0000-0002-9879-2928, Scopus ID 24483922300; e-mail bsumre@rediffmail.com

Mohan Vithalrao Aware – Ph. D. (Electrical Engineering), Professor, Department of Electrical Engineering, Visvesvaraya National Institute of Technology, Nagpur, India; ORCID 0000-0003-3806-7908, Scopus ID 6602631834; e-mail mvaware@eee.vnit.ac.in

Lalit Kumar Sahoo – Principal Investigator, CSIR-Central Institute of Mining & Fuel Research, Nagpur Research Centre, Nagpur, India; ORCID 0000-0001-8924-6741, Scopus ID 55901599900; e-mail lalitsahoo@yahoo.co.in

Received 23.03.2023
Revised 17.07.2023
Accepted 15.08.2023

MINING SCIENCE AND TECHNOLOGY (RUSSIA)
ГОРНЫЕ НАУКИ И ТЕХНОЛОГИИ
eISSN 2500-0632
https://mst.misis.ru/
2023;8(3):245–259

POWER ENGINEERING, AUTOMATION, AND ENERGY PERFORMANCE

Research paper

https://doi.org/10.17073/2500-0632-2022-12-70
UDC 621.316.575

Simulation of protection against unbalanced high-voltage asynchronous drive of recycle compressor in fuel hydrotreating unit

V.V. Dmitrieva ✉, **A.B. Khammatov**
I.M. Gubkin Russian State Oil and Gas University, Moscow, Russian Federation
✉ *dm-valeriya@yandex.ru*

Abstract
In the oil and gas industry, continuous processes such as oil and gas refining play a great role and are sensitive to many external factors. Such processes require special procedures for stopping and restarting. In order to maintain a sustainable process, the entire system needs to be cleaned by removing of unreacted components. Rejected raw materials are often dumped into a flare leading to tangible environmental problems and significant economic disadvantages. Electrotechnical systems (ETS) play an important role in ensuring continuous technological processes in oil and gas industry. Electric motors are one of the key elements of ETS. The majority of the electrical machines used in industry today are Asynchronous motors (AM) – no less than 80 %. Ensuring their trouble-free operation is one of the key factors in the design, simulation, and analysis of asynchronous motor relay protection systems, including unbalanced conditions of their operation. These conditions can occur due to unbalanced AM connection circuits, supply voltage unbalance, or as any faults in a machine itself. Operating a motor under these conditions will result in shorter motor life, reduced power, wear and aging of the insulation. The study subject was an Asynchronous motor drive of a recycle compressor of a gasoline hydrotreating unit at the fuel hydrotreating integrated unit at the Astrakhan Gas Refining Plant (AGRP). The authors used Matlab simulations to study the facility and its protection systems/devices operation. The method of symmetrical components was selected as the main theoretical method. The authors developed a model of an asynchronous motor drive of a recycle compressor. This involved establishing a set of relay protections (RP) and developing the models of the following protections: sequence filter (symmetrical component filter) (SF), negative sequence (nps) O/C protection, and overload protection. It was demonstrated that the specified relay protection complex fully protects the motor from unbalanced operation conditions. The authors conducted a study of the protection complex operation under different supply voltage unbalances, with different motor loads. They formed a conclusion about the performance of the developed protection complex, and gave recommendations for its technical implementation in a business environment. The study findings can be used as a basis for the development and testing of relay protection components of the entire electrical system of the fuel hydrotreating unit at the Astrakhan Gas Refining Plant.

Keywords
asynchronous motor, unbalanced conditions of operation, unbalanced supply voltage, relay protection, structural simulation, sequence filter, negative sequence O/C protection, overload protection, Sepam1000+, Matlab, Simulink

For citation
Dmitrieva V.V., Khammatov A.B. Simulation of protection against unbalanced high-voltage asynchronous drive of recycle compressor in fuel hydrotreating unit. *Mining Science and Technology* (*Russia*). 2023;8(3):245–259. https://doi.org/10.17073/2500-0632-2022-12-70

ЭНЕРГЕТИКА, АВТОМАТИЗАЦИЯ И ЭНЕРГОЭФФЕКТИВНОСТЬ

Научная статья

Моделирование защиты от несимметричных режимов работы высоковольтного асинхронного привода циркуляционного компрессора в установке гидроочистки топлив

В.В. Дмитриева ✉, **А.Б. Хамматов**
РГУ нефти и газа (НИУ) им. И.М. Губкина, г. Москва, Российская Федерация
✉ *dm-valeriya@yandex.ru*

Аннотация
В нефтегазовой промышленности большую роль играют непрерывные технологические процессы, например, нефте- и газопереработка, которые чувствительны к многим внешним факторам. Такие процессы требуют реализации специальных процедур для остановки и повторного пуска. Для на-

ладки технологического процесса необходимы очистка всей системы от непрореагировавших компонентов и их удаление. Забракованное сырьё зачастую сбрасывается на факел, что влечет за собой ощутимые экологические проблемы и значительный экономический ущерб. Важную роль в обеспечении непрерывных технологических процессов в нефтегазовой промышленности играют электротехнические системы (ЭТС), одним из ключевых элементов которых являются электродвигатели. Большую часть, не менее 80 %, используемых сегодня в промышленности электрических машин, составляют асинхронные двигатели (АД). Безаварийная их работа является одной из ключевых задач, что обеспечивает актуальность проектирования, моделирования и анализа действия систем релейных защит асинхронного двигателя, включая несимметричные режимы их работы. Эти режимы могут возникнуть при несимметричных схемах включения АД, несимметрии питающего напряжения, а также в результате каких-либо неисправностей в самой машине. Работа двигателя в таких условиях приведет к сокращению срока его службы, снижению мощности, износу и старению изоляции. В качестве исследуемого объекта выбран асинхронный электропривод циркуляционного компрессора блока гидроочистки бензина в комбинированной установке гидроочистки топлив, расположенного на Астраханском газоперерабатывающем заводе (АГПЗ). Для исследования работы и его защит авторы использовали моделирование в программе Matlab. В качестве основного теоретического метода выбран метод симметричных составляющих. Авторы разработали модель асинхронного электропривода циркуляционного компрессора; сформировали комплекс релейных защит (РЗ) и разработали модели следующих защит: «фильтр симметричных составляющих» (ФСС), максимальная токовая защита обратной последовательности «МТЗ $I_{\max\ \text{обр}}$», защита от перегрузки. Продемонстрировано, что указанный комплекс релейной защиты полностью защищает двигатель от несимметричных режимов работы. Авторами было проведено исследование работы комплекса защит при различных несимметриях питающего напряжения, при различной загрузке двигателя, сделан вывод о работоспособности разработанной защиты, а также даны рекомендации по его технической реализации на производстве. Выполненная работа может быть положена в основу разработки и тестирования релейной защиты элементов всей электротехнической системы установки гидроочистки топлив на Астраханском ГПЗ.

Ключевые слова
асинхронный двигатель, несимметричные режимы работы, несимметрия питающего напряжения, релейная защита, структурное моделирование, фильтр симметричных составляющих, максимальная токовая защита, защита от перегрузки, Sepam1000+, Matlab, Simulink

Для цитирования
Dmitrieva V.V., Khammatov A.B. Simulation of protection against unbalanced high-voltage asynchronous drive of recycle compressor in fuel hydrotreating unit. *Mining Science and Technology* (*Russia*). 2023;8(3):245–259. https://doi.org/10.17073/2500-0632-2022-12-70

Introduction. Statement of problem

In the oil and gas industry, continuous processes such as oil and gas refining play a great role and are sensitive to many external factors. Such processes require special procedures for stopping and restarting. In order to maintain a sustainable process, the entire system needs to be cleaned by removing unreacted components. The rejected raw materials are often dumped into a flare leading to tangible environmental problems and significant economic disadvantages. Electrotechnical systems (ETS) play an important role in ensuring continuous technological processes in oil and gas industry. Electric motors are one of the key elements of ETSs. The majority of the electrical machines used in industry today are Asynchronous motors (AM) – no less than 80 %. Ensuring their trouble-free operation is one of the key factors in the design, simulation, and analysis of asynchronous motor relay protection systems, including unbalanced conditions of their operation.

This paper discusses the design and simulation of a number of relay protections against unbalanced conditions of operation of an asynchronous motor [1]. The causes of such conditions can be both external, such as unbalance in the voltage supplied to the motor [2], and defects in the machine itself. If unbalance occurs due to imperfections in the rotor circuit of the motor, the torque is the sum of the torques of the positive-phase-sequence M_1 and negative-phase-sequence M_2:

$$M(s) = M_1 + M_2, \tag{1}$$

and this dependence curve will have a dip at torque creep $s \approx 0.5$. Since a negative-phase-sequence field is stationary with respect to the stator, it does not create currents in the stator. Therefore, the torque due to this field will be zero. If $0 \le s \le 0.5$. The magnetic field will rotate relative to the stator in the negative direction, and the torque M_2 will act on the rotor in the direction of rotation. If $0.5 \le s \le 1$, the field rotates relative to the stator in the positive direction, and the torque M_2 created by this field will act on the rotor against the direction of rotation. If there is significant resistance unbalance in the secondary circuit, the motor will not reach normal R.p.m. This effect is maximal when one rotor phase fails.

MINING SCIENCE AND TECHNOLOGY (RUSSIA)
ГОРНЫЕ НАУКИ И ТЕХНОЛОГИИ
2023;8(3):245–259
eISSN 2500-0632
https://mst.misis.ru/

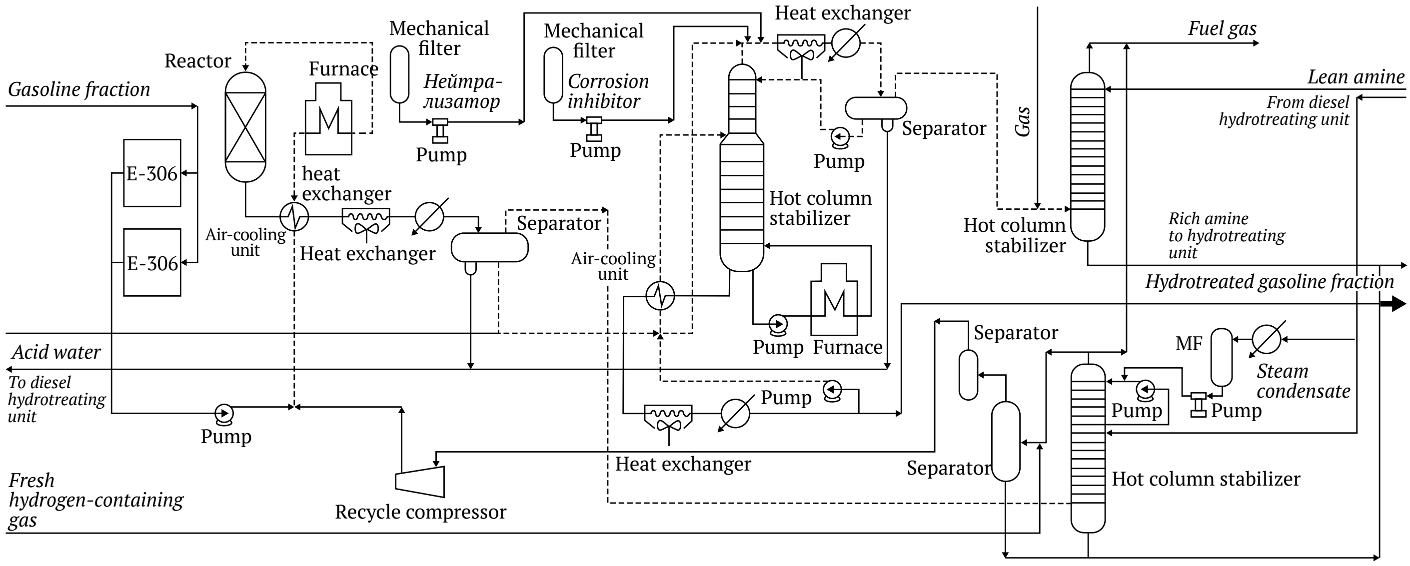

Fig. 1. Basic process flow diagram of gasoline fraction hydrotreating unit

If the cause of unbalanced AM operation conditions is the unbalance of voltages supplied to the stator winding ($U_{AB} \neq U_{BC} \neq U_{CA}$), the phase voltages will not be equal to each other ($U_A \neq U_B \neq U_C$). The influence of unbalance [3] on the operation of an asynchronous motor is investigated by the method of symmetrical components. In the case of an unbalanced power supply, the maximum $M_{\max}$ and starting M_{start} torques of the motor are reduced and the torque creep increases, while the loading torque remains unchanged due to the influence of the negative-phase-sequence. In addition, when the motor is supplied with unbalanced voltage, its efficiency decreases, the losses increase, and consequently motor heating also increases. This can affect the life of the winding insulation. For example, with a voltage unbalance of 2 %, the service life of a motor is reduced by 10 % due to additional losses of active power. For this reason, if there is a strong voltage unbalance, the motor power has to be reduced. Thus, the work of an asynchronous motor at unbalanced supply voltage is undesirable, and the study of asynchronous motor protection systems is an urgent task.

Currently, in Russia, the quality indicators of electrical energy according to the national technical standard GOST 32144-2013 are standardized in terms of the negative-phase-sequence voltage unbalance factor K_{2U} and zero-phase-sequence voltage unbalance factor K_{0U}. The maximum permissible values for these quality indicators are 2% and 4% respectively, which are averaged in the time interval of 10 minutes for 95% and 100% of the time for a week[1].

[1] GOST 32144–2013. Quality standards of electrical energy in power supply systems of general purpose. Moscow: Standards Publishers; 2014. 15 p.

Description of the research subject

The study subject was an asynchronous motor drive of a recycle compressor of a gasoline hydrotreating unit of the fuel hydrotreating integrated unit at the Astrakhan Gas Refining Plant (AGRP). It is a more rational choice to study unbalanced motor operation conditions on powerful motors, as the effect of unbalance in this case will be better expressed.

The hydrotreating unit is designed for hydrotreating of 2 million tons/year of straight-run broad gasoline fraction NK-180°C (with possible weighting of the boiling point to 230°C) produced from Astrakhan gas condensate, broad fraction of light hydrocarbons, and distillate gasoline from a diesel hydrotreating unit. The working hours of the hydrotreating unit are 8000 hours per year. The operating regime of the unit is continuous. The process flow sheet of the gasoline hydrotreating is shown in Fig. 1. The process flow sheet of the gasoline hydrotreating unit includes:

– hydrotreating of raw feedstock with alumina-cobalt-molybdenum catalyst;

– cold separation of the gas-feedstock mixture;

– hydrotreated feed stabilization;

– gas-air regeneration of the catalyst;

– purification of hydrogen-containing gas and hydrocarbon gas with diethanolamine;

– corrosion inhibitor protection.

Fig. 1 shows the main unit components: a reactor, column-stabilizers, mechanical filters, pumps, heat exchangers, separators, and storage tanks (E-306). The direction of movement of NK-180 gasoline fraction is indicated by arrows. The facility under study is a **recycle compressor**, which pressurizes hydrogen-containing gas to produce a gas-feedstock mixture, which then goes through various process cycles: heating, hydrogenation, stabilization, cooling, and the resulting hydrogenate is taken out of the unit.

Control of the technological processes of the gasoline hydrotreating unit and the facilities of the gasoline hydrotreating unit with a pumping station is managed from an automated control system (APCS) from a single workplace of a process control operator. The APCS is a hierarchical multifunctional commercial design-composable software and hardware complex based on microprocessor hardware with modular architecture [4]. The system provides on-line monitoring and control of all process operations of the unit, collection, accumulation, processing and displaying of information on the technological process, stabilization of key parameters, alarming of equipment operation and valve positions, blocking and protection of the unit from emergency situations, emergency alarms, and equipment fault detection.

The power supply system of the gasoline hydrotreating unit includes a distribution point. The scheme is shown in Fig. 2:

– TsK-1, TsK-2 are VSG 2GC2-47/35-44M UHL4 recycle compressors (complete with 1000/TF/LB/D00908 dry gas seals control panel). Asynchronous electric motors 4 AZMP-2000/6000 UHL4 (U_{rated} = 6000 V; P_{rated} = 2000 kW; n = 3000 rpm; explosion protection IExdIIBT4) are installed as drives;

– N-1/1, N-1/2, N-1/3 — 1NPS-E200/700 centrifugal vertical split casing oil pumps (with flat body connector). IBAO-560S-4Y2,5-T asynchronous motors are installed as drives. The product to be refined is a gasoline fraction. These pumps are used to feed gasoline fraction to the hydrotreating unit;

– UK-1 is capacitor unit (U_{rated} = 6000 V; Q = 450 kVAr (reactive kilovolt-ampere)) included in the scheme for compensation of reactive power, released on the electric motors TsK-1 (TsK-2);

– 1T, 2T are double-winding three-phase power transformers TSZL-1600/6/0.4 for powering transformer substation low-voltage load.

Research techniques

In order to study the operation of an asynchronous motor under unbalanced conditions, we used mathematical simulation. *Matlab* software package was used [5, 6] as a simulation program. We traditionally used the method of symmetrical components [7] in compiling the mathematical model of an AM.

The most suitable way of protecting electric motors is the development of protection equipment [8]. The complexity of its design, cost-effectiveness, accuracy of operation, and reliability are considered when evaluating the equipment. In order to avoid technological losses associated with asynchronous motor unbalanced operation conditions, a range of protection methods are applied [9, 10]. Since abnormal operation conditions will affect not just the motor, but also the protection itself, the protection equipment must have a high level of reliability [10, 11]. The methods of protection of electric motors from damage at unbalanced conditions of operation can be divided into preventive and technical. This requires the development and implementation of up-to-date protective means made on a microprocessor base [12, 13].

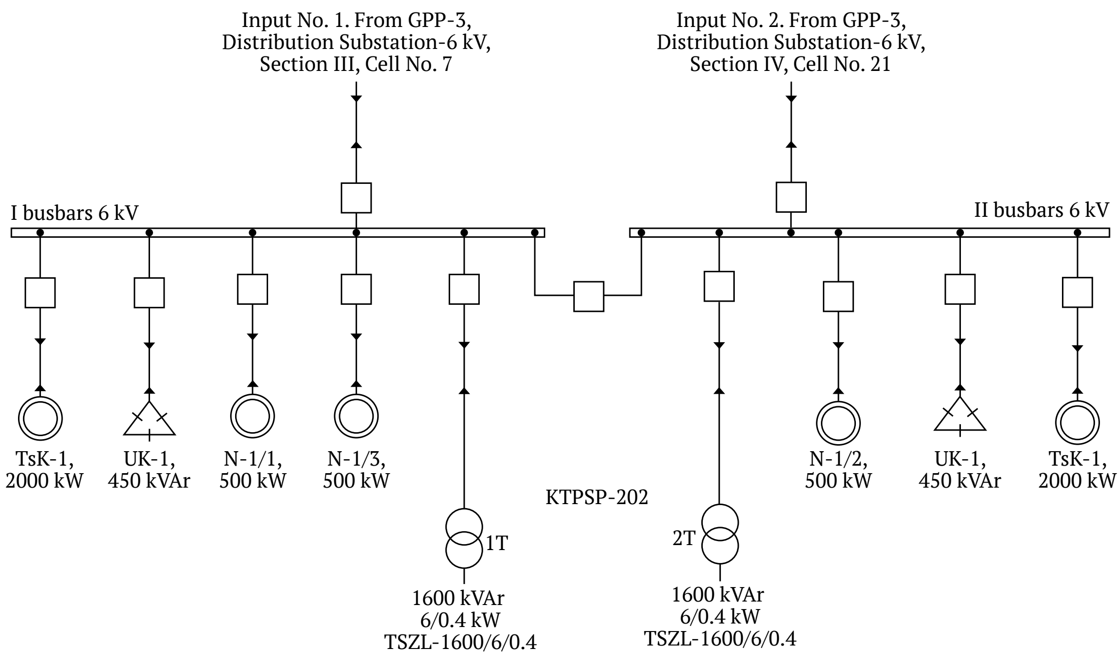

Fig. 2. Power supply diagram for gasoline hydrotreating unit

Devices of indirect type, tripping when stator windings temperature exceeds a preset level (devices of built-in temperature protection, phase-sensitive protection) and those of direct action, reacting to occurrence of negative- or zero-phase-sequence of voltage or current can be used to protect electric motors from unbalanced and single-phase conditions [14, 15].

Because these protections correspond not to the unbalance itself, but to its consequences, their operation is characterized by a large error of tripping, low reliability and response speed. Other disadvantages of these protections are complicated circuits, large mass and dimensions, and a high cost. In this regard, direct action devices are more promising, namely, special protection devices based on sequence filters.

Devices for AM protection against supply voltage unbalance can be based on zero and negative sequence filters and react to current or voltage unbalances.

Let us consider the advantages and disadvantages of relay protection based on current relays. Current protections with negative and zero sequence filters respond to all unbalanced conditions. These devices monitor the current as it flows through the stator phase circuits. Tripping of protections based on them does not depend on the point of connection. However, the use of current transformers decreases the protection reliability, increases power consumption and mass and dimensions of the devices. In addition, due to transformer core saturation, the protection has insufficient tripping accuracy [16]. Biased protections are used to increase the sensitivity of current filter protections.

If a protection is implemented on a voltage relay, it should be borne in mind that voltage relays do not have versatility, because they detect only one failure. The most suitable type of AM protection is the use of so-called voltage monitors which monitor several types of accidents (failures). Such monitors are bases on microprocessor devices. They are versatile, highly reliable, simple, inexpensive, and ensure timely shutdown of an electric motor in the event of unbalanced and single-phase conditions [12, 17].

At present, series 80 Sepam 1000+ microprocessor protection is being implemented at the facility in question, in order to ensure the protection of electrical equipment.

Let us consider the capabilities of Sepam 1000+ in the area of unbalanced power supply protection. In order to protect an asynchronous motor from overloads caused by unbalanced line voltage, a positive-phase-sequence minimum voltage protection $U^{(1)}$ is used. This protection trips when the component $U^{(1)}$ of a three-phase voltage system falls below the design tripping set-point of the protection U_{trip}. Protection against phase imbalance is implemented by measuring $U^{(2)}$. The time delay of both protections is independent.

Sepam 1000+ for implementing these protections operates on line or phase voltage and allows tuning out based on negative-phase-sequence voltage unbalance factor [14]

$$K_{2U} = \frac{U^{(2)}}{U^{(1)}} 100\,\%.$$

Negative-phase-sequence voltage unbalance factor and time delay set-points are set, in order to provide the protection against unbalance: K_{2U} = 20 % and t = 10 s. Current protections which identify unbalanced operation conditions include negative sequence overcurrent (O/C) protection, overload protection, and thermal protection. Negative sequence overcurrent protection produces a value of unbalance factor based on the negative-phase-sequence current. The protection has a dependent and independent time delay. Overload protection and thermal protection are designed to protect a motor against the overloads caused by unbalanced loads in operating conditions or abnormal grid regimes. They also detect the consequences of unbalance rather than unbalance itself, and are therefore less accurate.

The range of set-points of these protections is shown in Table 1[2].

Table 1

Range of set-points of Series 80 Sepam 1000+ protections

Protection function	Setting range	Time delay range, s
Protection against unbalanced supply voltage	K_{2U} = 0 ÷ 50 %	0.05–300
Negative sequence O/C protection with independent Δt	22.3–1130 A	0.1–300
Negative sequence O/C protection with dependent Δt	22.3–1130 A	0.1–1
Overload protection with independent Δt	1–6250 A	0.05–300
Overload protection with dependent Δt	1–6250 A	0.1–12.5 for 2260 A
Thermal protection	60–200°C	1–600 min

[2] Sepam 1000+ (Series 80) Installation and Application Manual.

Development of an asynchronous motor model and models of devices for relay protection against unbalanced operation conditions in Matlab Simulink

We will use the Asynchronous Machine block in the Matlab Simulink software package [18] to simulate an AM. 4AZM-2000/6000 UHL4 motor nameplate data are given in Table 2.

Table 2

4AZM-2000/6000 UHL4 motor nameplate data

Power, kW	2000
Rotation velocity, rpm	2973
Weight, kg	5600
Stator current, A	226
Slip, %	0,9
KPI	96.7
Power factor, p.u.	0.88
Peak torque brevity	1.9
Starting torque brevity	0.77
Starting current brevity	4.7

Based on the motor nameplate data, let us calculate the values of the motor model parameters in Matlab Simulink by the method described in [19]. The obtained parameters required for simulation are presented in Table 3.

Table 3

Parameters of 4AZM-2000/6000 UHL4 motor in Simulink

Reduced rotor active resistance, Ohm	0.419724
Active stator resistance, Ohm	0.888812
Reduced stator and rotor leakage inductance, henry	0.003531
Excitation circuit inductance, henry	0.127834
Moment of inertia, kg·m^2	187.07

The model of asynchronous motor protection against unbalanced supply voltage modes is based on the existing Sepam 1000+ protection. The protection set-points to be reflected in the model are given in Table 4. In order to simulate the unbalanced operation conditions of a motor and the means of its protection against unbalance, a scheme was constructed using the Matlab Simulink software package. It is shown in Fig. 3.

Table 4

Protection model set-points in Matlab Simulink

	Tripping	Release (reset)	t_{tr}, s
Sequence filter-based protection	$K_{2U} = 8$ %	$K_{2U0} = 6$ %	10
Overload protection	$I_{trip} = 350$ A	$I_{rel} = 300$ A	18
Negative sequence O/C protection	$I_{negative\ sequence\ O/C\ protection\ tripping} = 60$ A	$I_{rel} = 20$ A	10

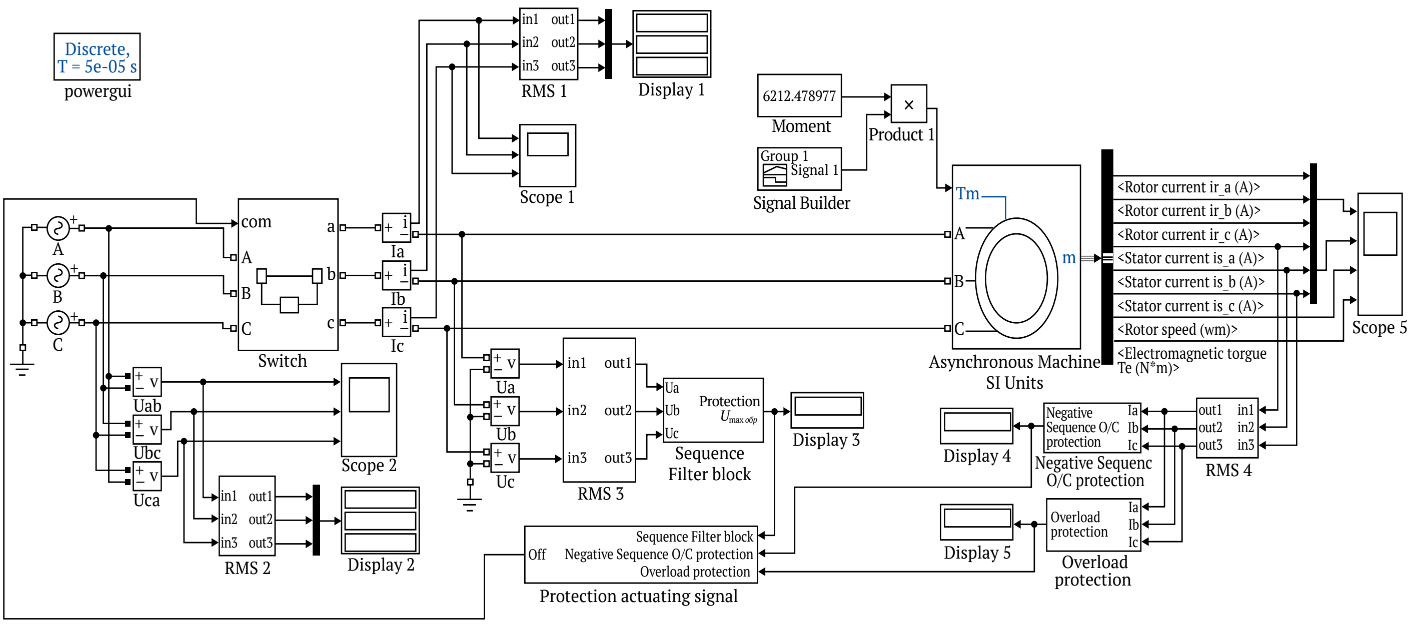

Fig. 3. Schematic of an asynchronous motor simulation in Simulink:
in1 – input 1; in2 – input 2; in3 – Input 3; out1 – output 1; out2 – Output 2; out3 – Output 3

Explanations for the scheme of simulation of an asynchronous motor in Simulink:

1. The input three-phase voltage is formed by three single-phase sources in the form of AC *Voltage Source* elements of *SimPowerToolbox* package: amplitude $A = 4898.98$ V, frequency $f = 50$ Hz; initial phase: 0° for phase A, −120° for phase B, and 120° for phase C.

2. Asynchronous motor: set by *Asynchronous Machine* block. The block parameters are selected in accordance with Table 3. The torque is set by *Signal Builder*, *Constant*, *Product*1 blocks for the soft start of a motor.

3. Three-phase breaker: set by *Three-Phase Breaker* block. This block is controlled by a signal, the open and closed key position resistances are stored by default at 10^6 и 10^{-2} ohms, respectively.

4. Current and voltage meters are set by *Current Measurement* and *Voltage Measurement*.

5. RMS1-RMS4 blocks are designed to measure rms current or voltage values.

6. Sequence filter protection: input quantities for the block are effective (rms) phase voltages, while the output quantities are the protection tripping signal and the value of negative-phase-sequence voltage unbalance factor. The measured voltages are converted into balanced (symmetrical) components of the positive- and negative-phase-sequence with the use of *Magnitude-Angle to Complex* block. *Divide* block is used to calculate K_{2U}; when the set-point set by *Relay* block $K_{2U} = 0.08$ is exceeded, a tripping signal is given with a time delay of 10 s.

7. Negative Sequence O/C protection: the input values are the motor stator rms currents, while the output is a tripping (protection actuating) signal. Similarly to the sequence filter, based on the measured line currents, negative-phase-sequence current is obtained and compared with a set-point. If the set-point is exceeded ($I_{trip} = 60$ A), the protection system gives a signal for tripping with a time delay of 10 s.

8. Overload protection: the input values are the motor stator rms currents, while the output is a tripping (protection actuating) signal. Maximum effective current is calculated using MinMax block and then compared with a corresponding set-point. If the set-point $I_{trip} = 350$ A is exceeded, a signal for tripping is given with a time delay of 18 s.

9. "Tripping signal": the input values are signals of tripped sequence filter, Negative Sequence O/C protection, and overload protection, while the output value is a tripping signal. *Logical Operator* 1–3 and Monostable blocks are used to open a breaker, and since this is accompanied by tripping the protections, no signal is given to activate the motor, so there is no looping of the simulation.

The internal structure of the above blocks complies with the protection algorithms. For a more compact and concise presentation, all of the above protections are enclosed in *Subsystem* blocks. As an example, Fig. 4 presents the "Sequence Filter" protection circuit.

The developed motor model and its protection circuit can be verified by simulating its rated operating conditions. Simulation of a motor operation at rated operating conditions presents transients which coincide with the reference processes of an asynchronous motor in terms of phase currents, line voltages, rotor and stator currents, rotor rpm, and electromagnetic torque of a motor.

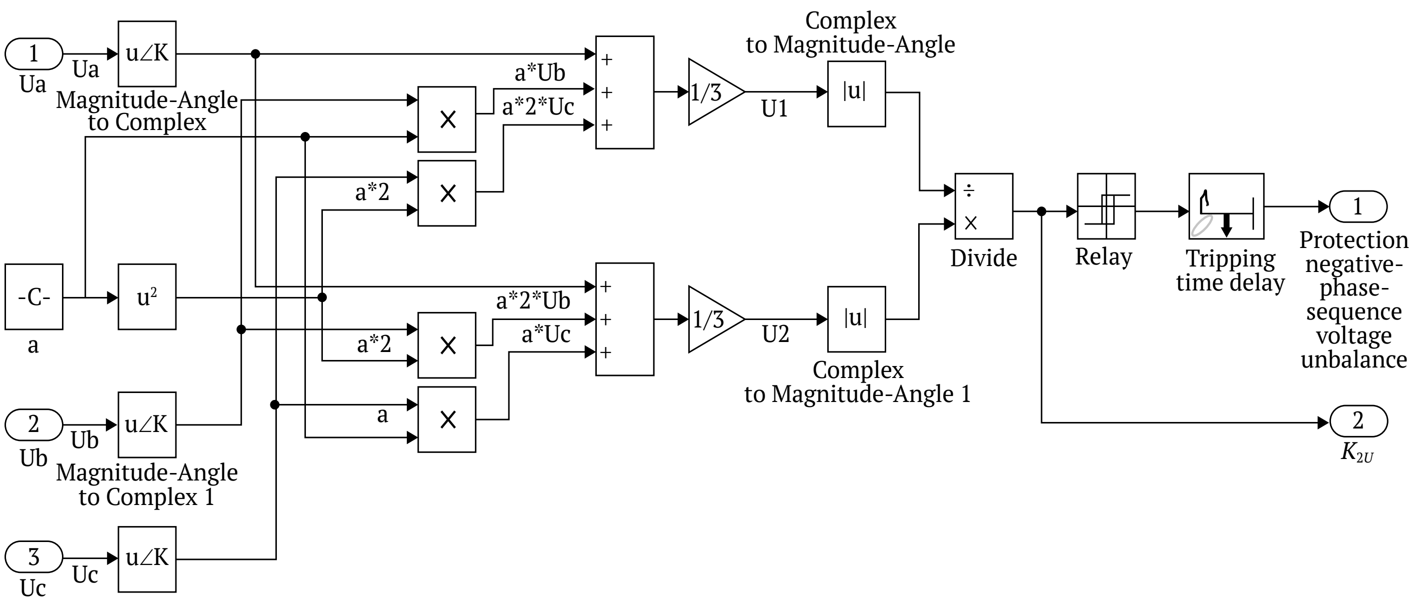

Fig. 4. Internal structure of the Sequence Filter block

1. Line currents during start-up (t = 0–8 c) are about 6 times the rated current; this corresponds to the motor nameplate data. When the motor reaches the rated r.p.m., the currents decrease and reach the rated values I_{rated} = 226 A.

2. Line voltages corresponding to the rated value throughout the simulation time $U_{l\text{-}rated}$ = 6000 V.

3. Signals formed by the protections models demonstrate that at the rated operating conditions, the protections do not trip, forming signal 0 on their outputs. These conditions correspond to 1 on the "Tripping Signal" block output, since when such a signal is applied to the circuit breaker, the breaker is closed.

Let us check the functionality of the installed protections by considering their operation under abnormal conditions of motor operation. The tests conducted by the authors have shown that when the load torque increases by 50 %, the overload protection trips. The other protections do not trip, since there are no negative-phase-sequence currents and voltages. The time diagrams show the protection tripping at time t = 18 s.

Let us now consider the operation of the protections when voltage changes in one of phases. When the voltage in phase A increases by 20 %, in line with voltage unbalance, current unbalance arises. However, at a given deviation, the level of negative-phase-sequence voltage unbalance factor K_{2U} = 6.07 % < $K_{2U\max}$ = 8 % is not enough for tripping a corresponding protection. The current deviation is sufficient to cause a negative-phase-sequence current exceeding the set-point of the negative sequence O/C protection I_2 = 80 A > $I_{2\max}$ = 60 A. The time diagrams show the protection tripping at time t = 10 s. The overload protection does not trip, since the stator currents decrease before reaching the time set-point t = 18 s.

If the voltage in one of the phases is reduced, the currents will decrease. However, a deviation of more than 20 % is necessary for the negative-phase-sequence voltage unbalance protection to trip. In this case, K_{2U} = 8.95 % > $K_{2U\max}$ = 8 %, and therefore the voltage unbalance protection trips, but I_2 = 50 A < $I_{2\max}$ = 60 A, so the negative sequence overcurrent protection does not trip.

We can see that the protections operate selectively and protect the motor from unbalanced operation conditions within the preset set-point limits. Consequently, the digital model developed allows not only motor operation at unbalanced supply voltage to be studied, but also conditions with the use of overload protection detected, negative sequence overcurrent protection. It also allows for protection based on a sequence filter.

Performance Results. Simulation of the processes in an asynchronous motor with unbalanced supply voltage

Let us consider model operation when the supply voltage is unbalanced [20]. By varying the voltages in each phase by ΔU = ±15 % U_{rated}, we can consider the deviations (changes) of negative-phase-sequence currents and voltage unbalance factor K_{2U}. Fig. 5 shows these voltage deviations. This diagram shows the values of deviation ΔU, %, in phases in the course of 43 tests. The legend of the diagram explains the display color of each phase. The same diagram shows the deviations in K_{2U} factor.

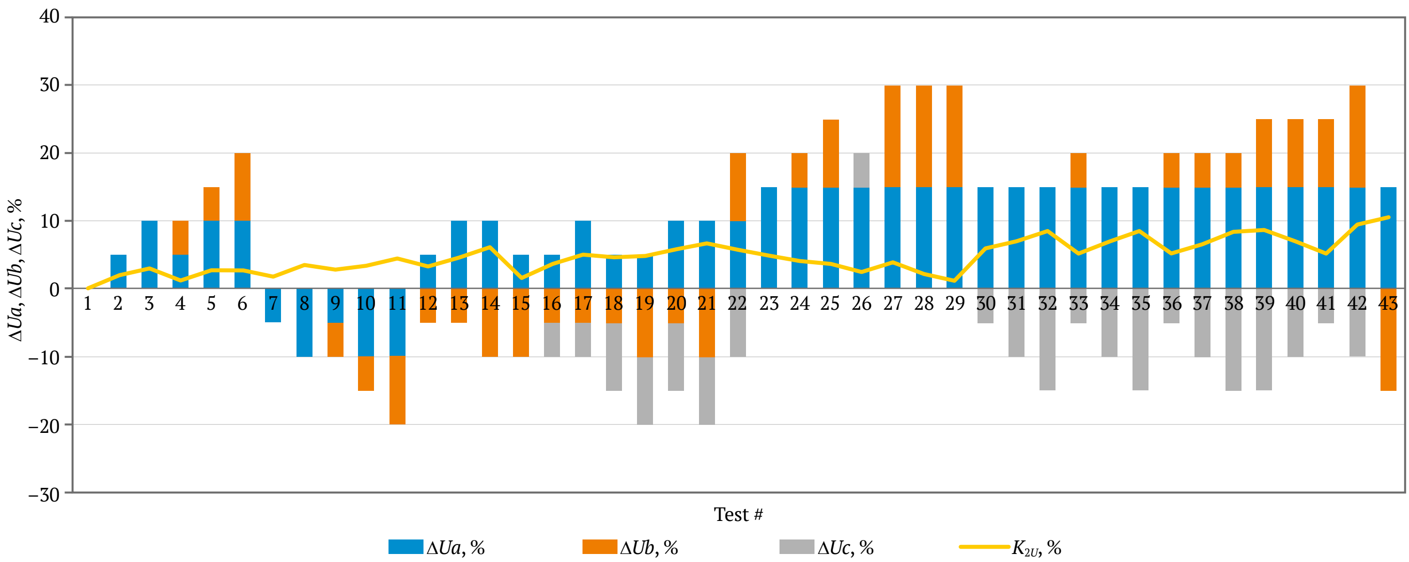

Fig. 5. Values of deviations in supply voltage phases

Next, Fig. 6 shows the dependence of negative-phase-sequence voltage unbalance factor K_{2U} on the deviations of the voltages in the phases.

The third diagram (Fig. 7) presents the currents in the motor phases *Ia*, *Ib*, *Ic* as functions of the voltages unbalance in the phases.

The tripping of simulated protections is also of interest. Table 5 presents the operations of protections operation and shows the results of the most representative part of the tests (those in which the protections trip).

Analysis of research findings

Fig. 8 shows an example of the simulation results in Simulink. The simulation results show that the negative-phase-sequence overcurrent (O/C) protection trips more often when the supply voltage is unbalanced. This can be explained by the fact that when the voltage level changes even in one of the phases of the source, this causes a change in currents in all motor phases. This, in turn, causes the unbalance of currents and arising negative-phase-sequence currents [21]. If the negative-phase-sequence current exceeds the set-point level of the time-delayed protection, the protection trips and the power supply is switched off. The simulation results allow the conclusion that the protection does not always respond equally to the same levels of voltage unbalance. For example, at K_{2U} = 4,9 % in one case (ΔUa = 5 %; ΔUb = 0 %; ΔUc = −10 %) the negative sequence overcurrent protection trips, while in another case it does not (ΔUa = 15 %; ΔUb = 0 %; ΔUc = 0 %). In cases where the level of unbalance is K_{2U} > 5 %, negative sequence overcurrent protection trips, and when it is K_{2U} > 8 %, the sequence filter protection also trips.

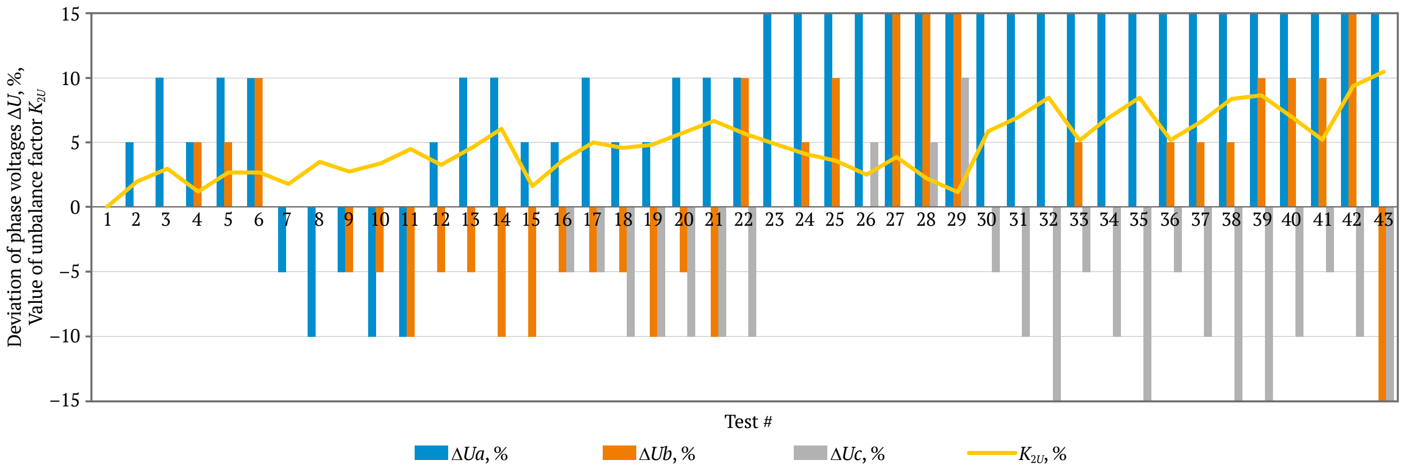

Fig. 6. Dependence of negative-phase-sequence voltage unbalance factor K_{2U} on phase voltage deviations ΔU, %

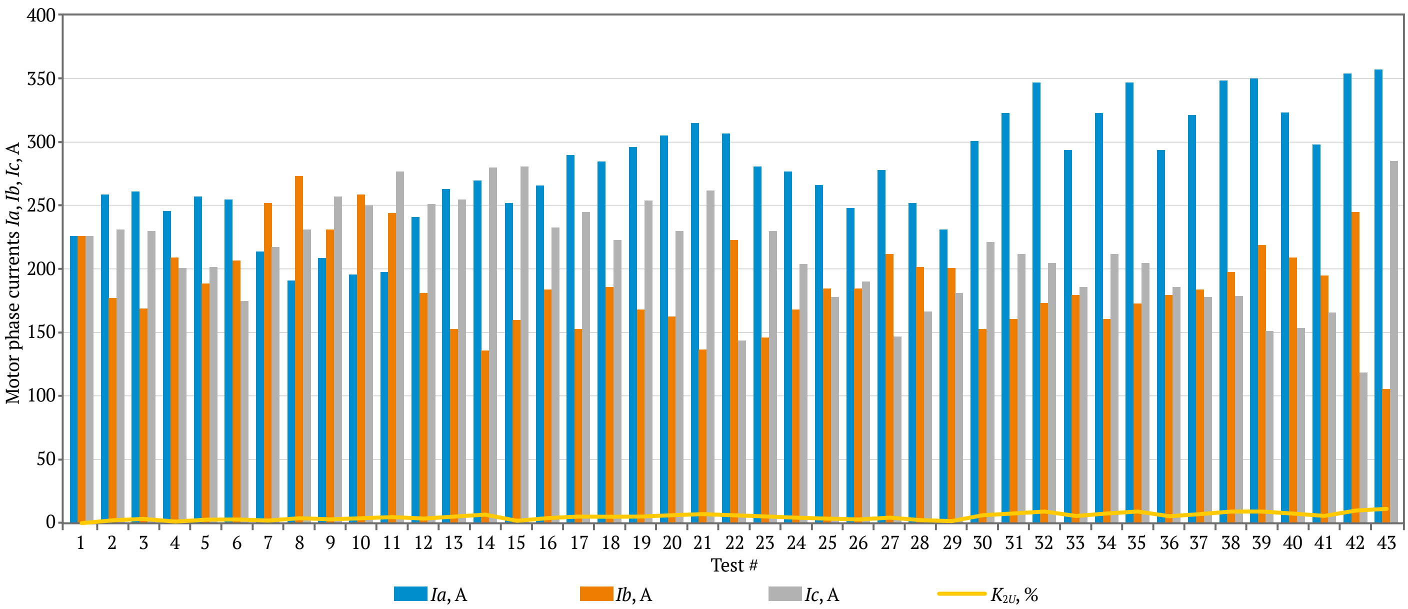

Fig. 7. The currents in a motor phases *Ia*, *Ib*, *Ic* as functions of the negative-phase-sequence voltage unbalance factor K_{2U}

eISSN 2500-0632
https://mst.misis.ru/

Analysis of the dependence of currents in phases on the unbalance factor shows that significant current unbalance occurs even at small values of the unbalance factor K_{2U}. This means that for full-fledged motor protection, in addition to sequence filter protection, negative sequence overcurrent protection should be in place, since it is under the action of negative-phase-sequence currents a motor heating occurs, losses increase, and thereby the service life is reduced.

Now let us consider the effect of voltage unbalance on motor phase currents at different shaft loads. For this purpose the load will vary from 0 to 120 %. The examples of the study results for no-load, rated conditions, and overload are presented in Tables 6–8.

It is important to note that when the load on the motor shaft is 120% of the rated load, and when the voltages in phases A, B, C deviate by −10, −10 and 0 % respectively, the overload protection trips. This is because even a small voltage unbalance during overload causes currents in excess of the protection set-point.

The data presented in the tables shows that at the same deviations in phase voltages, the currents have greater unbalance at higher load factors. This is because the more loaded motor produces greater currents, and with an unbalanced supply voltage, the magnitude of these increased currents has a greater effect on the unbalance, thus causing greater negative-phase-sequence (nps) current. Therefore, unbalanced supply voltage conditions are unacceptable at high motor loads.

Table 5

Simulation results for AM operation under conditions of unbalanced supply voltage

Phase voltage deviations, %			Currents in motor phases, A			K_{2U}, %	Tripping
ΔUa	ΔUb	ΔUc	*Ia*	*Ib*	*Ic*		
10	−10	0	270	136	280	6,1	Negative Sequence O/C protection
5	−10	−10	296	168	254	4,9	Negative Sequence O/C protection
10	−5	−10	305	163	230	5,8	Negative Sequence O/C protection
10	−10	−10	315	137	262	6,7	Negative Sequence O/C protection
10	10	−10	307	223	144	5,7	Negative Sequence O/C protection
15	0	−5	301	153	221	5,9	Negative Sequence O/C protection
15	0	−10	323	161	212	7	Negative Sequence O/C protection
15	0	−15	347	173	205	8,5	Negative Sequence O/C protection, sequence filter
15	5	−5	294	180	186	5,2	Negative Sequence O/C protection
15	0	−10	323	161	212	7	Negative Sequence O/C protection
15	0	−15	347	173	205	8,5	Negative Sequence O/C protection, sequence filter
15	5	−5	294	180	186	5,2	Negative Sequence O/C protection
15	5	−10	321	184	178	6,6	Negative Sequence O/C protection
15	5	−15	348	198	179	8,4	Negative Sequence O/C protection, sequence filter
15	10	−15	350	219	151	8,7	Negative Sequence O/C protection, sequence filter
15	10	−10	323	209	154	7	Negative Sequence O/C protection
15	10	−5	298	195	166	5,2	Negative Sequence O/C protection
15	15	−10	354	245	119	9,4	Negative Sequence O/C protection, sequence filter
15	−15	−15	357	106	285	10,5	Negative Sequence O/C protection, sequence filter

Let us now consider the rotor rpm and torque produced by the motor under different unbalanced supply voltage conditions as a function of time. We will investigate the operation of the motor with rated load when the voltage in the phases deviates from the rated value as follows:

1) phase voltage deviations: $\Delta Ua = 15$ %; $\Delta Ub = 10$ %; $\Delta Uc = 0$ %;

2) phase voltage deviations: $\Delta Ua = 10$ %; $\Delta Ub = 5$ %; $\Delta Uc = 0$ %;

3) phase voltage deviations: $\Delta Ua = -15$ %; $\Delta Ub = -5$ %; $\Delta Uc = 0$ %;

4) phase voltage deviations: $\Delta Ua = -10$ %; $\Delta Ub = 0$ %; $\Delta Uc = 0$ %.

In the conditions under consideration, the motor has time to reach steady-state operation conditions before the overload protection trips Thus, the negative sequence overcurrent protection and sequence filter-based protection do not trip. To obtain a more illustrative study, the stator and rotor currents, as

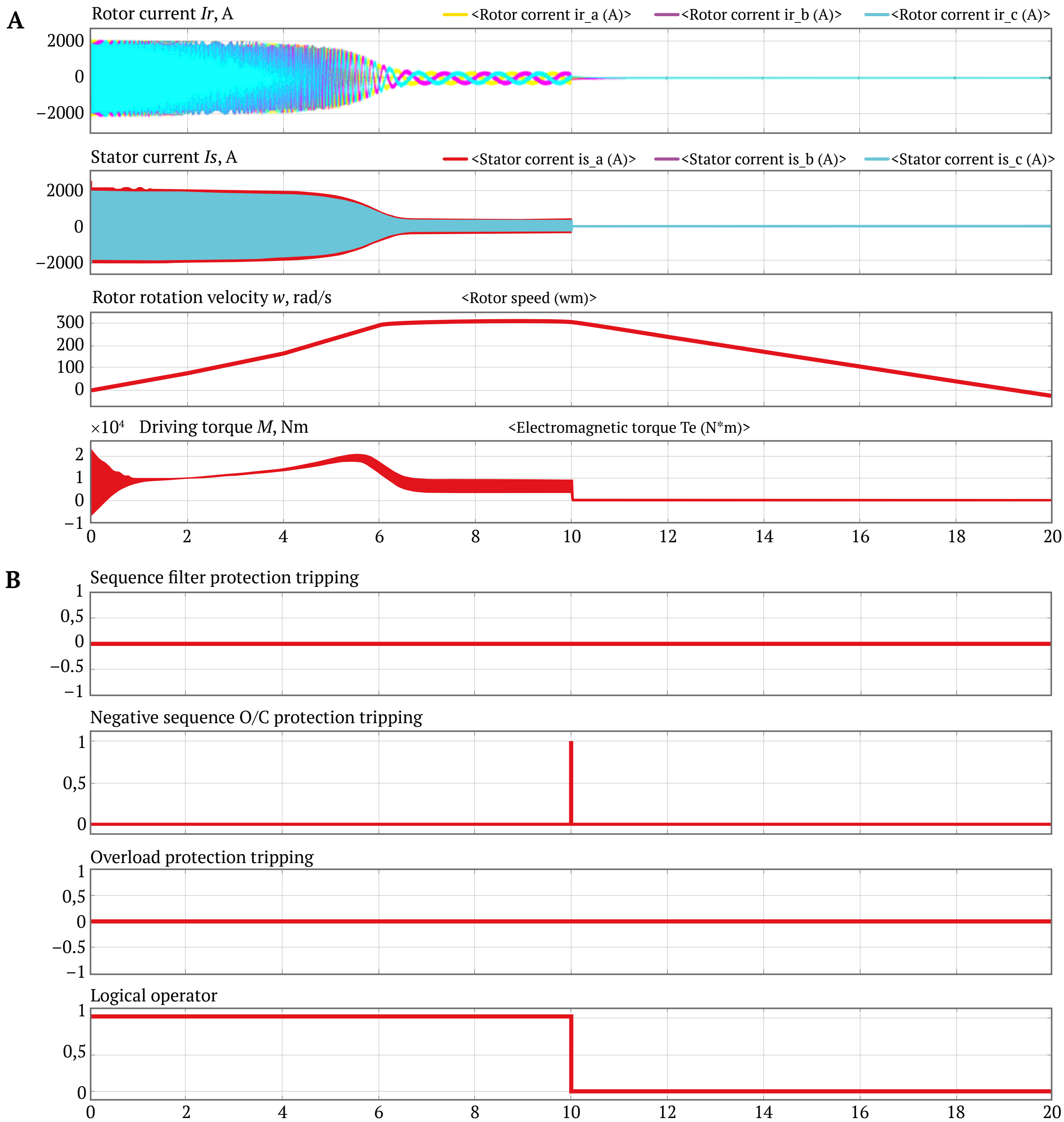

Fig. 8. Timing diagrams: *A* – line rotor currents, stator currents, rotor rpm, and electromagnetic torque of a motor with an increase in phase A voltage by 20 %; *B* – protection signals with an increase in phase A voltage by 20 %

eISSN 2500-0632
https://mst.misis.ru/

well as the rotor rpm and the motor torque for 13 s of simulation are considered. The simulation results are presented in Table 9. Fig. 9 shows examples of the graphs of changes in the rotor currents, stator currents, rotation velocity and drive torque of an asynchronous motor at the considered negative-phase-sequence voltage unbalance factor values K_{2U}.

The figures presented show that the supply voltage unbalance causes currents unbalance and, consequently, negative-phase-sequence current. This violates the normal regime of motor operation by changing the shape of stator and rotor current curves, as well as the rotor rpm and the motor torque, that is, by creating oscillations of these parameters. The

Table 6

Simulation of unbalanced motor operation conditions at 100% load

Voltage deviations in phases, %			K_{2U}, %	Motor phase currents, A			Tripping
Δ*Ua*	Δ*Ub*	Δ*Uc*		*Ia*	*Ib*	*Ic*	
−10	−10	0	4	197.7	244.1	277.2	Protections fall to function
10	−5	−10	6	304.8	162.8	229.9	Negative Sequence O/C protection
15	0	−5	6	300.5	153.4	221.4	Negative Sequence O/C protection
15	0	−10	7	322.6	161.2	211.9	Negative Sequence O/C protection
15	10	−15	9	350.2	219.1	151.0	Negative Sequence O/C protection, sequence filter
15	−15	−15	11	356.9	106.0	285.2	Negative Sequence O/C protection, sequence filter

Table 7

Simulation of unbalanced operation conditions at 0% load

Voltage deviations in phases, %			K_{2U}, %	Motor phase currents, A			Tripping
Δ*Ua*	Δ*Ub*	Δ*Uc*		*Ia*	*Ib*	*Ic*	
−10	−10	0	4	81.6	23.5	117.7	Protections fall to function
10	−5	−10	6	162.6	92.3	70.6	Negative Sequence O/C protection
15	0	−5	6	178.4	120.3	58.8	Negative Sequence O/C protection
15	0	−10	7	192.8	145.6	56.4	Negative Sequence O/C protection
15	10	−15	9	205.2	204.0	60.3	Negative Sequence O/C protection, sequence filter
15	−15	−15	11	237.6	148.2	126.2	Negative Sequence O/C protection, sequence filter

Table 8

Simulation of unbalanced operation conditions at 120% load

Voltage deviations in phases, %			K_{2U}, %	Motor phase currents, A			Tripping
Δ*Ua*	Δ*Ub*	Δ*Uc*		*Ia*	*Ib*	*Ic*	
−10	−10	0	4	243.2	300.0	327.6	Overload protection
10	−5	−10	6	348.8	205.4	275.0	Negative Sequence O/C protection
15	0	−5	6	341.6	192.2	261.7	Negative Sequence O/C protection
15	0	−10	7	365.1	198.9	250.3	Negative Sequence O/C protection
15	10	−15	9	383.5	245.4	188.6	Negative Sequence O/C protection, sequence filter
15	−15	−15	11	396.2	148.6	333.6	Negative Sequence O/C protection, sequence filter

Table 9

Motor dynamic characteristics simulation results

Voltage deviations in phases, %			Phase voltages, V			Motor phase currents, A			Unbalance factor K_{2U}, %
Δ*Ua*	Δ*Ub*	Δ*Uc*	Δ*Ua*	Δ*Ub*	Δ*Uc*	*Ia*	*Ib*	*Ic*	
15	10	0	5634	5389	4899	274.1	196.2	181.7	4.1
10	5	0	5389	5144	4899	257.9	196.6	203.4	2.8
−15	−5	0	4164	4654	4899	184.9	292.7	262	4.7
−10	0	0	4409	4899	4899	198	277.5	232.2	3.4

resulting oscillations have a larger amplitude with a higher negative-phase-sequence voltage unbalance factor. Unbalanced voltage conditions have an adverse impact on motor operation, since it causes fluctuations in the motor torque and rotor rpm, resulting in vibrations that reduce the motor service life. For better visualization let us display graphically the signals of rotor rpm and motor torque from identical circuits working in parallel with different ratios of supply voltages, according to Table 9. Fig. 10 shows such graphs of changes in the effective values of rotation velocity and torque of the asynchronous motor at different negative-phase-sequence voltage unbalance factors.

The graphs show that the changes in the rotor rpm and motor torque depend mostly on the nature of the voltage change rather than on the unbalance factor. At lowered voltage, it is more difficult to start the motor and the rated rotation velocity is reached more slowly. Let us compare the graphs of the torque changes at K_{2U} = 0, 4.7, 3.4 %. Since K_{2U} = 0 % at the ra-ted supply voltage conditions, no negative-phase-sequence torque occurs $-M_2 = 0$, and the motor torque is fully determined by positive-phase-sequence torque $-M_{rated} = M_1$. In order to assess the effect of unbalanced voltage on the motor torque, we assume that at K_{2U} = 4.7, 3.4 % the positive-phase-sequence torque is approximately equal to the torque at the rated motor operating conditions. This statement is justified by the fact that the voltage level in the cases under consideration does not differ significantly from the rated voltage. Consequently, the character of the curves depends on this to a lesser extent. Since negative-phase-sequence currents arise when the supply voltage is unbalanced, negative-phase-sequence torque also arises. It has a negative value of $M_2 < 0$: the resulting torque equal to the sum of positive- and negative-phase-sequence torques $-M = M_1 + M_2 = M_{rated} + M_2$ will decrease by increasing the unbalance factor as clearly expressed in the peaks of the curves in question. A similar statement is true for the change in torques at K_{2U} = 4.1, 2.48%. However, this is due to the fact that the voltage unbalance was introduced by increasing the voltages in the phases, both positive- and negative-phase-sequence currents increased along with the voltage which caused an increase in the corresponding torques. In this case, with a higher unbalance factor, the torque becomes greater when compared to the rated one. It may thus be concluded that a deviation from voltage balance is accompanied by a decrease in the resulting torque and, consequently, by an increase in losses and a decrease in motor efficiency, as well as by heating of the windings as a result of negative-phase-sequence currents.

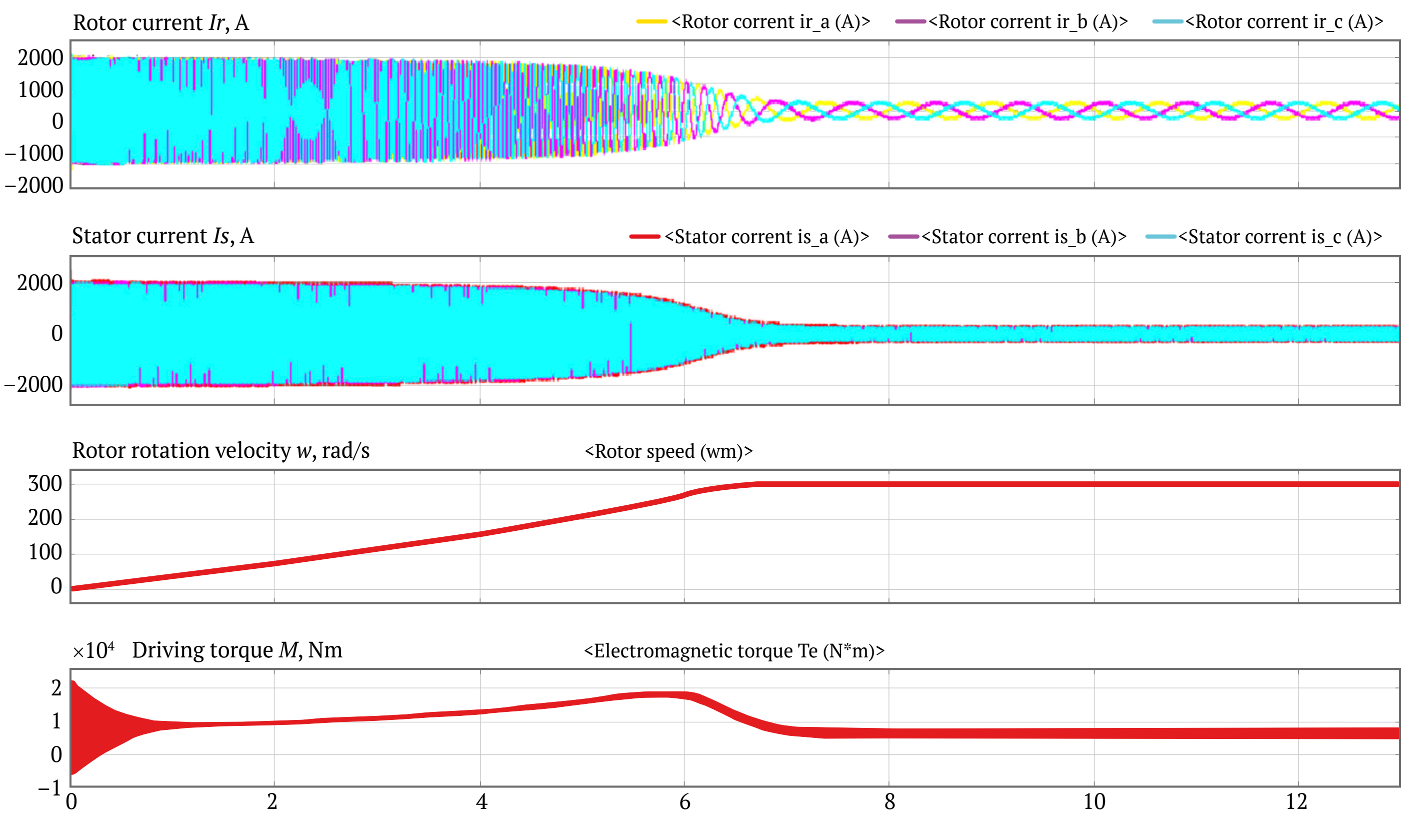

Fig. 9. Graphs of changes in rotor currents, stator currents, rotation velocity and drive torque of an asynchronous motor at the considered negative-phase-sequence voltage (unbalance) factor K_{2U} = 4.1 %

eISSN 2500-0632
https://mst.misis.ru/

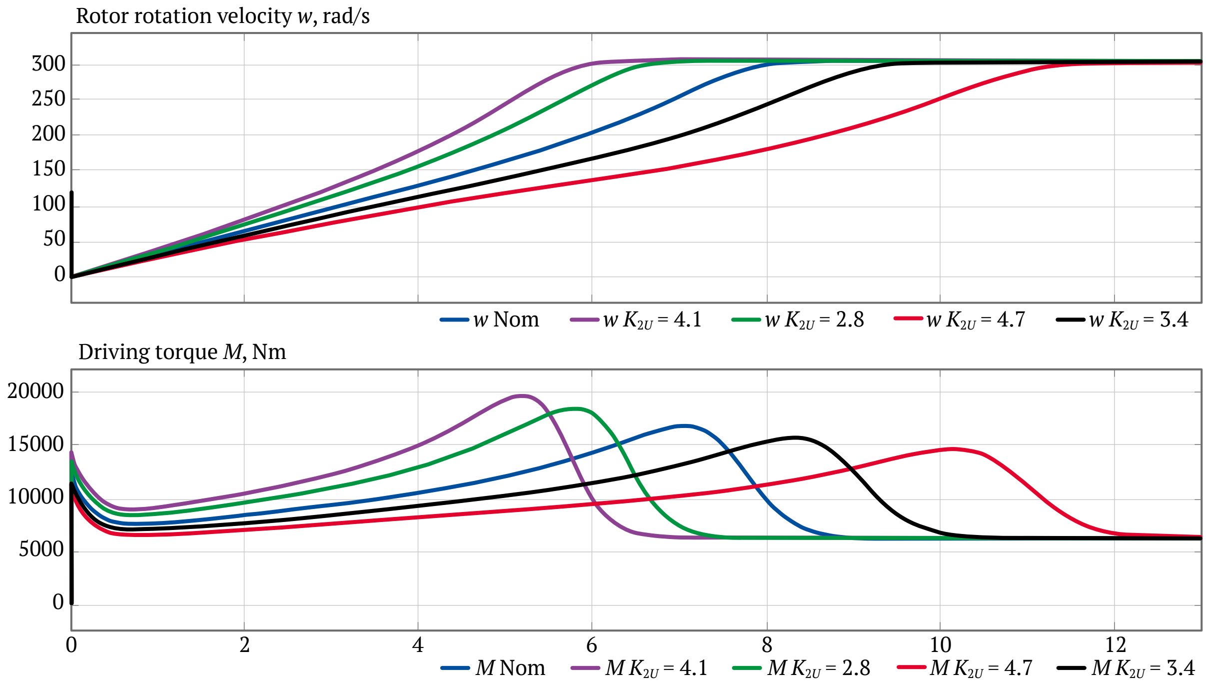

Fig. 10. Graphs of changes in the effective values of rotation velocity and torque of the asynchronous motor at rated operating conditions (K_{2U} = 0 %) and at different negative-phase-sequence voltage unbalance factor values K_{2U} = 4.1, 2.8, 3.4, 4.7 %

Conclusions

The authors conducted a study of high-voltage asynchronous motor drive protections of a recycle compressor in the fuel hydrotreating unit at the Astrakhan Gas Refining Plant. The studies showed that sequence filter relay protections, negative-phase-sequence protection, and overload protection should be selected in the aims of protecting the motor against supply voltage unbalance. A simulation of the joint operation of the AM and its protections was performed. The study findings allow for quantitative assessment of the effect of supply voltage unbalance on the operation of a high-voltage asynchronous motor. The analysis of the protections operation showed that, in the event of voltage unbalance, the negative sequence overcurrent protection trips more often, because an unbalance of currents arises. The authors conclude that this protection must be implemented, because the consequence of unbalanced voltage supply conditions, namely, the unbalance of currents, creates a negative-phase-sequence torque. This leads to a reduction of motor efficiency and service life. Evaluation of the protections operation at different motor load factors showed that the effect of voltage unbalance has a greater influence on the motor operation at higher load factors. The analysis of the motor characteristics at different unbalances of the supply voltage allowed changes in the effective values of the motor rpm and torque at different unbalance factors to be assessed. The feasibility of implementation of the developed relay protection system on the basis of series 80 Sepam 1000+ microprocessor protection has been confirmed.

In terms of commercial application, the study findings can be used as a basis for relay protection of all components of the fuel hydrotreating unit at the Astrakhan gas refining plant. The authors are currently further developing this system.

References

1. Panchenko V., Turenko A. Analysis of the influence of voltage asymmetry on the operation of the traction asynchronous electric motor using the simulation model. *Collected Scientific Works of Ukrainian State University of Railway Transport*. 2021;(198):145–150. (In Ukranian) https://doi.org/10.18664/1994-7852.198.2021.256648

2. Romanova V.V., Khromov S.V., Batukhtin A.G., Suslov K.V. Analysis of the degree of influence of supply voltage asymmetry on the operational reliability of low-voltage asynchronous electric motors. *Power Engineering: Research, Equipment, Technology*. 2022;24(4):131–141. (In Russ.) https://doi.org/10.30724/1998-9903-2022-24-4-131-141

3. Shakirov V.A., Syroveshkin A.M., Buyanina O.A. Study of the effect of voltage unbalance on the operation of asynchronous motors. *Trudy Bratskogo Gosudarstvennogo Universiteta. Seriya: Estestvennye i Inzhenernye Nauki – Razvitiyu Regionov Sibir*. 2011;(2:8):11. (In Russ.)

4. Dmitrieva V.V., Avkhadiev I.F., Sizin P.E. Use of advance hardware/software in multiple conveyor system automation. *Mining Informational and Analytical Bulletin*. 2021;(2):150–163. (In Russ.) https://doi.org/10.25018/0236-1493-2021-2-0-150-163

5. Ershov Yu.A., Maleew A.V. Microprocessor Relay Protection Modeling in MATLAB. *Journal of Siberian Federal University. Engineering & Technologies*. 2010;3(2):220–228. (In Russ.) URL: https://elib.sfu-kras.ru/bitstream/handle/2311/1672/09_ershov.pdf?sequence=1

6. Andreev M.V., Ruban N.Yu., Suvorov A.A. Mathematical modeling of digital differential transformer protection in Matlab Simulink environment. *Bulletin of Irkutsk State Technical University*. 2018;22(1):134–150. https://doi.org/10.21285/1814-3520-2018-1-134-150

7. Kopylov I.P. *Mathematical modeling of electric machines*. Moscow: Vysshaya Shkola; 2001. 327 p. (In Russ.)

8. Andreev V.A. *Relay protection of power supply systems in examples and tasks*. Moscow: Vysshaya Shkola; 2008. 256 p. (In Russ.)

9. Hou L., Li B., Hu X., Liu Ch. Research on motor relay protection of high-voltage variable frequency motor drive system. *Journal of International Council on Electrical Engineering*. 2014;4(4):330–335. https://doi.org/10.1080/22348972.2014.11011892

10. Kuprienko V.V. Relay protection features of frequency-adjustable electric drive. In: *IOP Conference Series: Materials Science and Engineering*. 2018;327(5):052021. https://doi.org/10.1088/1757-899X/327/5/052021

11. Popa G.N., Duinis C.M. Complex electronic protection for low-voltage three-phase induction motors. *WSEAS Transactions on Electronics*. 2020;11:11–17. https://doi.org/10.37394/232017.2020.11.2

12. Polishchuk V.I., Kritsky M.V., Bannov D.M., Malyshev S.V. Application of unified microprocessor relay protection units in electrical machine diagnostics. *Power Engineering: Research, Equipment, Technology*. 2019;21(6):93–100. (In Russ.) https://doi.org/10.30724/1998-9903-2019-21-6-93-100

13. Neftisov A.V., Sarinova A.Zh., Talipov O.M. Possibility of building microprocessor relay protection devices on open architecture. *Bulletin of Toraigyrov University. Energy Series* 2022;(3):277–292. https://doi.org/10.48081/IKLZ1109

14. Zeng Q., Zhang Zh., Xu M., Zhu J. A coordinated relay protection strategy of distribution network based on fault current limiting. *Energy Reports*. 2022;8(3):380–387. https://doi.org/10.1016/j.egyr.2022.08.036

15. Kholiddinov I.Kh., Misinova G., Yulchiev M.E., Tuychiev Z.Z. Modeling of calculation of voltage unbalance factor using Simulink (Matlab). *The American Journal of Engineering and Technology*. 2020;2(10):33–37. https://doi.org/10.37547/tajet/Volume02Issue10-07

16. Novobritsky V.A., Fedosov D.S. The main types of wind turbines-generators in the power supply system. *Power Engineering: Research, Equipment, Technology*. 2021;23(5):71–85. (In Russ.) https://doi.org/10.30724/1998-9903-2021-23-5-71-85

17. Nedelchev N., Matsankov M. Increasing the sensitivity of the digital relay protection against turn-to-turn short circuits and asymmetries in wind power generators. In: *The 3rd International Conference on Electrical Engineering and Green Energy (CEEGE 2020)*. 2020;186(4):03001. https://doi.org/10.1051/e3sconf/202018603001

18. Romanova V.V., Khromov S.V. Construction of a computer model to study the operating regimes of an asynchronous motor. In: *Collection of scientific papers based on the results of the international scientific-practical conference "Development of Technical Sciences in the Modern World". Vol. II*. Voronezh, December 8, 2015. Voronezh: ITsRON Publishing House; 2015. Pp. 35–38. (In Russ.)

19. Pantel O.V. Asynchronous motor parameters calculation methodology for simulation of its operating regimes in Matlab/Simulink environment. *Academy*. 2015;(2):7–11. (In Russ.)

20. Nemykina V.V., Ryabchenok N.L., Alekseeva T.L., Astrakhantsev L.A. Analysis of current and voltage unbalance in stator windings of asynchronous motors of the auxiliary machine drive. *Modern Technologies. System Analysis. Modeling*. 2020;(4):85–92. (In Russ.) https://doi.org/10.26731/1813-9108.2020.4(68).85-92

21. Suvorov I.F., Sidorov A.I., Khromov S.V. Investigation of the effect of unbalanced line voltages in networks up to 1000 V on the modes of induction motors. *Electrical Safety*. 2014;(3):17–30. (In Russ.)

Information about the authors

Valeria V. Dmitrieva – Cand. Sci. (Eng.), Associate Professor of the Department of Theoretical Electrical Engineering and Electrification of Oil and Gas Industry, National University of Oil and Gas "Gubkin University", Moscow, Russian Federation; ORCID 0000-0002-8740-9380, Scopus ID 56007868500; e-mail dm-valeriya@yandex.ru

Aldiyar B. Khammatov – Master Student of the Department of Theoretical Electrical Engineering and Electrification of Oil and Gas Industry, National University of Oil and Gas "Gubkin University", Moscow, Russian Federation; ORCID 0009-0007-6286-6845; e-mail khammatov.aldik@mail.ru

Поступила в редакцию	25.12.2022	**Received**	25.12.2022
Поступила после рецензирования	27.03.2023	**Revised**	27.03.2023
Принята к публикации	28.03.2023	**Accepted**	28.03.2023